Summer 8-9-2019

Synthesis and Characterization of Long-Acting Rilpivirine Prodrugs

James R. Hilaire
University of Nebraska Medical Center

Follow this and additional works at: https://digitalcommons.unmc.edu/etd

Part of the Immune System Diseases Commons, Medicinal and Pharmaceutical Chemistry Commons, Nanomedicine Commons, Pharmaceutics and Drug Design Commons, and the Virus Diseases Commons

Synthesis and Characterization of Long-Acting Rilpivirine Prodrugs

by

James Hilaire

A DISSERTATION

Presented to the Faculty of

the University of Nebraska Graduate College

in Partial Fulfillment of the Requirements

for the Degree of Doctor of Philosophy

Pharmacology and Experimental Neuroscience
Graduate Program

Under the Supervision of Professor Howard E. Gendelman

University of Nebraska Medical Center
Omaha, Nebraska

July, 2019

Supervisory Committee:

Dr. Benson Edagwa, Ph.D.   Dr. JoEllyn McMillan, Ph.D

Dr. Joseph Vetro, Ph.D   Dr. Tatiana Bronich, Ph.D

DEVELOPMENT AND CHARACTERIZATION OF

LONG-ACTING RILPIVIRINE PRODRUGS

James R. Hilaire, Ph.D.

University of Nebraska, 2019

Supervisor: Howard E. Gendelman, M.D.

Antiretroviral therapy (ART) requires lifelong daily dosing to suppress viral replication, restore or maintain immune function and improve quality of life. As an alternative, long-acting (LA) antiretrovirals (ARVs) aim to deliver therapeutic drug concentrations over an extended period, ultimately requiring monthly or even more extended dosing intervals. Specifically, the success of recent clinical trials examining LA cabotegravir and rilpivirine (CAB and RPV LA) highlight the advent of these novel HIV-1 therapeutics. Further optimization of LA dosage forms are required and rests upon improving dosing frequency, injection volumes and tissue distribution to viral compartments. To this end, we report the synthesis of a library of RPV prodrugs specifically designed to provide sustained drug plasma concentrations and enhance tissue distribution. Lead prodrug candidate M3RPV was nanoformulated to develop a stable LA injectable dosage form (NM3RPV). Specifically, NM3RPV provided RPV plasma concentrations above the PA-IC$_{90}$ for 25 weeks, while concurrently generating a substantial tissue depot after in single injection in *BALB/cJ* mice. Furthermore, NM3RPV provided 13 and 26-fold increases in t$_{1/2}$ and MRT compared with NRPV respectively. Therefore, these results provide proof-of-concept nanoformulated RPV prodrugs can

effectively extend the apparent half-life and improve tissue distribution compared to nanoformulated RPV (NRPV), warranting further investigation and optimization

ACKNOWLEDGEMENTS

The journey towards the conclusion of my doctoral training did not start at the University of Nebraska Medical Center, but with the conversations I had with my Popop as a child. He was a thinker and a learner, someone who taught me to ask questions and never be hesitant to ask "why". At a young age he instilled in me a spirit of learning and discovery. These characteristics remain embedded in my personality and direct my course in life; even if he is not here to see his impact. Furthermore, I would like to thank my mother, father, and sister supported my goals, interests, and dreams. They gave me space to grow, yet were always there for support when I needed them the most. My mother was a teacher and helped me fall in love with education and generate a thirst for knowledge. My father taught me about work ethic and how hard I would need to work to achieve my goals. My sister provided me with an example of how to be responsible and take care of my business in a proper manner. Along with my immediate family, all my New York family has supported in this process, making me feel the space between NY and Nebraska is shorter than the measured 1,200 miles.

My time in Nebraska has been accompanied by scientific successes and failures. Outside the lab has been a resounding success, as I met my wife Shannon in Omaha, NE. Her continued and persistent love, support, and belief in me have propelled me to personal and professional heights I could not have achieved alone. In addition to being an outstanding professional in her respective field, Shannon is a great mother to our 2-month-old daughter Holiday. She has juggled her career and our new baby to support my educational endeavors and I am thankful for all her love and support. In addition, Shannon's family, including Jan, Gary, Andy, Aaron, Joe, Elisabeth, Laura, Reece, and Dr. Peter's have provided me a Nebraska family for which I am truly thankful.

Surrounding yourself with people you love makes your successes more enjoyable and your failures manageable. Thank you to the whole Stawniak crew for your love and support.

On a professional level Dr. Gendelman has been an instrumental in my development as a scientist. As a mentor, Dr. Gendelman has exhibited patience, as my early projects were not as fruitful and productive as desired. He stood by me and continually supported me, engendering confidence that I would eventually breakthrough scientifically. Besides Dr. Gendelman scientific lessons, it is his work ethic that will leave a lasting impact on me. To witness an accomplished leader of his field continually outworking the competition and pushing for continued success is inspiring. He taught me when you have success it is time to work even harder, as those special moments are often fleeting. Additionally, Dr. Gendelman taught me that no idea is too outside the box and in science it is okay and sometimes necessary to push the boundaries because that is where true innovation lies.

Additionally, I would like to thank the members of my advisory committee: Drs. Benson Edagwa, Tatiana Bronich, JoEllyn McMillan, and Joseph Vetro. All committee members have provided valuable insight not only towards my research, but also how to think and develop into a better scientist. Dr. Edagwa has been very patient and provided excellent guidance in chemistry, scientific discussions, and insightful perspectives on life. Dr. McMillan has been a steady source of support for me, continually displaying a willingness to listen and discuss ideas and improve my scientific directions. Furthermore, I want to thank Dr. Bronich for pushing me to think more in depth about my research, her insightful critiques have added significant value to my education. Moreover, I would like to thank Dr. Vetro who also provided me with excellent research feedback and urged me to put my research and scientific ideas in context of the bigger picture.

and Siddhi Bade for their support and friendship as the hard work was definitely offset with lots of fun.

TABLE OF CONTENTS

LIST OF ABBREVIATIONS

^{1}H NMR	proton nuclear magnetic resonance spectroscopy
3TC	lamivudine
^{13}C NMR	carbon nuclear magnetic resonance spectroscopy
ACN	acetonitrile
AIDS	acquired immunodeficiency syndrome
ART	antiretroviral therapy
ARV	antiretroviral drugs
BD	biodistribution
C_{trough}	trough concentration
CAB	cabotegravir
DCM	dichloromethane
DMF	dimethylformamide
DMSO	dimethyl sulfoxide
DTG	dolutegravir
EC_{50}	50% effective concentration
ESI-MS	electrospray ionization mass spectrometry
INI	integrase inhibitor
FTIR	Fourier-transformation infrared spectroscopy
HIV-1	human immunodeficiency virus type-one
HCL	hydrochloric acid

IC$_{90}$	90% inhibitory concentration
IM	intramuscular
IP	intraperitoneal
IS	internal standard
LA	long-acting
LASER-ART	long-acting slow effective release antiretroviral therapy
MDM	monocyte-derived macrophages
MOI	multiplicity of infection
MRT	mean resonance time
MVC	maraviroc
MS/MS	tandem mass spectrometry
NaOH	sodium hydroxide
NNRTI	non-nucleoside reverse transcriptase inhibitor
NRTI	nucleoside reverse transcriptase inhibitor
P407	poloxomer 407
P338	poloxomer 338
PA-IC$_{90}$	protein-adjusted 90% inhibitory concentration
PBS	phosphate buffered saline
PDI	polydispersity index
PK	pharmacokinetics
PrEP	pre-exposure prophylaxis
RPV	rilpivirine
RT	reverse transcriptase
SEM	standard error of the mean
SC	subcutaneous
t$_{1/2}$	half-life

TEM   transmission electron microscopy

UPLC   ultra-performance liquid chromatography

UV/Vis   dual-wavelength ultraviolet/visible light detection

LIST OF FIGURES

LIST OF TABLES

CHAPTER 1- INTRODUCTION

1.1 Global Impact of HIV/AIDS

Since the beginning of the HIV/AIDS epidemic in early 1980s, 77.3 million people have become infected with HIV, with 35.4 million dying from AIDS-related illnesses during this timeframe.[1] Antiretroviral therapy (ART) has revolutionized patient care for HIV-1 infected individuals providing a life span approaching that of the general population.[2,3] In particular, between 2000 and 2017, coinciding with the advent of ART, new HIV infections and HIV-related deaths have decreased by 36 and 38% respectively.[4] Notwithstanding, as of 2017 only 59% of HIV-infected adults were receiving ART.[1] Furthermore, HIV is still endemic in eastern and southern Africa where an estimated 19.6 million people are currently living with HIV, a substantial 53% of the global disease burden.[1] Therefore future treatment strategies must focus on delivering ART is a more efficient, discrete, and reliable manner to increase drug access and effective use.

1.2 HIV-1 Pathobiology

HIV-1 infection requires viral entry into its target cells (CD4+ T-cells; monocytes; dendritic cells and macrophages). Cellular entry is facilitated by viral envelope (env) glycoprotein 120 (gp120) and glycoprotein 41 (gp41). Specifically, gp120 binds to CD4 on the host cell surface.[5] This interaction facilitates a conformational change in gp120, whereby the newly exposed V3 loop binds its co-receptor target (CCR5 or CXCR4).[6] Co-receptor binding exposes HIV-1gp41 enabling interaction between viral and host cell

membranes, ultimately generating membrane fusion and exposure of viral RNA to the cytoplasm.[7] HIV-1 is a retrovirus, thus after cellular entry conversion of its single stranded RNA genome into double stranded circular DNA is required and accomplished by reverse transcriptase (RT).[8] Viral DNA is subsequently transported into the nucleus as a pre-integration complex (PIC) and integrated into the host cell genome with the help of the virally encoded integrase enzyme.[9] Integrated proviral DNA can remain latent or be expressed at low levels using host cell machinery. Expression of HIV-1 DNA in turn produces viral proteins such as trans-activator of transcription (Tat) which stimulate more efficient HIV-1 transcription.[10] Furthermore, HIV-1 gag polyprotein facilitates the assembly, budding, and with assistance from HIV-1 protease, the production of infectious virions destined to infect more host cells.[11] (Figure 1.5.1)[12]

In the human host, HIV-1 infection is a major threat to immunity. Patients typically experience a severe depletion of CD4+ CCR5+ T-cells in the gut with the onset of infection.[13] Clinical manifestations of early infection often present as flu-like symptoms, but as the disease progresses and plasma viremia reach their set point, patients can become asymptomatic for an extended period of time. Within the host body, destruction of the CD4+ T cell population is accompanied by robust immune activation. If a patient is left untreated, a depleted immune system would eventually succumb to opportunistic infections. Therefore, means to monitor HIV-1 plasma viral load and CD4+ T cell counts is essential. ART is essential not only prolong the life span of infected individuals but in reducing the propagation and further spread of infection to other human hosts.

1.3 ART

Between the first clinical observations of HIV (1981) and clinical trials for zidovudine (AZT; 1987), clinicians were relegated to the treatment of opportunistic infections associated with HIV/AIDS.[14,15] It became apparent that combination ART was

necessary to slow disease progression, avoid development of resistance, and reduce morbidity and mortality due to opportunistic infections.[16-19] As the basic understanding of HIV-1 and its viral life cycle improved, more targets were identified for medicinal chemists to develop novel antiretroviral compounds. Thus, protease inhibitors (PIs) were discovered in 1995 (saquinavir), while the first non-nucleoside reverse transcriptase inhibitors (NNRTIs) were approved 1996 (nevirapine).[20,21] Quickly new classes of compounds emerged and attained FDA approval, such as fusion inhibitors (enfuvirtide; 2003), entry inhibitors (maraviroc; 2007), and integrase inhibitors (raltegravir; 2007).[22-24] Patient quality of life continued to improve as ART more readily managed HIV-1 infection, although a significant number of pills and multiple daily dosing schedules remained a requirement. Further advances included the development of single tablets containing multiple drug classes, first exemplified by efavirenz (EFV), emtricitabine (FTC), and tenofovir disoproxil fumarate (TDF).[25] Strict adherence to modern ART therapy reduces plasma viral loads below the limit of detection, offers comparable life spans to the general population, and provides a 96% reduction in sexual transmission between HIV-1 serodiscordant couples.[2,26] General guidelines for current ART suggest the use of two nucleoside reverse transcriptase inhibitors (NRTIs) administered with an nonnucleoside reverse transcriptase inhibitor (NNRTI), integrase inhibitor (INSTI) or a protease inhibitor (PI), with a booster).[27] Common ART combinations include bictegravir-tenofovir alafenamide-emtricitabine (biktarvy) and dolutegravir-abacavir-lamivudine (triumeq). Furthermore, new potent compounds continue to be developed (cabotegravir, CAB), as well as the repurposing of existing ARVs for monthly delivery by intramuscular injection (rilpivirine, RPV and CAB LA).[28] Certainly, ART has been one of most significant achievements in modern medicine, enabling millions of infected individuals to live with HIV-1 and have productive lives. Specifically, between 2000 and 2017 an estimated 11.4 million lives were saved due to ART.[4] Notwithstanding, significant

progress is still required considering only 75% of infected individuals know their status, of which 79% are accessing ART, and 81% which are virally suppressed.[1] Therefore, the 90-90-90 initiative has been implemented to strive for 90% of all HIV infected individuals to be aware of their status, receive ART treatment, and ultimately achieve viral suppression by 2020.[29] Thus, next generation ART will focus on improving drug access and utilization in underserved communities, as well as improving the compliance and ease of use for individuals already on ART.

1.3.1 RPV

Non-nucleoside reverse transcriptase inhibitors (NNRTIs) bind to a hydrophobic binding pocket near the reverse transcriptase (RT) catalytic site, thus acting as allosteric inhibitors. Rilpivirine is a highly active diarylpyrimidine NNRTI with sub-nanomolar activity against wild-type virus (0.73 nM).[30] RPV is more active against a broad range of viral mutants, differentiating it from other NNRTIs such as Nevirapine (NVP) and Efavirenz (EFV).[31] The broad-spectrum inhibitory nature of RPV across NNRTI resistant strains is likely due to its flexibility within the RT binding pocket.[31] Furthermore, RPV is associated with less reported adverse events than NVP and EFV, which have been observed to generate hepatotoxic and neuropsychiatric side effects respectively.[32,33] RPV is slowly metabolized by liver hepatocytes, thus its observed slow metabolic clearance results in a long half-life (~45 hours), allowing for once-daily dosing.[31,34] Currently RPV is indicated for once-daily oral delivery (25 mg) in adults with HIV-1 RNA ≤ 100,000 copies/mL in treatment naïve patients in two fixed-dose combinations, Complera (RPV-TFV-FTC) and Odefsey (RPV-TAF-FTC).[35] Moreover, the first two-drug fixed dose once-daily oral regimen (Juluca) was approved for treatment experienced patients exhibiting viral suppression (HIV-1 RNA < 50 copies/mL) consisting of DTG (50 mg) and RPV (25 mg).[35,36] Furthermore, RPV has been investigated as a long-acting

injectable formulation for monthly delivery.[37,38] Particularly, its combination of high potency and low solubility selected RPV for LA formulation development securing its status as highly important compound for the next generation of ART.[39]

1.3.2 Maraviroc (MVC)

MVC is a small molecule allosteric antagonist of CCR5 and represents the first and only FDA approved HIV-1 entry inhibitor. Specifically, MVC bound to CCR5 generates a conformational change whereby efficient interaction between HIV-1gp120 and CCR5 is no longer possible. Entry inhibitors such as MVC have been attractive drug targets due to the cure of the "Berlin patient", as well as observations of delayed disease progression in individuals heterozygous for the Δ32 CCR5 deletion mutation.[40,41] Furthermore, its significant distribution to vaginal and rectal tissue, as well as semen has garnered MVC interest in pre-exposure prophylaxis (PrEP).[42,43] MVC is only effective against R5 tropic HIV-1 stains, thus requires a tropism test before use and is currently recommended for used in treatment experienced patients that have experienced previous virologic failure.

1.4 Clinical History of LA Therapy

LA dosage forms are available for indications ranging from contraceptives to antipsychotics.[44-46] In particular, LA contraceptives are available as implants or injectable formulations. For example, Depo-Provera, comprised of medroxyprogesterone acetate microcrystals, requires quarterly injections eliminating the need for daily pills.[46] Furthermore, reversible methods of LA contraception, such as intrauterine devices (IUDs) and subdermal hormonal implants continue to permeate the market.[47] Specifically, levonorgestrel-releasing IUDs such as Liletta and Mirena are effective for 3 and 5 years respectively. Furthermore, subdermal implants, such as the esonogestrel-

releasing Nexplanon is highly efficient during its 3-year effectiveness window. In addition, LA antipsychotics utilize multiple dosage forms such as oil depots, aqueous suspensions of prodrugs or hydrophobic salts, and/or polymeric microparticles to increase patient compliance and reduce adverse neurological side effects.[45] Recently, Invega Trinza, a microsuspension of the prodrug paliperidone palmitate received approval for quarterly dosing for the treatment of schizophrenia.[48] Therefore, clinically approved LA dosage forms for birth control and schizophrenia provide important examples of extended release delivery; technologies which will need optimization to meet the unique needs and requirements of HIV-1 treatment.

1.5 LA HIV-1 Therapy

ART compounds were originally synthesized and designed for oral delivery. Therefore drug physicochemical properties were tailored to achieve high bioavailability by providing stability in the gastrointestinal tract (GI), adequate absorption into the blood stream, and limited first-pass metabolism.[49] Thus a balance of low molecular weight, suitable aqueous solubility, moderate lipophilicity, and low hydrogen bonding capacity define solid drug candidates for oral delivery. Therefore, translating existing ARV compounds into LA therapeutics requires careful considerations and ultimately determines their formulations design (Implant; Injectable formulation; Prodrug).

1.6 LA Parenterals (LAP)

Translating LA injectable formulations used for antipsychotic and/or contraceptives into LA treatments for HIV-1 requires careful examination of drug solubility, potency, and half-life. For example, antipsychotic paliperidone and contraceptive medroxyprogesterone acetate require just 3-12 and 2.5-10 mg daily oral dosages respectively.[39] In comparison, some ARVs such as 3TC (300 mg/day), EFV

(600 mg/day) and RAL (800 mg/day) require significantly higher doses.[50] Therefore, in order to facilitate formulation, limit injection volumes, and deliver efficacious concentrations of drug, injectable HIV-1 treatments have focused on the development on hydrophobic compounds such as CAB and RPV that require daily oral doses of (10-60 mg) and 25 mg respectively.

RPV-LA is an investigational LA formulation under development by Janssen. Early proof of concept work focused on optimizing drug form (RPV-free base or RPV-HCL), nanoparticle size (200, 400, 800 nm), surfactant selection (P338, d-alpha-tocopheryl polyethylene glycol 100 succinate; TPGS), and route of administration (IM; subcutaneous; SC)[37] Dose response (300, 600, 1200 mg) pharmacokinetic studies in HIV-1 seronegative patients established RPV-LA as well tolerated and able to produce clinically relevant RPV plasma concentration for an extended period of time.[38]

Cabotegravir, an investigational integrase inhibitor and structural analogue of DTG is currently in clinical development as both an oral therapy and LA injectable formulation (CAB-LA).[51] CAB-LA is produced by wet-milling using polysorbate 20 and polyethylene glycol 3350 as stabilizers to generate 200 nm nanocrystals.[51] Phase I clinical trials demonstrated CAB-LA was well tolerated and provided plasma CAB concentrations above its IC_{90} for 16 weeks in healthy patients, thereby offering proof of concept for its potential application in HIV-1 treatment.[52] Furthermore, rhesus macaque studies determined the effectiveness of CAB-LA protection against viral challenge though multiple routes of infection.[53-55]

Ultimately, proof-of-concept studies with RPV-LA and CAB-LA culminated in their combination to determine efficacy in multiple clinical trials for HIV-1 maintenance therapy. Specifically, the LA Antiretroviral Treatment Enabling (LATTE-2) trial demonstrated CAB-LA (400; 600 mg) and RPV-LA (600; 900 mg) in combination every 4 or 8 weeks was non-inferior to daily oral therapy (CAB-ABC-3TC; 30-600-300

mg)(Figure 1.5.2).[28] These results were reinforced by successful phase 3 clinical trials (ATLAS and FLAIR) and positive patient feedback, thereby generating strong support for the future of LA ARVs.[56,57]

1.7 HIV-1 LA Implantable Formulations and Technologies

Implantable technologies provide sustained drug concentrations for an extended period of time and also provide a platform to integrate more hydrophilic ARVs. In addition, sub-Saharan Africa, which bears the largest global burden of HIV-1, has observed increased use of implants for contraception, thereby setting precedent for their use in a resource-limited setting.[58,59]

To this end, a sustained release implantable formulation of TAF was developed using a PVA-coated silicone cylinder loaded with TAF powder.[60] In particular, the TAF implant delivered detectable concentrations of TAF, TFV, as well as, the pharmacologically active TFV-diphosphate (TFV-DP) over a period of 40 days in beagle dogs.[60] Moreover, TFV-DP was detected at concentrations 30 times higher than observed in HIV-1 human PrEP studies, lending credence to its importance as a continued research objective.[60]

Furthermore, biodegradable implants consisting of poly(lactic-co-glycolic acid) (PLGA), N-methyl-2-pyrrolidone (NMP), and integrase inhibitor dolutegravir generated detectable DTG concentrations 9 months after insertion.[61] Such implants require subcutaneous injection for insertion and are inspired by Eligard, which uses Atrigel technology and is commercially available to treat prostate cancer.[62] Biodegradable implants delivered by subcutaneous injection have substantial advantage of other implants, which require surgical insertion and removal. Therefore the report of a biodegradable implant capable supplying sustained ARV concentration has tremendous potential, especially in the context of HIV-1 PrEP.

MK-8591 is an investigational nucleoside reverse transcriptase translocation inhibitor (NRTTI) currently under development by Merck.[63] Research detailing MK-8591 incorporation into a LA implantable formulation consisting of biodegradable polymers polylactic acid (PLA), polycaprolactone (PCL), or polyethylene vinyl acetate (EVA) has recently been reported.[64] Specifically, when administered to rhesus macaques, MK-8591 PCL implants provided detectable drug concentrations up to 6 months.

Moreover, phase III clinical trials investigating the efficacy of dapivirine vaginal rings were recently reported.[65] Specifically, dapivirine rings administered monthly, generated a 27% reduction in HIV-1 incidence compared with placebo.[65] Interestingly, the efficacy of treatment differed amongst age groups where 65% efficacy was observed in patients over the age of 25, but just 10% in participants under 25.[65] These results underscore the importance of adherence for PrEP efficacy, even in the context of sustained release dosage forms.

1.8 HIV-1 LASER-ART Formulations

In short order, HIV-1 infected patients will have options that rest outside standard oral therapy. Current iterations of LA injectable formulations and/or implants are limited by large injection volumes, injection site reactions (ISR), dosing frequency, and lack of tissue reservoir penetrance. To address these issues and generate the next generation of LA HIV therapeutics, long-acting slow effective release antiretroviral therapy (LASER-ART) was developed (Figure 1.5.3)[66,67]. Incorporating rationally designed hydrophobic and lipophilic prodrugs of existing ARVs into a LAP; a number of limitations can be subverted or improved.

Briefly, prodrugs are considered bioreversible chemical modifications of an active compound.[68] Therefore, chemical or enzymatic cleavage is required *in vivo* to yield the active molecule. Reversible chemical modification provides flexibility to add chemical

moieties specifically designed to alter a compounds hydrophobicity, lipophilicity, and/or membrane penetrance without negatively effecting the drug's action. Thus, in the context of HIV-1, prodrugs can be designed to improve upon suboptimal characteristics of existing ARVs, thereby facilitating their transition into LA dosage forms. Prodrug synthesis is dependent on the presence of reactive functional groups such as hydroxyl, amine, carboxylic, or phosphate moieties, which can generate a range of bonds including ester, amide, carbamates, ethers, and phosphates.[69] Furthermore, bond stability prominently affects systemic release kinetics; therefore, the design of prodrugs requires knowledge of the biological system and desired pharmacological outcome. Specifically in the context of LA HIV-1 therapeutics, tailoring the release kinetics to generate efficacious plasma concentrations and sufficient tissue penetrance is essential.

To this end, long acting slow effective release ART (LASER ART) preparations of integrase inhibitors DTG and CAB were recently reported.[70,71] Specifically, a myristoyl ester prodrug of DTG (MDTG) was synthesized and subsequently nanoformulated (NMDTG) using poloxamer 407 (P407).[70] Murine pharmacokinetic studies generated DTG plasma concentrations above the PA-IC$_{90}$ for 8 weeks after a single IM injection. Additionally, DTG concentrations in tissue (spleen, lymph node, GALT, liver, lung, kidney) were significantly higher in groups treated with NMDTG compared to those treated with nanoformulated DTG (NDTG). Furthermore, NMDTG administered in rhesus macaques observed DTG concentrations above the PA-IC$_{90}$ for 35 days following a single 45 mg/kg IM injection.[72] Of utmost importance, treatment with NMDTG generated significant protection against HIV-1$_{ADA}$ in a CD34+ humanized mouse model, underscoring the long-term efficacy of LASER-ART.

Furthermore, a myristoylated prodrug of CAB (MCAB) afforded further proof of concept LASER-ART can improve the apparent half-life and tissue distributions better than LA formulations of unmodified ARVs. Specifically, nanoformulated MCAB (NMCAB)

was compared against CAB-LA, which is currently in phase III clinical trials.[71] NMCAB generated a 4x increase in terminal CAB apparent half-life compared with CAB-LA in *BALB/cJ* mice. PK improvements were paired with significant biodistribution enhancements. Furthermore, rhesus macaques administered with NMCAB (45 mg/kg-CAB eq.) displayed CAB plasma concentrations above the PA-IC_{90} for 12 weeks.[73]

LA injectable formulations require hydrophobic ARVs, which are incorporated into solid drug nanosuspensions. Therefore, numerous compounds, especially NRTIs have not been incorporated into this subset of LA therapeutics. Applying the conceptual framework of LASER ART, in which hydrophobic prodrugs are synthesized and subsequently nanoformulated, NRTIs were successfully included in the LA injectable paradigm. Proof of concept studies involving myristoylated 3TC and ABC laid the groundwork for what could be done with NRTIs in this arena.[74,75] Building off this work and the concept of ProTide technology, a series of abacavir (ABC) prodrugs specifically designed to mask parent drug monophosphates with cleavable hydrophobic groups were synthesized.[76] Furthermore, nanoformulations of these novel ABC prodrugs produced long-acting cellular depots of active carbovir-tripohsphate (CBV-TP).

Together these results suggest altering the physicochemical properties of ARVs by generating hydrophobic prodrugs can confer benefit in terms of PK and BD, as well as incorporating a broader range of ARVs into the LA injectable paradigm.

1.9 Figures
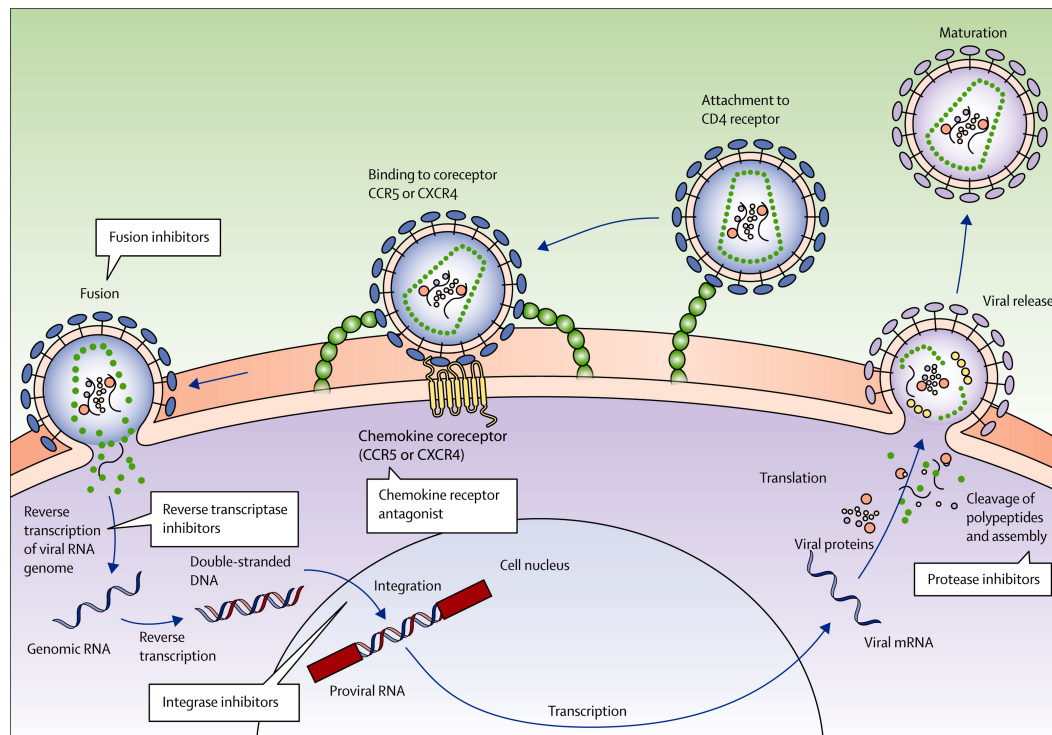
Figure 1.9.1 HIV-1 Life cycle and ART targets.[12]

HIV-1 must attach to the CD4 receptor and subsequently a coreceptor (CCR5 or CXCR4) to gain cellular entry. Entry inhibitors such as MVC bind to CCR5 and prevent HIV-1 cellular entry. Furthermore, membrane fusion facilitated by HIV-1gp41 merges the viral and host cell membranes exposing viral RNA into the cytoplasm. Membrane fusion is disrupted by the fusion inhibitor Enfuvirtide. Reverse transcriptase converts single stranded RNA into double stranded DNA. This stage of the viral life cycle is inhibited by NRTIs, such as FTC, and NNRTIs, such as RPV. Viral DNA integration into the host cell genome is inhibited by integrase inhibitors (INI, DTG). Moreover, protease inhibitors prevent new virions from becoming mature and infectious by inhibiting the actions of protease (PI; Darunavir; DRV). Figure adapted from Maartens et al., HIV infection: epidemiology, pathogenesis, treatment, and prevention. *Lancet,* 2014.
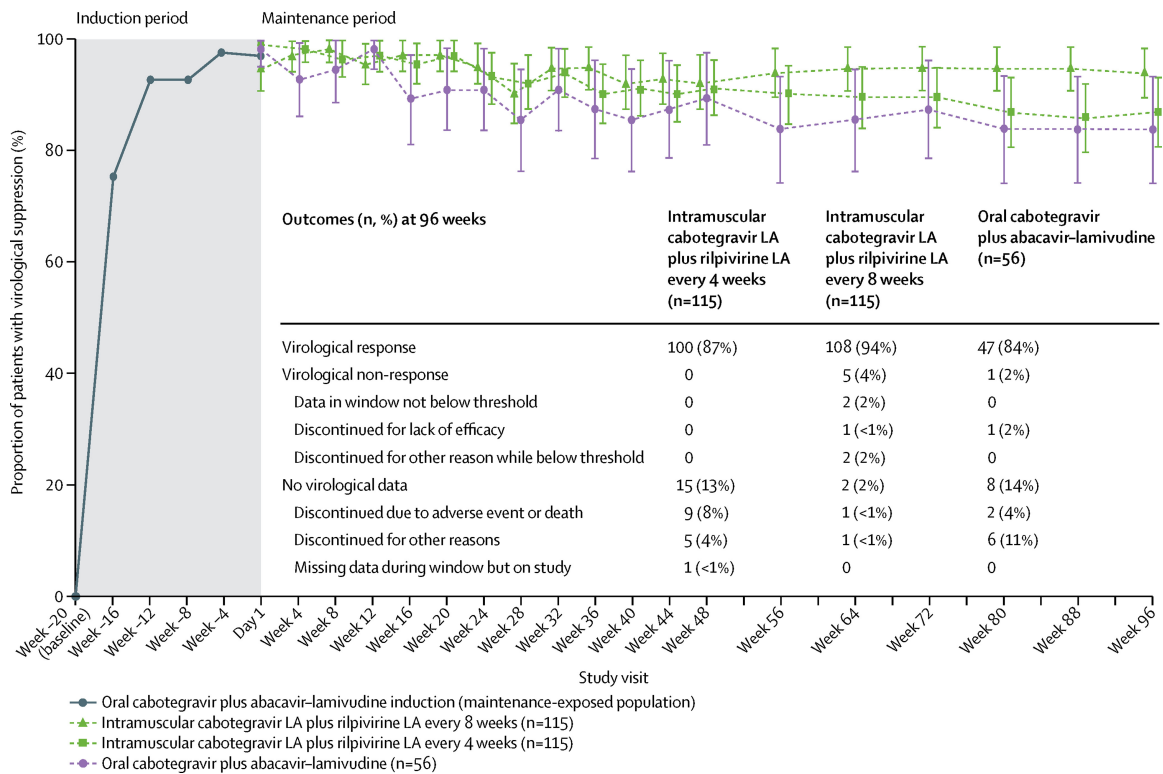
Figure 1.9.2 LA HIV-1 maintenance therapy (LATTE-2).[28]

Following an oral induction period to achieve viral suppression, patients were administered CAB LA + RPV LA every 4 or 8 weeks or continued oral therapy (CAB,ABC,3TC). LA therapy demonstrated non-inferiority compared to oral therapy in this study. Figure adapted from Margolis et al., Long-acting intramuscular cabotegravir and rilpivirine in adults with HIV-1 infection (LATTE-2): 96-week results of a randomized, open-label, phase 2b, non-inferiority trial. *Lancet*, 2017
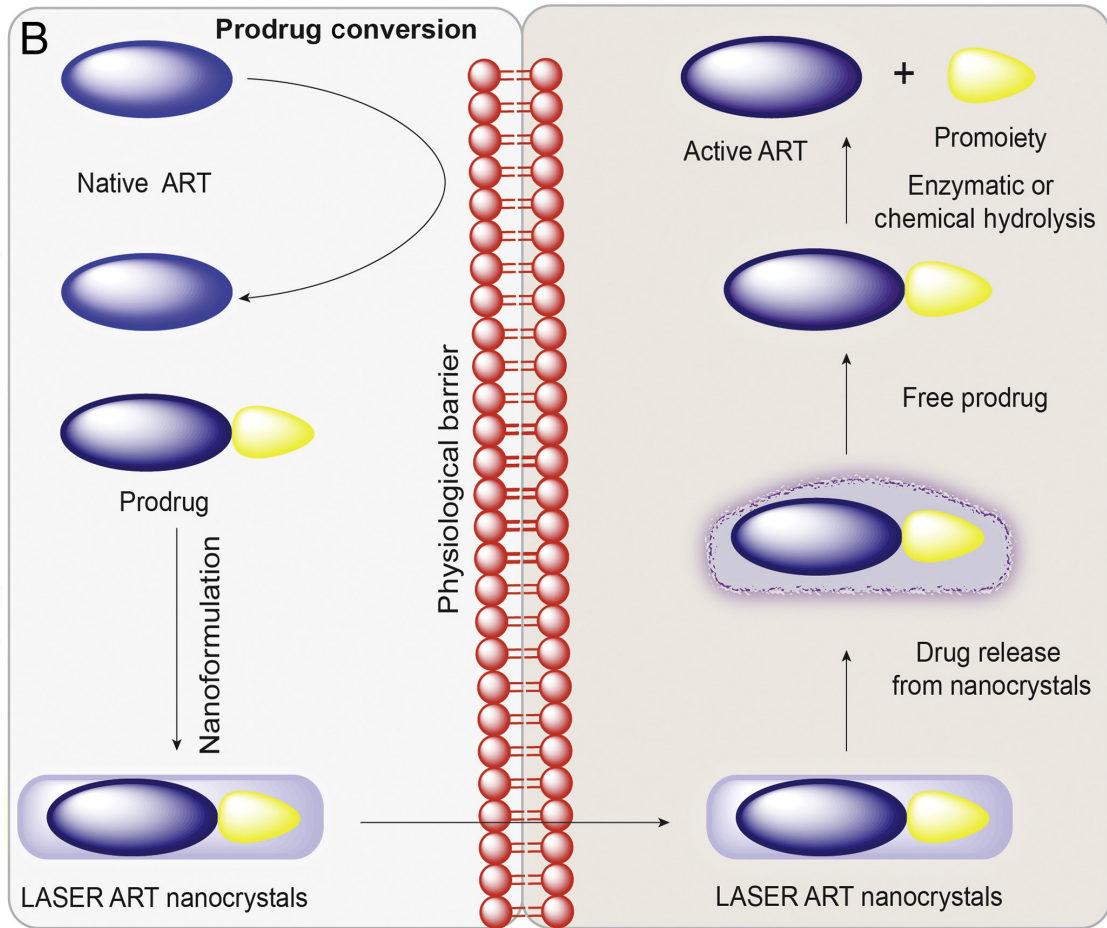
Figure 1.9.3 LASER ART[66]

The apparent half-life of ART compounds can be potentially increased by prodrug modification and subsequent nanocrystal manufacture. Together, increased cellular uptake, storage, and slow intracellular release confer advantages over conventional LA ART. Figure adapted from Gendelman et al., The Promise of Long-Acting Antiretroviral Therapies: From Need to Manufacture, *Trends in Microbiology*, 2019.

CHAPTER 2

SYNTHESIS AND CHARACTERIZATION OF AN RPV PRODRUG LIBRARY

2.1 Abstract

RPV, a NNRTI, has been developed as a LAP (RPV LA). Combinations of RPV LA and CAB LA administered to HIV-1 infected individuals restrict HIV-1 replication and restores immune function. LA injectable formulations simplify treatment and prevention regimens. Notwithstanding, targeting HIV-1 cellular and anatomical reservoirs, and limiting injection volumes and dosage frequency remain ongoing obstacles for treatment optimization. In attempts to improve upon existing drug formulations, our laboratories developed LASER-ART, defined as synthesized prodrugs encased in nanocrystals with the intent to further extend drug half-life and improve viral reservoir delivery. To this end, an RPV prodrug library was synthesized and tested for its antiviral activity, nanoformulation capacity, as well as pharmacokinetics (PK) and biodistribution (BD) to ultimately generate a lead prodrug candidate for more extensive studies.

2.2 Introduction

ART has revolutionized the treatment of HIV-1 infected people from what was certain death to a life free of most co-morbid conditions. Nonetheless, strict adherence to daily drug regimens is required to suppress viral replication and maintain CD4+ T cell numbers and functional immunity. Nevertheless, a life span approaching that of the general population has been achieved[2,3]. The requirement for lifelong daily drug administration may soon be supplanted by LA dosage forms of ARVs such as implants

and injectable formulations[77,78]. LA formulations of common drugs have previously found utility as contraceptives and antipsychotics and parallel directives are now being considered for HIV-1 prevention and maintenance.[79-81] As of now, HIV-1 LA agents have focused on parenteral cabotegravir (CAB-LA) and rilpivirine (RPV-LA) [52,82,83]. Early success in the First LA Injectable Regimen (FLAIR) phase 3 trial examining monthly intramuscular (IM) injections found combination LA ART non-inferior to standard oral DTG, ABC, and 3TC.[56] These results support prior LATTE and ATLAS trials with positive patient feedback and support for future LA ARVs.[28,56,57] Therefore, anticipating a paradigm shift towards LA medicines, innovative approaches to advance formulation design are essential to limit current dosage volumes, injection site reactions, together with optimal tissue penetrance and dosing frequency.[66] Alternative implantable devices also exhibit consistent and sustained drug release.[60,61,64,84] However, the latter approaches require more sophisticated insertion and removal procedures and do not affect ARV delivery to viral reservoirs. As an alternative our own laboratories LASER-ART utilizes ARV prodrug modifications to provide slow dissolution, penetrance of biological membranes, as well as sustained delivery of efficacious drug concentrations to both plasma and tissue reservoirs.[67] LASER ART has been developed across a broad spectrum of ARVs and represents an innovative approach to improving existing LA formulations.[70,71,76] Therefore, we aimed to synthesize a library of prodrugs for the non-nucleoside reverse transcriptase inhibitor (NNRTI) rilpivirine (RPV), with the objective of developing a LA formulation designed to improve tissue distribution and prolong exposure of clinically relevant RPV concentrations. To this end, we synthesized a group of N-acyloxyalkyl RPV prodrugs of varying carbon chain length. Furthermore, prodrugs were evaluated based on their antiviral activity, nanoformulation capacity, and pharmacokinetic and tissue distribution profile in *BALB/cJ* mice to select a lead compound (M3RPV) for more extensive studies.

2.3 Materials and Methods

2.3.1 Materials

RPV was purchased from LeapChem (Hangzhou, China). Dichloromethane (DCM), tetrahydrofuran (THF), *N,N*-dimethylformamide (DMF), sodium(trimethylsilyl) amide (NaHMDS;1 M in THF), hexanes, ethyl acetate, dimethyl sulfoxide (DMSO), anhydrous pyridine, chloromethyl chlorosulfate, tetrabutylammonium hydrogen sulfate, potassium carbonate, heptanoic acid, lauroyl chloride, myristoyl chloride, stearic acid, zinc chloride ($ZnCl_2$), sodium iodide (NaI), deuterated chloroform, paraformaldehyde (PFA), and Pluronic F127 (P407) was purchased from Sigma-Aldrich (St. Louis, MO). Pluronic F108 (P338) was purchased from BASF (Florham Park, NJ). Acetonitrile (ACN), methanol (MeOH), cell-culture grade water (endotoxin-free), and KH_2PO_4 were purchased from Fisher Scientific (Hampton, NH). Flash column chromatography was performed on 32-63 μm flash silica gels, while thin layer chromatography utilized pre-coated silica plates (250 μm, F-254) both from SiliCycle Inc. (Quebec, Canada).

2.3.2 Synthesis of chloromethyl heptanoate; chloromethyl stearate

Heptanoic acid (or stearic acid) (1.0 eq.) was added to a mixture of K_2CO_3 (4.0 eq.), tetrabutylammonium hydrogen sulfate (0.1 eq.), and H_2O:DCM (1:1) at 0°C under argon atmosphere. Reaction mixture was warmed to RT for 10 min. Next, additional ice was added to cool the reaction and a solution of chloromethyl chlorosulfate (dissolved in DCM) was added dropwise and allowed to react overnight. After 16+ hours, the reaction was diluted with water and extracted with DCM (3x). Combined organic extracts were washed with brine and subsequently dried with sodium sulfate. Extracted samples were concentrated using a rotary evaporator to yield an oil. Silica column chromatography purification using 9:1 hexanes: ethyl acetate yielded a distinct band not visible by UV.

The purified compound was visualized by thin layer chromatography (TLC) staining with potassium permanganate. Furthermore, isolated samples was collected, concentrated and analyzed by ^{1}H NMR.

2.3.3 Synthesis of chloromethyl tetradecanoate; chloromethyl dodecanoate

Myristoyl chloride (or Lauroyl chloride) was reacted with 1.0 eq. paraformaldehyde (PFA) and 0.025 eq. zinc chloride ($ZnCl_2$) under reflux conditions for a minimum of 16 hours. The reaction mixture was cooled to RT and partitioned between dichloromethane (DCM) and saturated aqueous sodium bicarbonate in a separatory funnel. The aqueous layer was back-extracted twice with DCM. Organic extracts were combined, washed with brine and dried from sodium sulfate. The solvents were evaporated on a rotary evaporator followed by isolation of the desired compound using silica column chromatography eluting with a mobile phase of 9:1 hexanes-ethyl acetate and stained with potassium permanganate. ^{1}H NMR characterized the isolated product to confirm appropriate chemical structure.

2.3.4 Synthesis of iodomethyl heptanoate; dodecanoate; tetradecanoate; stearate

Chloromethyl tetradecanoate (heptanoate; dodecanoate; stearate; 1 eq.) and sodium iodide (NaI, 2.5 eq.) were dissolved in a 2:1 mixture of ACN/DCM under an argon atmosphere. The reaction mixture proceeded for a minimum of 90 hours at RT under protection from light. Upon completion, the mixture was concentrated and partitioned between DCM and water. The aqueous layer was further extracted with DCM followed by sequential washing of the combined organic extracts with saturated sodium bicarbonate and brine. The sample solution was then dried from sodium sulfate, concentrated and purified by silica column chromatography eluting with 9:1 hexanes-

ethyl acetate. Isolated compounds were analyzed by ^{1}H NMR to confirm their chemical structure.

2.3.5 M1RPV, M2RPV, M3RPV, M4RPV synthesis and characterization

Rilpivirine hydrochloride (RPV HCl) was suspended in a mixture (1:1) of anhydrous tetrahydrofuran (THF) and dimethylformamide (DMF) under an argon atmosphere. The reaction flask was then cooled to -46°C (ACN; dry ice) followed by addition of 3 eq. of sodium bis(trimethylsilyl)amide (NaHMDS; 1M in THF) base and allowed to react for 30 min. to deprotonate the secondary amine in RPV. A solution of iodomethyl tetradecanoate (or heptanoate; dodecanoate; stearate) (1.5 eq.) in anhydrous THF was added dropwise, followed by gradual warming of the reaction mixture to room temperature and allowed to proceed for 48 hours. The mixture was then cooled to -78°C (Acetone; Dry Ice), quenched using MeOH and concentrated to remove solvents. The concentrated sample was purified by silica column chromatography eluting with 1:1 hexanes-ethyl acetate to isolate M1RPV, M2RPV, M3RPV, or M4RPV. M3RPV was precipitated by hexanes for final product. Nuclear magnetic resonance (NMR) and Fourier-transform infrared (FTIR) spectroscopy, as well as positive electrospray ionization mass spectrometry (ESI-MS) were used to characterize each prodrug. Proton (^{1}H)- and carbon (^{13}C)- NMR spectra were recorded on a Varian Unity/Inova-500 NB (500 MHz; Varian Medical Systems Inc., Palo Alto, CA). FTIR was performed on a PerkinElmer universal attenuated total reflectance (UATR) Spectrum Two (Waltham, MA). **M1RPV**: ^{1}H NMR (500 MHz, CDCl$_3$): 7.98 (d, J = 5.8 Hz, 1H), 7.80 (d, J = 8.5 Hz, 2H), 7.60 (d, J = 8.6 Hz, 2H), 7.23-7.34 (m, 4H), 5.88 (app. s, 2H), 5.51 (d, J = 5.8 Hz, 1H), 2.33 (t, J = 7.4 Hz, 2H), 2.21 (s, 6H), 1.59 (p, J = 7.3 Hz, 6H), 1.18-1.34 (m, 6H), 0.84 (t, J = 6.5 Hz, 3H). ^{13}C NMR (125 MHz, CDCl$_3$): δ 173.5, 161.5, 158.9, 157.4, 149.4, 143.9, 141.2, 138.2, 133.8, 133.2, 128.2, 119.4, 118.4, 117.8, 104.4, 97.6,

97.2, 73.0, 34.7, 34.3, 31.3, 28.7, 25.0, 24.7, 22.4, 18.1, 13.9. MS-ES+ (m/z): calcd. for $C_{30}H_{32}N_6O_2$, 508.26 (100%), 509.26 (32.4%), 510.27 (2.7%); found, 509.2 [M+H$^+$].

M2RPV: ^{1}H NMR (500 MHz, CDCl$_3$): 7.97 (d, J = 5.8 Hz, 1H), 7.81 (d, J = 8.6 Hz, 2H), 7.60 (d, J = 8.6 Hz, 2H), 7.24-7.32 (m, 4H), 5.58-6.0 (m, 2H), 5.50 (d, J = 5.8 Hz, 1H), 2.32 (t, J = 7.6 Hz, 2H), 2.21 (s, 6H), 1.59 (p, J = 7.3 Hz, 6H), 1.18-1.35 (m, 16H), 0.87 (t, J = 6.9 Hz, 3H). ^{13}C NMR (125 MHz, CDCl$_3$): δ 173.5, 161.6, 158.9, 157.0, 149.4, 143.9, 141.2, 138.2, 133.9, 133.2, 128.2, 119.5, 118.5, 117.8, 104.4, 97.7, 97.1, 73.1, 34.3, 31.9, 29.6, 29.5, 29.4, 29.3, 29.2, 29.1, 25.1, 24.8, 22.7, 18.2, 14.1. MS-ES+ (m/z): calcd. for $C_{35}H_{42}N_6O_2$, 578.34 (100%), 579.34 (37.9%), 580.34 (7.0%); found, 579.4 [M+H$^+$]. **M3RPV**: ^{1}H NMR (500 MHz, CDCl$_3$): 7.98 (d, J = 5.4 Hz, 1H), 7.79 (d, J = 8.6 Hz, 2H), 7.60 (d, J = 8.3 Hz, 2H), 7.23-7.32 (m, 4H), 5.86-5.95 (m, 2H), 5.51 (d, J = 5.8 Hz, 1H), 2.33 (t, J = 7.2 Hz, 2H), 2.21 (s, 6H), 1.51-1.68 (m, 6H), 1.17-1.32 (m, 17H), 0.87 (t, J = 6.9 Hz, 3H). ^{13}C NMR (125 MHz, CDCl$_3$): δ 173.5, 161.5, 158.9, 157.7, 149.4, 143.9, 141.2, 138.2, 133.8, 133.2, 128.2, 119.4, 118.3, 117.8, 104.4, 97.6, 97.3, 73.0, 34.3, 31.9, 29.6, 29.5, 29.4, 29.3, 29.2, 29.1, 24.8, 22.6, 18.2, 14.1. MS-ES+ (m/z): calcd. for $C_{37}H_{46}N_6O_2$, 606.37 (100%), 607.37 (40.0%), 608.37 (7.8%); found, 607.2 [M+H$^+$]. **M4RPV**: ^{1}H NMR (500 MHz, CDCl$_3$): 7.97 (d, J = 5.8 Hz, 1H), 7.81 (d, J = 8.5 Hz, 2H), 7.59 (d, J = 8.5 Hz, 2H), 7.23-7.32 (m, 4H), 5.57-6.0 (m, 2H), 5.50 (d, J = 5.8 Hz, 1H), 2.33 (t, J = 7.5 Hz, 2H), 2.21 (s, 6H), 1.60 (p, J = 7.1 Hz, 2H), 1.18-1.32 (m, 27H), 0.88 (t, J = 6.9 Hz, 3H). ^{13}C NMR (125 MHz, CDCl$_3$): δ 173.5, 161.5, 158.9, 157.6, 149.4, 143.8, 141.2, 138.2, 133.8, 133.2, 128.2, 119.4, 118.3, 117.8, 104.4, 97.6, 97.3, 73.0, 34.3, 31.9, 29.7, 29.6, 29.5, 29.4, 29.3, 29.2, 29.1, 24.8, 22.7, 18.2, 14.1. MS-ES+ (m/z): calcd. for $C_{41}H_{54}N_6O_2$, 662.43 (100%), 663.43 (44.3%), 664.44 (9.6%); found, 663.2 [M+H$^+$].

2.3.6 Analysis of RPV prodrugs (M1-M4RPV) by UPLC-UV/Vis

Analytical methods for drug quantitation were developed on UPLC-UV/Vis for RPV and each synthesized prodrug. Specifically, a Waters ACQUITY ultra performance liquid chromatography (UPLC) H-Class system with TUV detector and Empower 3 software (Milford, MA) was used for quantification. RPV and all prodrugs (M1-M4RPV) were separated on a Phenomenex Kinetex 5 μm C18 column (150 x 4.6 mm) (Torrance, CA) with a flow rate of 1.0 mL/min. All compounds were quantified comparing peak areas to known standards (0.048-50 μg/mL) generating a linear standard curve.

2.3.7 Macrophage half-maximum effective concentration (EC$_{50}$) assays

Studies to determine the EC$_{50}$ of RPV and RPV prodrugs (M1RPV, M2RPV, M3RPV, and M4RPV) in MDMs were performed in 96-well plates at a density of 0.15 x 10^6 cells/well. Specifically, cells were treated with 0.1-1000 nM (RPV or M1-M4RPV) for 2 hours, followed by HIV-1$_{ADA}$ challenge at a multiplicity of infection (MOI) of 0.1 for 4 hours. Following viral challenge, cells were washed with PBS, and given fresh drug (0.1-1000 nM) containing media. Subsequently, cell supernatants were collected 10 days later and assayed for RT activity.[85,86]

2.3.7 Manufacture of nanoformulated RPV and RPV prodrugs

Nanoformulations of RPV and RPV prodrugs (M1-M4RPV) were manufactured using an Avestin EmulsiFlex-C3 high-pressure homogenizer (Ottawa, ON, Canada). NRPV was prepared to best replicate Janssen's RPV-LA currently in clinical trials.[37] Therefore, NRPV was prepared by dispersing P338 (0.5% w/v) in water and subsequently mixing RPV-free base (1% w/v) overnight at RT. Next, the pre-suspension was homogenized (20,000 psi) to generate homogeneous nanocrystals. Nanoformulation physicochemical properties were evaluated by dynamic light

scattering (DLS, Malvern Nano-ZS Worcestershire, UK) for size (nm), polydispersity index (PDI), and zeta potential (mV). Following homogenization, formulations were centrifuged (5,000 g for 5 min.) at which point the pellet was saved and the supernatant underwent a second round of centrifugation (10,000 g for 10 min). Resultant pellets were resuspended with desired volume of water and vortexed for 5 min or until a uniform suspension was observed. Next, to remove aggregated particles, formulations were centrifuged (200 g for 3 min) and supernatants were collected and analyzed. Nanoformulation of RPV prodrugs (M1-M4RPV) followed a similar protocol with subtle differences. Specifically, P407 (0.5 % w/v) was used a surface stabilizer for NM1RPV, NM2RPV, and NM3RPV. Additionally, NM4RPV required the use of P338 (0.5% w/v) and Tween 80 (0.5% v/v) during its manufacture. All RPV prodrugs utilized 1% (w/v) drug concentrations for initial pre-suspensions.

2.3.8 Murine PK and BD studies

Male *BALB/cJ* mice (6-8 weeks, Jackson Labs, Bar Harbor, ME) were treated with 45 mg/kg RPV eq. of NRPV, NM1RPV, NM2RPV, NM3RPV, or NM4RPV by intramuscular (IM; caudal thigh muscle) injection. Blood samples were collected into heparinized tubes by cheek puncture 24 hours after injection, followed by subsequent weekly collections. Isolated blood (25 µL) was immediately diluted in 1 mL of ACN and stored at -80°C until drug analysis. Remaining blood was centrifuged (2,000 g for 5 min) and plasma supernatants were collected and stored at -80°C. For tissue collection, animals were humanly euthanized with isoflurane, followed by cervical dislocation 4 and 8 weeks after drug treatment. Spleen, lymph nodes, liver, lungs, kidneys, gut, and brain were collected to assay drug content.

2.3.9 RPV plasma and tissue drug analysis by UPLC-MS/MS

Drug concentrations in plasma and tissue were determined by UPLC-MS/MS using a Waters ACQUITY UPLC-Xevo TQ-S micro mass spectrometry system (Milford, MA). RPV was separated using an AQUITY UPLC-BEH shield RP18 column (1.7 um, 2.1 mm x 100 mm) using a 7 min gradient mobile phase consisting of A (7.5 mM ammonium bicarbonate in Optima-grade water adjusted to pH 7 using acetic acid) and B (100% Optima-grade MeOH) at a flow rate of 0.25 mL/min. 70% mobile phase B remained for 4.75 min, followed by an increase to 95% B in 0.25 min and held constant for 0.75 min. Furthermore, mobile phase B was reset to 70% in 0.25 min and the column equilibrated for 1.0 min before the next injection. A cone voltage of 92 volts and collision energy of 56 volts was used to detect RPV. Multiple reaction monitoring (MRM) transitions used for RPV, Indinavir (IDV) and Lopinavir (LPV) were 367.032 > 127.859, 614.14 > 97.023, and 629.177 > 155.031 m/z respectively.

Collected plasma was stored at -80°C until processing and analysis. Samples were processed by adding 1 mL of ice-cold ACN to 25 µL of plasma in a 1.7 mL eppendorf tube. Subsequently, 10 µL of IS (IDV 250 ng/mL; LPV 500 ng/mL; final concentrations of 25 ng/mL IDV + 50 ng/mL LPV) and 10 µL of 50% MeOH was added to each tube and were vortexed for 3 min. Next, samples were centrifuged (17,000 *g* for 10 min) at 4°C and 1 mL of the supernatant was pipetted into a 2 mL tube. Furthermore, samples were dried under vacuum using a Thermo Scientific Savant SPD 1010 Speedvac Concentrator (Waltham, MA) with no temperature. Resultant samples were reconstituted in 100 µL of 50% MeOH and vortexed for 3 min, followed centrifugation (17,000 *g* for 10 min). Subsequently, 50-60 µL of supernatant were loaded onto a 96-well plate and used for UPLC-MS/MS analysis. Calibrations standards were prepared in a congruent fashion in which blank plasma was processed with IS and spiking solutions (2, 5, 10, 20, 50, 100, 200, 500, 1000, 2000, 5000, 8000, 10000 ng/mL) containing RPV

to generate standards with final analyte concentrations of 0.2, 0.5, 1, 2, 5, 10, 20, 50, 100, 200, 500, 800, 1000 ng/mL respectively.

Collected tissue was weighed (20-200 mg) and homogenized in 90% MeOH (5-20x) using a Qiagen TissueLyser II (Hilden, Germany). Next, 100 µL of homogenate is spiked with 280 µL of MeOH and 10 µL IS (mixture of 200 ng/ml MDTG, 200 ng/mL SDRV, IDV 250 ng/mL, LPV 500 ng/mL, DTG-d3 2000 ng/mL, 80 ng/mL Lamivudine-$^{15}N_2$-^{13}C, 40 ng/mL Abacavir-d4). Samples were vortexed for 30 seconds, settled for 5 min, and centrifuged (16,000 g for 15 min). For RPV analysis, 60 µL of supernatant was mixed with 40 µL of H2O and plated UPLC-MS/MS analysis. Calibration standards utilized a similar protocol using blank tissue homogenates and spiking solutions containing RPV at final analyte concentrations of 0.1, 0.2, 0.5, 1, 2, 5, 10, 20, 50, 100, 200, 500 ng/mL.

2.3.10 Statistics

In-vivo study results were expressed as mean ± SEM with a minimum of 4 biological replicates. GraphPad Prism 7.0 software (La Jolla, CA) was used for all statistical analysis. Specifically, comparisons between two groups utilized student's *t* test (two-tailed). Significant differences were denoted as follows: (* $P < 0.05$, ** $P < 0.01$, *** $P < 0.001$, **** $P < 0.0001$).

2.4 Results

2.4.1 M1RPV synthesis and characterization

M1RPV was synthesized by attaching a heptanoic acid moiety to RPV using a methylene ester linkage (Figure 2.6.1). ^1H NMR confirmed the successful synthesis of M1RPV (Figure 2.6.2). Specifically, signals between 1.18-1.34 ppm represent the

repeating (R-C**H₂**-R) protons, while protons of the methylene ester can be identified at 5.88 ppm. Furthermore, Cα and terminal methyl protons are observed at 2.33 and 0.84 ppm respectively. ^{13}C NMR confirmed the presence of carbon atoms of the attached heptanoic acid linkage with the appearance of multiples signals between 22.4 and 34.3 ppm. FTIR was used to further characterize the structure of M1RPV (Figure 2.6.2). Specifically, M1RPV generated absorption bands at 1730, as well and (2864,2928,2954 cm^{-1}), representing the carbonyl and alkane stretches of the heptanoic group respectively. To characterize and quantify M1RPV, an UPLC-UV/Vis method was developed (Figure 2.6.3). Specifically, using a mobile phase of 70% ACN and 30% H_2O, a flow rate of 1.0 mL/min, and a detection wavelength of 230 nm, M1RPV was eluted at 7.72 minutes. A linear standard curve covering concentrations between 0.048-50 µg/mL was used for quantitation and analysis of future studies.

2.4.2 M2RPV synthesis and characterization

To generate M2RPV, RPV was modified with a 12-carbon fatty acid (Lauric acid) via a methylene ester linkage (Figure 2.6.1). To confirm successful synthesis, ^{1}H NMR was performed (Figure 2.6.4). Specifically, signals at 0.84 and 2.32 ppm correspond to terminal methyl group and Cα protons respectively. Furthermore, multiplet signals between 1.18-1.35, as well as 5.58-6.0 represent (R-C**H₂**-R) and methylene ester protons respectively. In addition, ^{13}C NMR confirmed the presence of the aliphatic carbon atoms of the modifying lauric acid chain with signal between 22.7 and 34.3 ppm. Finally, FTIR further characterized the structure of M2RPV by revealing absorption bands at 1734 and (2854,2924 cm^{-1}) representing the lauric carbonyl and alkane stretches respectively (Figure 2.6.4). An UPLC-UV/Vis method for M2RPV was developed using 90% ACN and 10% H_2O as a mobile phase (Figure 2.6.5). Utilizing a flow rate of 1.0 mL/min and a detection wavelength of 230 nm, M2RPV was eluted at

5.61 minutes. Furthermore, a linear standard curve in the concentration range of 0.048-50 µg/mL was used for quantitation and analysis.

2.4.3 M3RPV synthesis and characterization

M3RPV, which contains a bioreversible myristic acid moiety, was synthesized with a chemical yield of 53% (Figure 2.6.1). The proton NMR spectrum of M3RPV exhibited multiplet signals in the range of 5.86-5.95 and 1.17-1.32 ppm corresponding to the methylene ester and repeating (R-C$\mathbf{H_2}$-R) protons of the modifying lipid chain (Figure 2.6.6). Additionally, chemical shifts at 0.87 and 2.33 ppm identified the terminal methyl group (C$\mathbf{H_3}$-R) and C_α protons of the fatty acid chain. The appearance of multiple signals between 22.6 and 34.3 ppm in the ^{13}C NMR spectrum of M3RPV confirmed the presence of carbon atoms of the conjugated aliphatic chain. FTIR analysis produced absorption bands at 1726 cm^{-1} corresponding to the carbonyl (C=O) within the myristoyl group (Figure 2.6.6). Absorption bands at 2856 and 2924 cm^{-1} represented alkane stretches along the aliphatic carbon chain. Nitrile stretches characteristic of the RPV backbone were observed at 2218 cm^{-1}. Detection by UPLC-UV/Vis was accomplished using a mobile phase of 90% ACN and 10% H_2O, wavelength of 230 nm, and a flow rate of 1.0 mL/min to elute M3RPV at 8.58 minutes (Figure 2.6.7). A linear standard curve between 0.048-50 µg/ml was used for quantitation and analysis.

2.4.4 M4RPV synthesis and characterization

RPV was modified with an activated methylene ester of stearic acid to generate M4RPV (Figure 2.6.1). To confirm successful synthesis, ^{1}H NMR was utilized (Figure 2.6.8). In particular, multiplet signals between 5.57-6.0 and 1.18-1.32 ppm represent the methylene ester and (R-C$\mathbf{H_2}$-R) protons respectively. Furthermore, signals at 2.33 and 0.88 ppm represent the Cα and terminal methyl group protons respectively. FTIR further

confirmed the structure of M4RPV (Figure 2.6.8). In addition to the characteristic nitrile absorption peak (2218 cm^{-1}), M4RPV generated bands at 1730, as well as (2864, 2928, 295 cm^{-1}) representing the carbonyl and alkane stretches of stearate respectively. UPLC-UV/Vis analysis of M4RPV required a mobile phase consisting of 95% ACN and 5% H$_2$O and a flow rate of 1.0 mL/min (Figure 2.6.9). In addition, M4RPV was eluted at 11.31 minutes using a detection wavelength of 230 nm. A linear standard curve between 0.048-50 μg/mL as used for quantitation and analysis.

2.4.5 Determination of half-maximum effective concentration of RPV prodrug

Antiretroviral activity of RPV and RPV prodrugs (M1RPV; M2RPV; M3RPV; M4RPV) were determined in human monocyte-derived macrophages (MDMs) Figure 2.6.10. RPV exhibited an EC$_{50}$ value of 1.91 nM congruent with its published low to sub-nanomolar in-vitro antiviral activities.[30,31] Furthermore, EC$_{50}$ values of RPV prodrugs decreased in conjunction with increased length of its carbon chain modification. Specifically, antiviral activities of 2.8, 3.1, 8.2, and 8.7 nM were observed for NM1RPV, NM2RPV, NM3PRV, and NM4RPV respectively.

2.4.6 Manufacture and characterization of NRPV and (NM1-M4RPV)

Nanoformulations were manufactured by a top-down approach utilizing high-pressure homogenization. NRPV was manufactured to replicate RPV-LA developed by Janssen.[37] Both NRPV and RPV-LA used P338 as a surface stabilizer, although the manufacturing technique differed, whereas NRPV used high-pressure homogenization, RPV-LA is manufactured by wet milling. Our laboratory generated NRPV exhibited an average size of 348 ± 51 nm compared with the reported 200 nm of RPV-LA. In terms of RPV prodrug formulations, NM1RPV (381 ± 119 nm, 0.3 ± .1, 32 ± 10 mV), NM2RPV (314 ± 59 nm, 0.3 ± .04, 15 ± 8 mV), NM3RPV (408 ± 41 nm, 0.2 ± .05, -17 ± 10 mV),

and NM4RPV (333 ± 32 nm, 0.3 ± .02, 19 ± 5 mV) all generated suitable nanoformulations for animal studies (Table 2.6.1).

2.4.7 Murine PK and BD

Nanoformulations of RPV and RPV prodrugs (NRPV; NM1RPV; NM2RPV; NM3RPV; NM4PRV) were administered to *BALB/cJ* mice to examine the effect of prodrug modification on plasma PK and tissue BD. Specifically, animals were administered a 45 mg/kg RPV eq. IM injection of NRPV or NM1RPV, NM2RPV, NM3RPV, or NM4RPV. Interestingly, 24 hours after injection, RPV concentrations in the plasma were dependent upon prodrug carbon chain length. (Figure 2.6.11) In particular, RPV plasma concentrations of 3370, 2714, 936.8, 111.2, and 133.52 ng/ml were observed for animals treated with NRPV, NM1RPV, NM2RPV, NM3RPV, and NM4RPV, respectively. Prodrug treatments of NM2RPV, NM3RPV, and NM4RPV all displayed shallower decay curves compared with NRPV and NM1RPV. Furthermore, 8 weeks after injection, RPV plasma concentrations in animals dosed with NM2RPV and NM4RPV were significantly higher than NRPV animals. Moreover, animals treated with select RPV prodrug formulations (NM2RPV, NM3RPV, NM4RPV) had significantly higher tissue concentrations compared with NRPV. Specifically, 8 weeks after injection, NM2RPV had significantly higher RPV concentrations in the liver and lymph nodes compared with NRPV. Additionally, treatment with NM3RPV provided RPV concentrations of 9.6, 39.3, and 100.6 ng/g in the liver, spleen, and lymph node respectively 8 weeks after injection. (Figure 2.6.12-14) Moreover, NM4RPV treated animals generated significantly higher RPV concentrations in the liver and lymph nodes compared with NRPV 8 weeks after injection.

2.5 Discussion

Our present study reports the synthesis of a diverse library of RPV prodrugs. Specifically, RPV was modified by aliphatic fatty acids of varying carbon chain lengths (7,12, 14, 18). Our investigation aimed to evaluate each prodrug on a number of metrics to ultimately determine a lead compound for more extensive study. To this end we evaluated the antiviral activity, nanoformulation capacity, and PK and BD characteristics of each prodrug. Synthesis of RPV prodrugs (M1-M4RPV) generated a library of compounds distinguished by their carbon chain length. We hypothesize that RPV was modified on its less hindered secondary amine. Our ^{1}H NMR and mass spectrometry analysis confirmed the synthesis of prodrugs containing a single fatty acid modification. The presence of structural isomers within our sample, in which modification occurred at the more hindered secondary amine, remains a possibility. Analytical techniques combining ion-mobility-mass spectrometry (IM-MS) and molecular modeling have the potential to differentiate between structural isomers if they display differences in their gas phase conformations.[87] Therefore, if it is deemed necessary, such a technology could be employed for a more precise chemical characterization.

Prodrug modification should be transient, ultimately releasing the active compound to exert its pharmacological purpose. To ensure modification of RPV with aliphatic carbon linkers did not completely abrogate antiviral activity we tested its ability to inhibit HIV-1$_{ADA}$ in MDMs. Interestingly, we observed a decrease in antiviral activity in the prodrugs modified with longer chain fatty acids. We hypothesize these observations are the result of slower bioconversion into RPV as the length of the fatty acid modification increases.[88] Therefore observed changes in EC$_{50}$ values could represent the presence of a mixture of intracellular species between the prodrug and active (RPV) form. Furthermore, with all prodrugs generating EC$_{50}$ values < 10 nM all compounds proceeded for further analysis.

PK and BD assessments in *BALB/cJ* mice revealed differences between NRPV and nanoformulated RPV prodrugs. Specifically, 24 hours after intramuscular injection, RPV plasma concentrations were higher for the shorter the fatty acid modifications (7, 12). This suggests differences in RPV bioconversion between the prodrugs based upon the fatty acid chain length.[88] Further studies testing the in vitro cleavage kinetics of each prodrug in mice plasma are required to confirm this hypothesis. Moreover, all prodrug formulations beside M1RPV produced shallower plasma decay kinetics compared with NRPV. Based on the observed differences in plasma kinetics, tissue samples (liver, lymph node, spleen) were processed to examine differences in distribution. Interestingly, significantly higher RPV concentrations were observed in the liver and lymph node for animals dosed with NM2RPV, NM3RPV, and NM4RPV when compared with NRPV. Furthermore, only NM3RPV generated significantly higher RPV concentrations in the spleen compared with NRPV.

Murine PK and BD provided evidence nanoformulated prodrugs of RPV may increase the apparent half-life and improved tissue distribution compared with NRPV. At the conclusion of our mouse study (8 weeks) NM2RPV and NM4RPV provided significantly higher RPV concentrations than NRPV, while NM3RPV trended towards significance. Furthermore, the lack of RPV present in the tissue of animals dosed with NRPV provided explanation for the continued decay of RPV plasma concentrations. In comparison, the significant RPV tissue distributions for NM2RPV, NM3RPV, and NM4RPV along with their shallow plasma decay curves generated our hypothesis that time points beyond 2 months could reveal significant differences in plasma and tissue RPV concentrations. Plasma concentrations of RPV were above the PA-IC$_{90}$ (12.5 ng/mL) for 35, 28, and 21 days following injection of NM2RPV, NM3RPV, and NM4RPV respectively. Our study used a dose of 45 mg/kg RPV eq. lower than clinical trials dosages (10 mg/kg) when converting for species differences between human and

mouse. Therefore future studies will deliver a more physiologically relevant dose of RPV to better evaluate the delivery of therapeutic plasma concentrations. Furthermore, follow-up studies should quantify prodrug concentrations in tissue to better understand the present data.

Our current study provided proof-of-concept that nanoformulated prodrugs of RPV could modify the tissue distribution and plasma decay kinetics compared with NRPV. To further optimize our approach we aimed to select a lead prodrug candidate from our research. In our mice studies, M1RPV exhibited precipitous decline of plasma RPV and was not detected in tissue, thus not recommended for further work. Nanoformulation of M2RPV (NM2RPV) yielded low drug concentrations and was difficult to resuspend after centrifugation. This required an injection in each mouse leg, not a single injection as with the other nanoformulations. While, M2RPV may have future application when using direct-manufacture formulation design, we decided to not move it forward to the next phase of our studies. M3RPV and M4RPV generated similar plasma RPV drug levels, but ultimately, NM3RPV generated significantly higher RPV levels in the spleen. Therefore, our future studies will center upon M3RPV and its potential as a long-acting HIV-1 therapeutic.

2.6 Figures
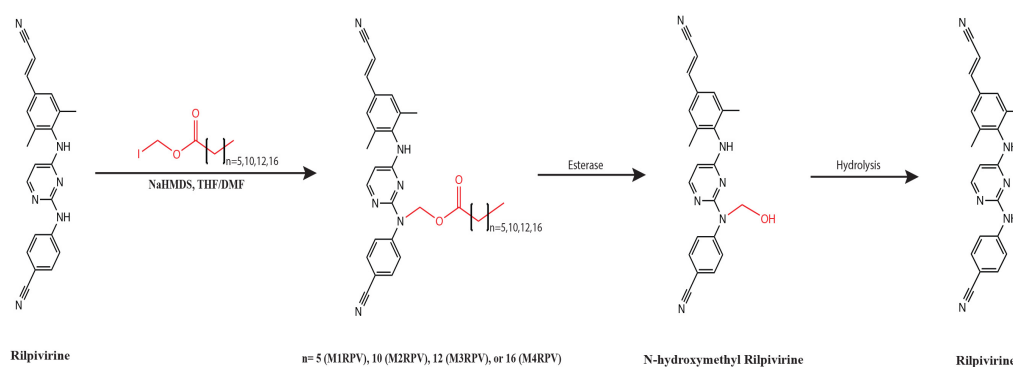
Figure 2.6.1 Synthesis and bioconversion of RPV prodrugs

Rilpivirine was modified with variable fatty acid chain lengths (7, 12, 14, 18) to develop a prodrug library (M1RPV, M2RPV, M3RPV, M4RPV). Prodrug bioconversion is hypothesized to first proceed by enzymatic cleavage of the methylene ester, yielding N-hydroxymethyl RPV.[89] Subsequently, hydrolysis will yield the original active compound (RPV).
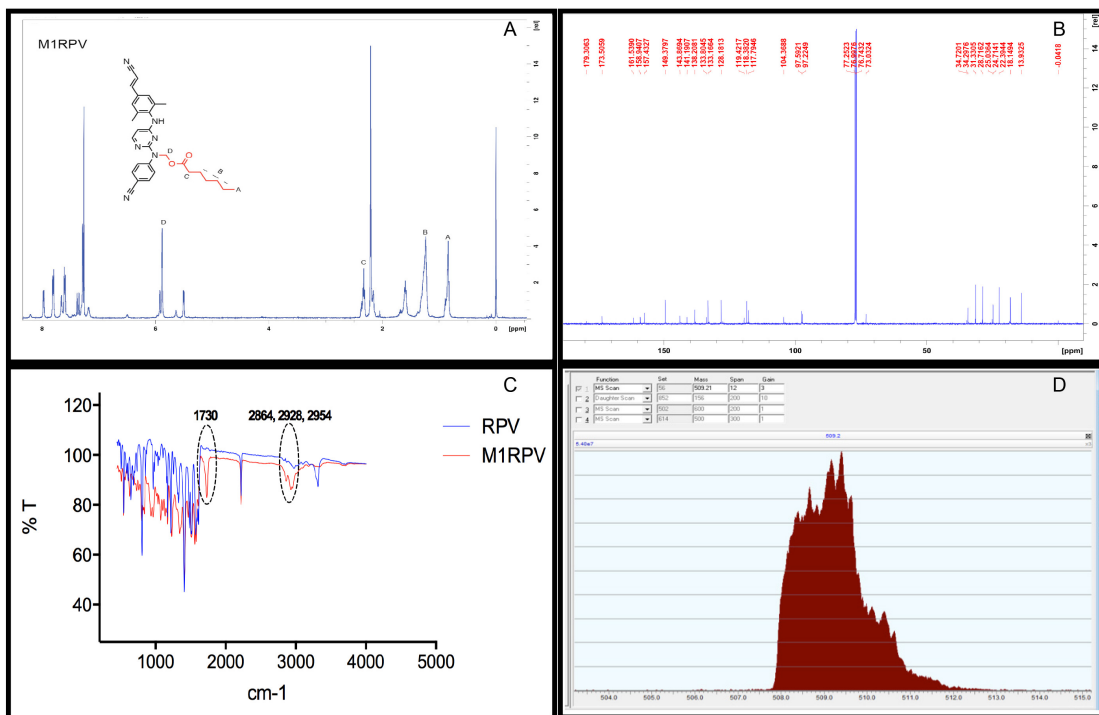
Figure 2.6.2 M1RPV chemical characterization

(A) Proton NMR spectra confirmed the synthesis of a heptanoyloxymethyl prodrug of RPV (M1RPV). Specifically, signals between 1.18-1.34 ppm represent the repeating (R-C**H₂**-R) protons, while protons of the methylene ester can be identified at 5.88 ppm. Furthermore, Cα protons, as well as those from the terminal methyl group are observed at 2.33 and 0.84 ppm respectively. **(B)** ^{13}C NMR spectra confirms the presence of aliphatic carbon chain with multiple signals between 22.4 and 34.3 ppm. **(C)** FTIR analysis of M1RPV generated absorption bands at 1730, as well as (2864, 2928, 2954), representing the heptanoic acid carbonyl and alkane stretches respectively. **(D)** Positive electrospray ionization mass spectrometry (ESI-MS) analysis generated a strong signal for M1RPV at 509.2 m/z.

Figure 2.6.3 Detection of M1RPV by UPLC-UV/Vis.

M1RPV (50 µg/mL) detected by UPLC-UV/Vis using a mobile phase of 70% (ACN) and 30% H_2O, wavelength of 230 nm, and a flow rate of 1.0 mL/min to produce a peak at 7.72 minutes. A linear standard curve between 0.048-50 µg/mL was used for quantitation and analysis.
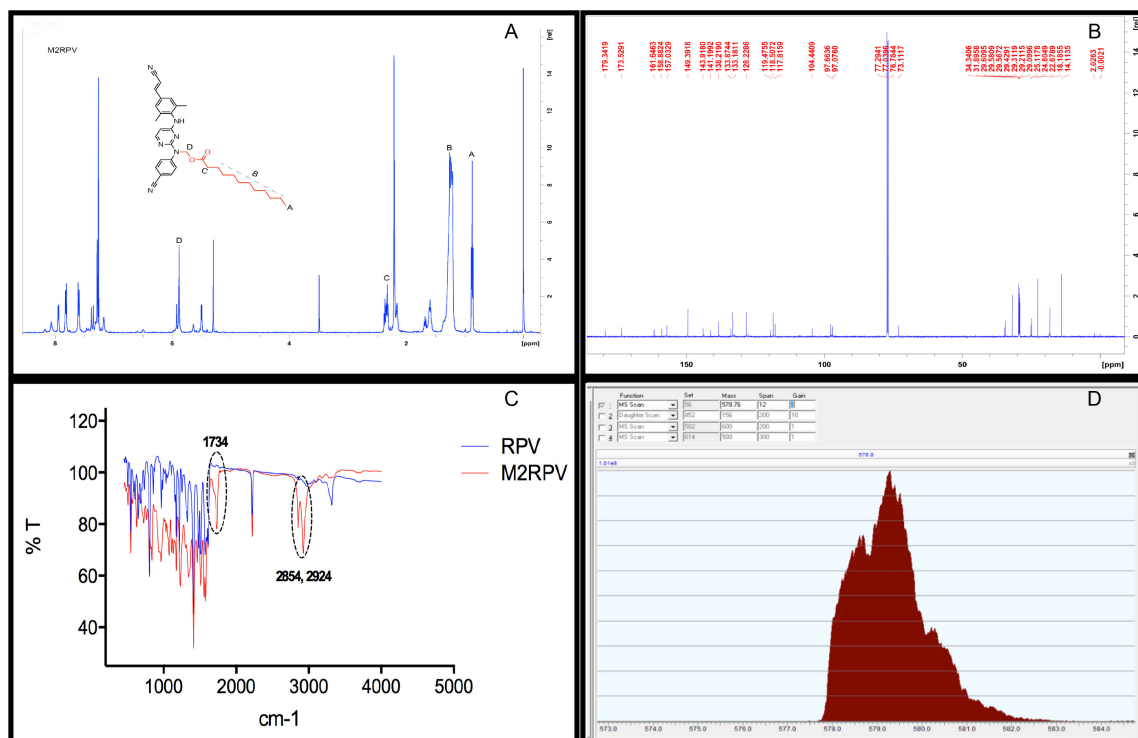
Figure 2.6.4 M2RPV chemical characterization

(A) Proton NMR confirmed the synthesis of a lauroyloxymethyl prodrug of RPV (M2RPV). Specifically, multiplet signals between 1.18-1.35 and 5.58-6.0 represent (R-C**H₂**-R) and methylene ester protons respectively. Moreover, signals at 0.84 and 2.32 correspond to terminal methyl group and Cα protons respectively. **(B)** ^{13}C NMR spectra confirms the presence of aliphatic carbon chain with multiple signals between 22.7 and 34.3 ppm. **(C)** FTIR analysis of M2RPV generated absorption bands at 1734, as well as (2854, 2924), representing the lauric acid carbonyl and alkane stretches respectively. **(D)** Positive electrospray ionization mass spectrometry (ESI-MS) analysis generated a strong signal for M2RPV at 579.4 m/z.
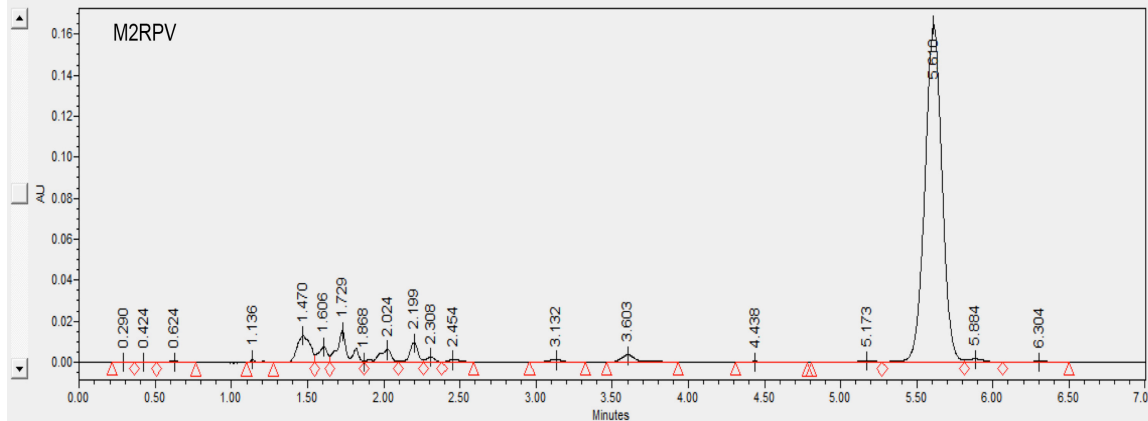
Figure 2.6.5 Detection of M2RPV by UPLC-UV/Vis.

M2RPV (50 µg/mL) detected by UPLC-UV/Vis using a mobile phase of 90% (ACN) and 10% H_2O, wavelength of 230 nm, and a flow rate of 1.0 mL/min to produce a peak at 5.61 minutes. A linear standard curve between 0.048-50 µg/mL was used for quantitation and analysis.
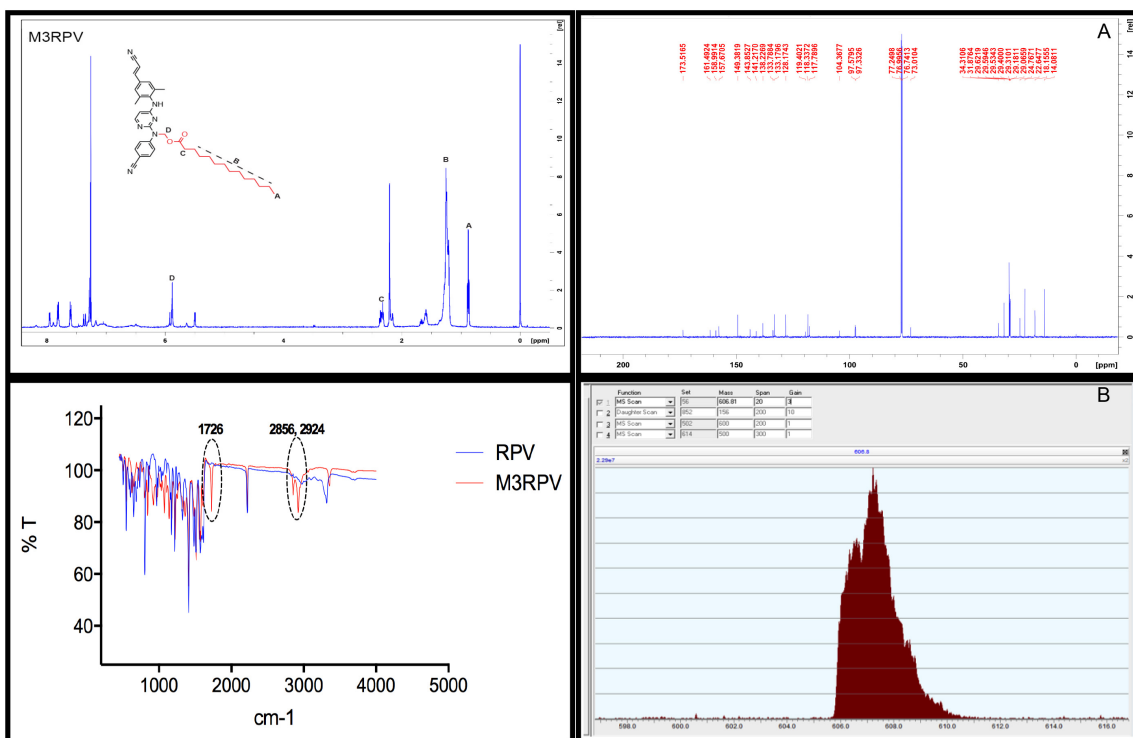
Figure 2.6.6 M3RPV chemical characterization

(A) Proton NMR spectra confirmed they synthesis of a myristoyloxymethyl prodrug of RPV (M3RPV). Specifically, multiplet signals between 5.86-5.95 and 1.17-.132 ppm, which correspond to the methylene ester and repeating (R-C$\mathbf{H_2}$-R) protons respectively. In addition, C$_\alpha$ and terminal methyl group protons are identified at 2.33 and 0.87 ppm respectively. **(B)** ^{13}C NMR spectra confirms the presence of aliphatic carbon chain with multiple signals between 22.6 and 34.3 ppm. **(C)** FTIR analysis of M3RPV generated absorption bands at 1726, as well as (2856, 2924), representing the myristoyl carbonyl and alkane stretches respectively. **(D)** Positive electrospray ionization mass spectrometry (ESI-MS) analysis generated a strong signal for M3RPV at 607.2 m/z.
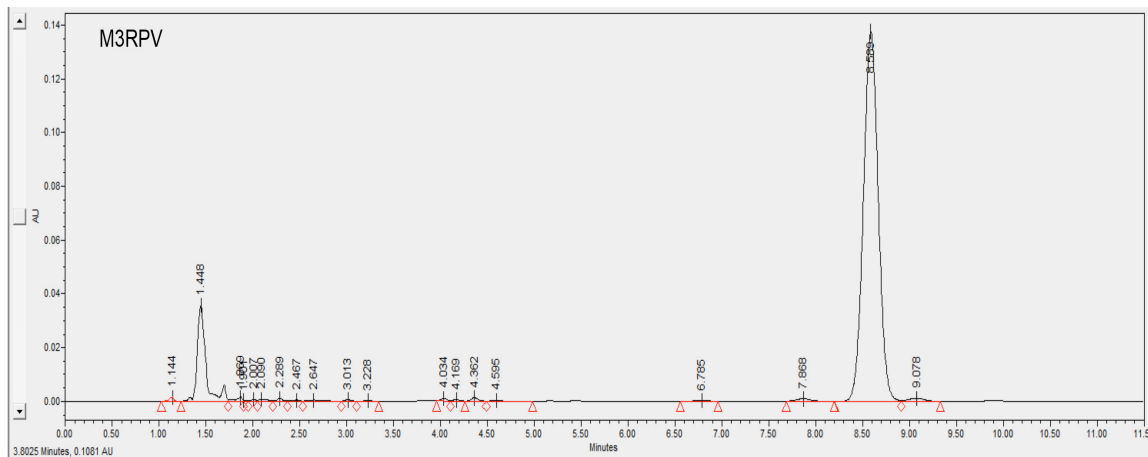
Figure 2.6.7 Detection of M3RPV by UPLC-UV/Vis.

M3RPV (50 µg/mL) detected by UPLC-UV/Vis using a mobile phase of 90% (ACN) and 10% H_2O, wavelength of 230 nm, and a flow rate of 1.0 mL/min to produce a peak at 8.58 minutes. A linear standard curve between 0.048-50 µg/mL was used for quantitation and analysis.
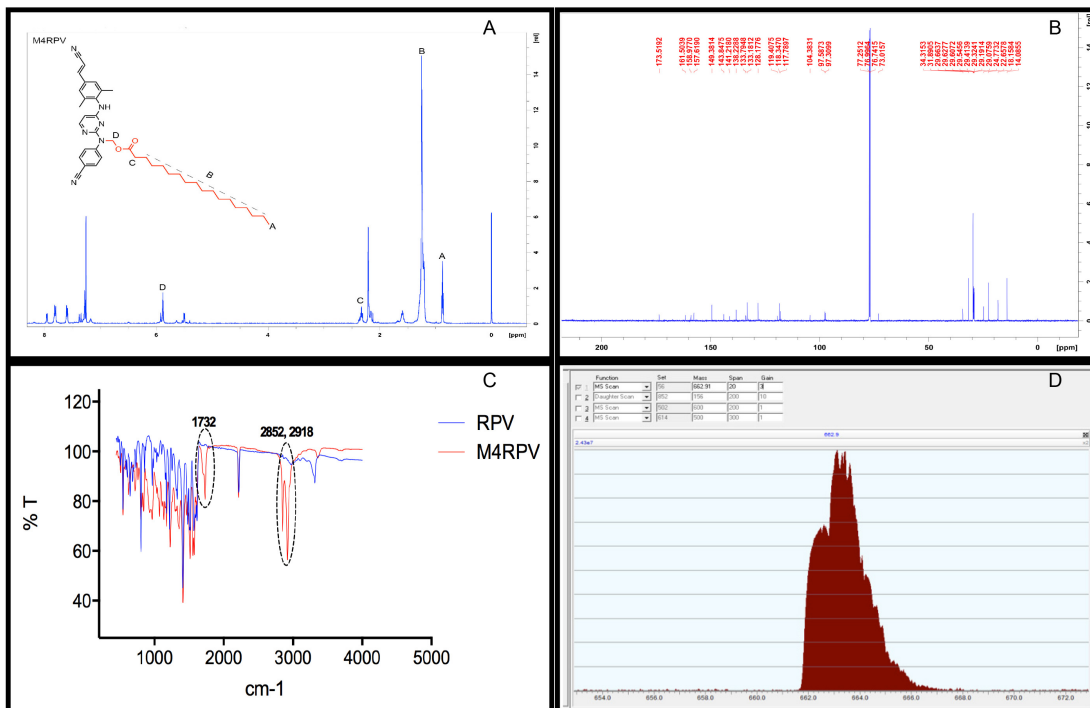
Figure 2.6.8 M4RPV chemical characterization

(A) Proton NMR spectra confirmed the synthesis of a stearoyloxymethyl prodrug of RPV (M4RPV). Specifically, multiplet signals between 5.57-6.0 and 1.18-1.32 ppm represent the methylene ester and (R-CH_2-R) protons respectively. In addition, signals at 2.33 and 0.88 ppm represent the Cα and terminal methyl group protons respectively. **(B)** ^{13}C NMR spectra confirms the presence of aliphatic carbon chain with multiple signals between 22.7 and 34.3 ppm. **(C)** FTIR analysis of M4RPV generated absorption bands at 1732, as well as (2852, 2918), representing the stearic acid carbonyl and alkane stretches respectively. **(D)** Positive electrospray ionization mass spectrometry (ESI-MS) analysis generated a strong signal for M4RPV at 663.2 m/z.
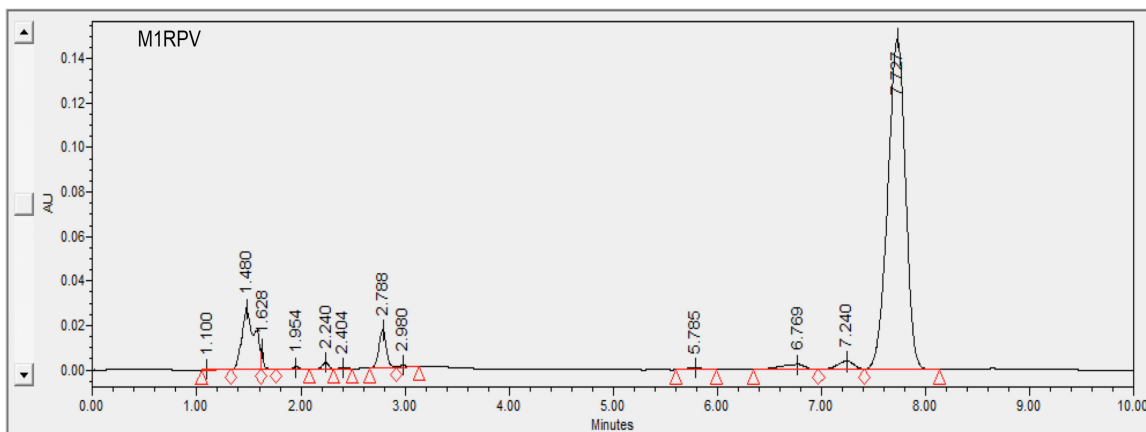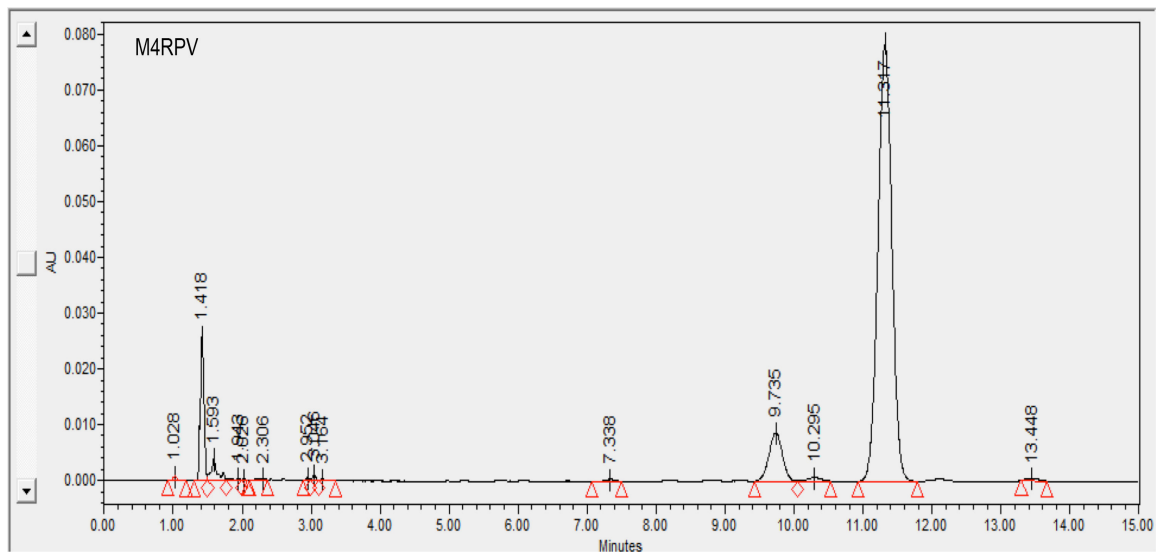
Figure 2.6.9 Detection of M4RPV by UPLC-UV/Vis.

M4RPV (50 µg/mL) detected by UPLC-UV/Vis using a mobile phase of 95% (ACN) and 5% H_2O, wavelength of 230 nm, and a flow rate of 1.0 mL/min to produce a peak at 11.31 minutes. A linear standard curve between 0.048-50 µg/mL was used for quantitation and analysis.
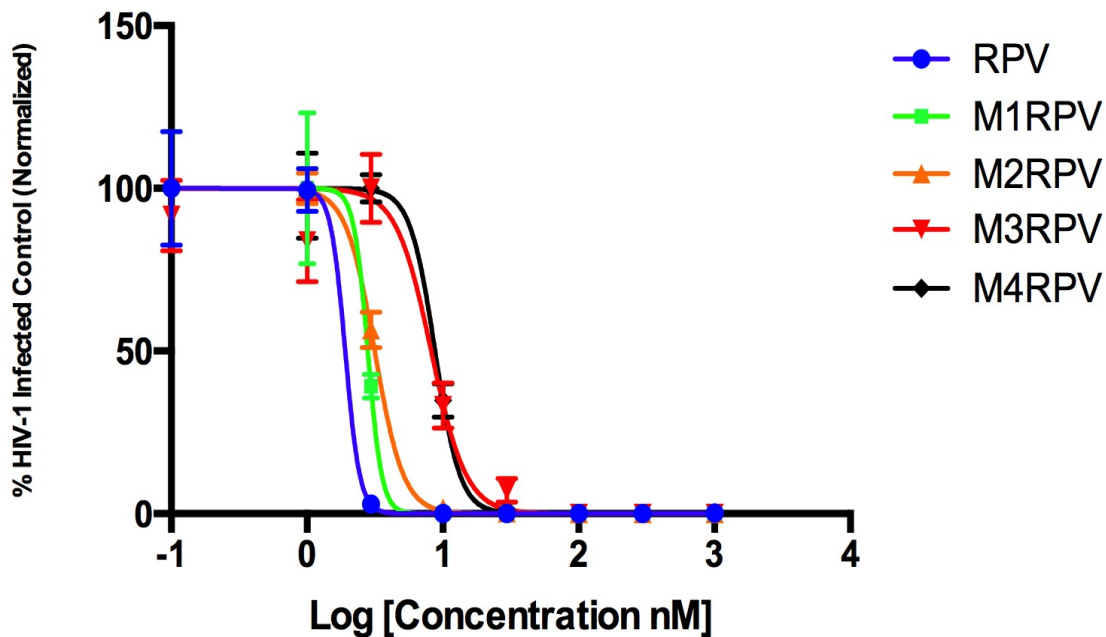
Figure 2.6.10 Antiviral activity of RPV prodrug in MDMs.

The antiviral activities of RPV and synthesized prodrugs (M1-M4RPV) were tested at a range of concentrations (0.1-1000 nm) in MDMs. RT activity was determined after viral challenge with HIV-1$_{ADA}$. Data was normalized and expressed as a percentage of HIV-1 control (mean ± SEM) with a minimum of 3 biological replicates.
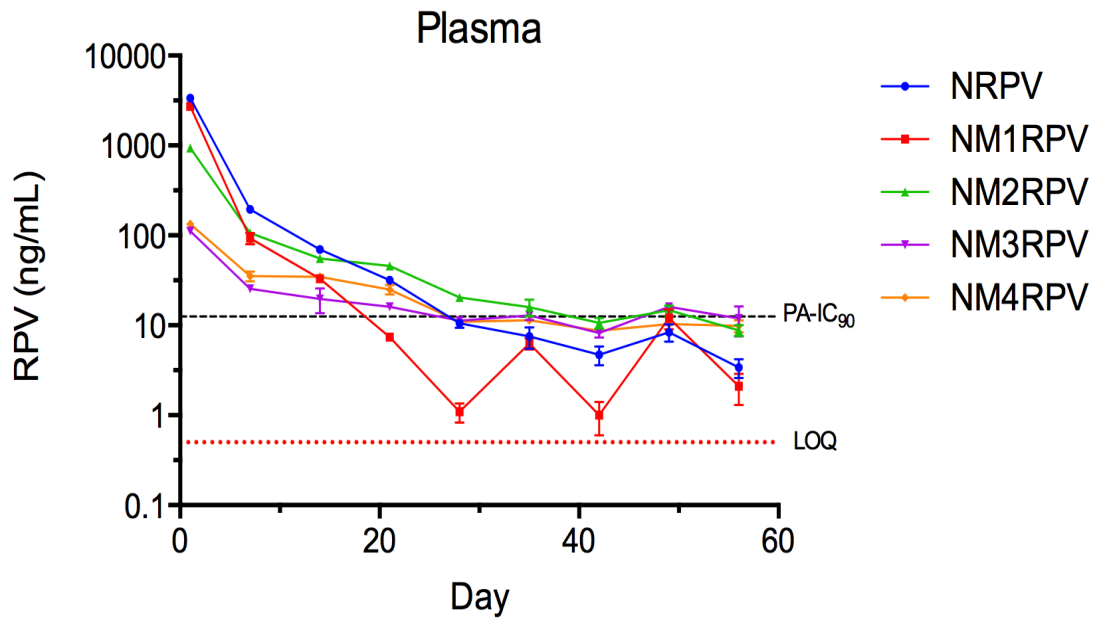
Figure 2.6.11 RPV prodrug PK

Male *BALB/cJ* mice were treated with 45 mg/kg RPV-eq. by intramuscular injection (IM) of NRPV, NM1RPV, NM2RPV, NM3RPV, or NM4RPV. RPV plasma concentrations were analyzed weekly for a period of 2 months by UPLC-MS/MS. Data is expressed as mean ± SEM where n = 4/5 biological replicates.
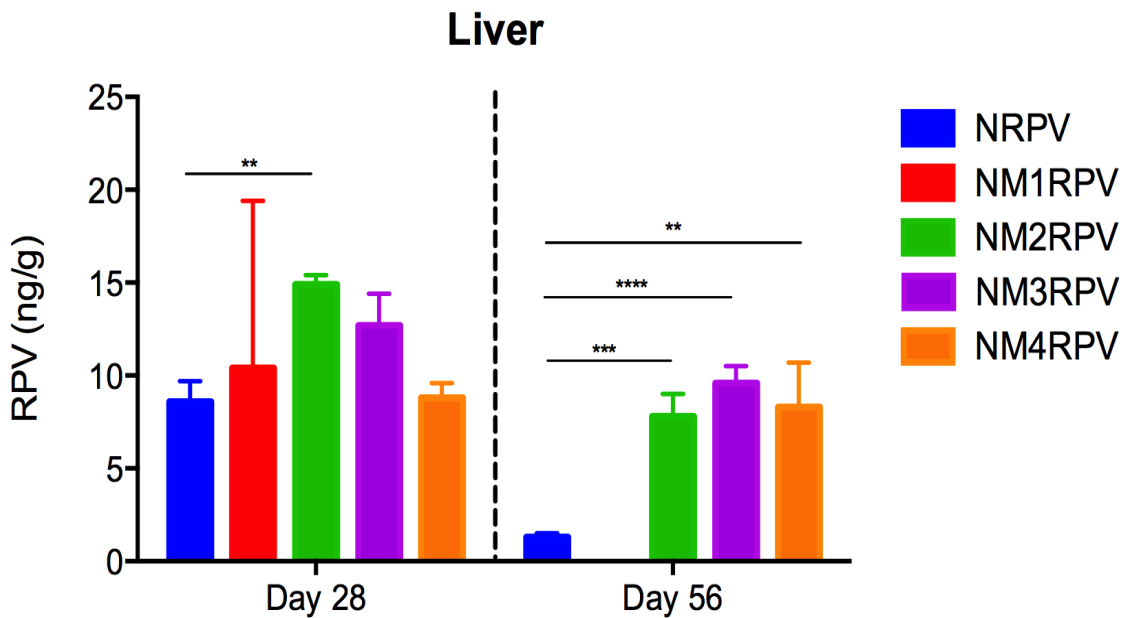
Figure 2.6.12 RPV prodrug liver tissue distribution

Male *BALB/cJ* mice were treated with 45 mg/kg RPV-eq. by intramuscular injection (IM) of NRPV, NM1RPV, NM2RPV, NM3RPV, or NM4RPV. Liver samples were collected 28 and 56 days post injection to assess RPV tissue concentrations by UPLC-MS/MS. Data is expressed as mean ± SEM where n = 4/5 biological replicates (**** $P < 0.0001$, *** $P < 0.001$, ** $P < 0.01$. by student's t-test).
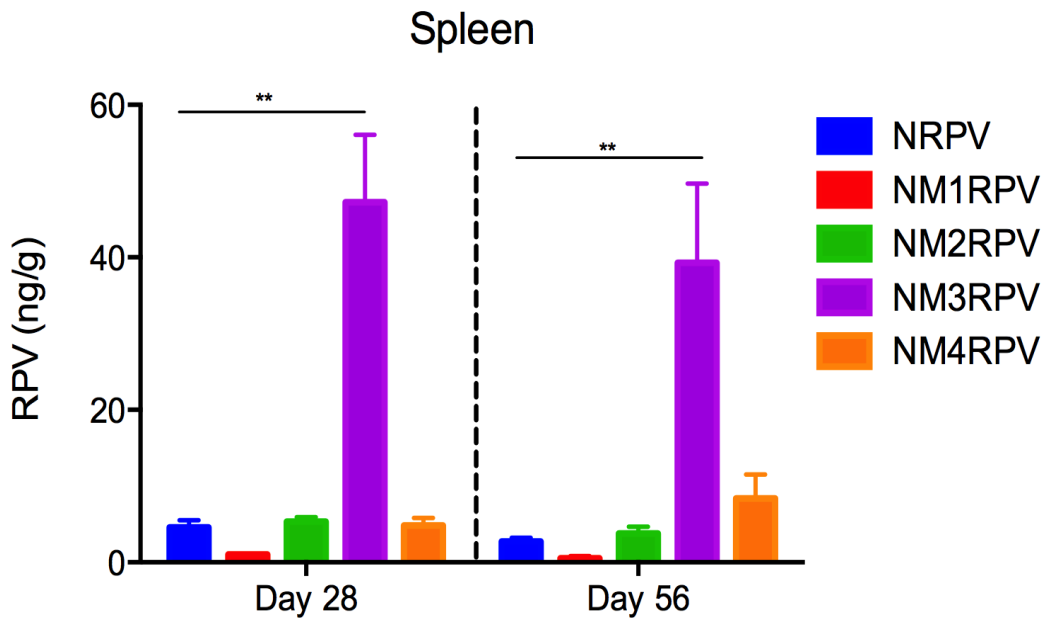
Figure 2.6.13 RPV prodrug spleen tissue BD

Male *BALB/cJ* mice were treated with 45 mg/kg RPV-eq. by intramuscular injection (IM) of NRPV, NM1RPV, NM2RPV, NM3RPV, or NM4RPV. Spleen samples were collected 28 and 56 days post injection to assess RPV tissue concentrations by UPLC-MS/MS. Data is expressed as mean ± SEM where n = 4/5 biological replicates (** $P < 0.01$ by student's t-test).
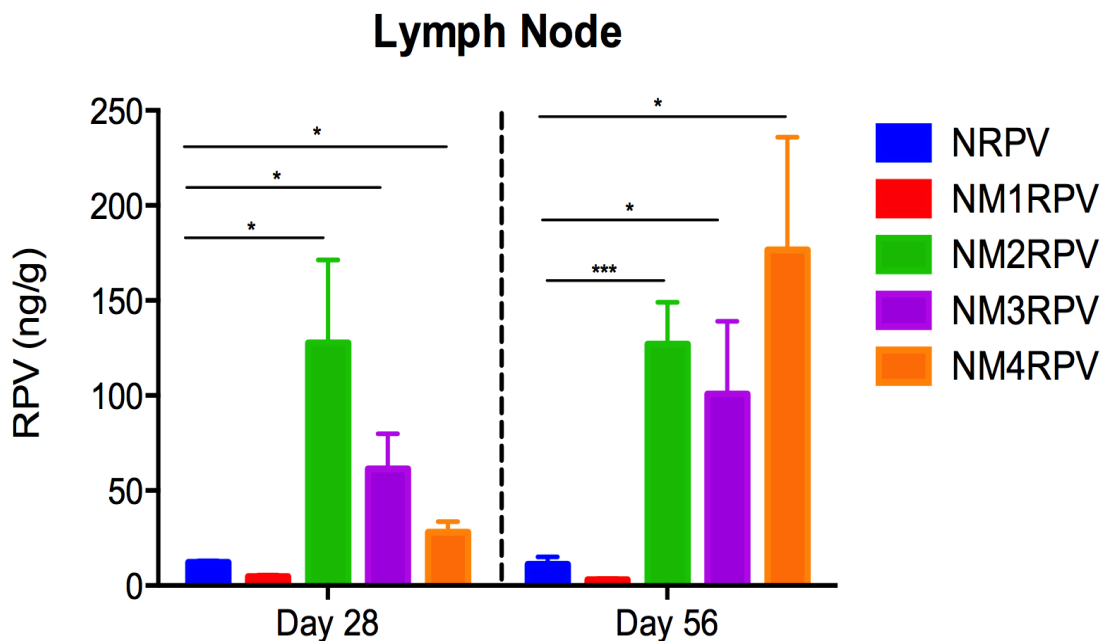
Figure 2.6.14 RPV prodrug lymph node tissue BD

Male BALB/cJ mice were treated with 45 mg/kg RPV-eq. by intramuscular injection (IM) of NRPV, NM1RPV, NM2RPV, NM3RPV, or NM4RPV. Lymph node samples were collected 28 and 56 days post injection to assess RPV tissue concentrations by UPLC-MS/MS. Data is expressed as mean ± SEM where n = 4/5 biological replicates (*** $P <$ 0.001, * $P <$ 0.05 by student's t-test).

2.7. Table

Table 2.7.1. Manufacture and characterization of nanoformulated RPV prodrugs

Formulation	Manufacture Process	Excipients	Purification
NRPV	High-Pressure Homogenization	P338	Centrifugation
NM1RPV	High-Pressure Homogenization	P407	Centrifugation
NM2RPV	High-Pressure Homogenization	P407	Centrifugation
NM3RPV	High-Pressure Homogenization	P407	Centrifugation
NM4RPV	High-Pressure Homogenization	P338, Tween 80	Centrifugation
Formulation	Hydrodynamic Diameter (nm)	Polydispersity (PDI)	Zeta Potential (mV)
NRPV	348 ± 51 nm	0.23 ± .03	10 ± 6 mV
NM1RPV	381 ± 119 nm	0.28 ± .12	32 ± 10 mV
NM2RPV	314 ± 59 nm	0.27 ± .04	15 ± 8 mV
NM3RPV	408 ± 41 nm	0.18 ± .05	-17 ± 10 mV
NM4RPV	333 ± 32 nm	0.32 ± .02	19 ± 5 mV

RPV and synthesized prodrugs (M1RPV, M2RPV, M3RPV, M4RPV) were nanoformulated using high-pressure homogenization and centrifugation as a means of purification and concentration respectively. Formulations were characterized in terms of size (nm), polydispersity (PDI), and zeta potential (mV) by dynamic light scattering (DLS). Data is expressed as mean ± SD for n ≥ 2 manufactured formulations.

CHAPTER 3

DEVELOPMENT AND CHARACTERIZATION OF A LA M3RPV FORMULATION

3.1 Introduction

Current ART has revolutionized patient care for those infected with HIV-1. Specifically, individuals faithfully adherent to oral ART experience undetectable plasma viral loads, improved immune function, as well as an extended life span.[2,3] Transitioning towards the next generation of ART, scientists have been learning from the past, specifically studying LA formulations developed for contraception and schizophrenia.[44,46] It is well established patient adherence is severely lacking, even in the context of clinical trials.[90] Lack of adherence in the context of HIV-1 can be particularly deleterious. Consistent, efficacious plasma concentrations of ARVs are necessary to achieve viral suppression. Moreover, suboptimal PK due to missed doses can cause low levels of viral replication and generate resistance mutations.[91] To address these concerns, LA formulations of RPV and CAB (RPV-LA; CAB-LA) are under development.[52,82] Phase 3 clinical trials demonstrated that LA regimens administered monthly were non-inferior to standard oral ART, thus a LA revolution in ART therapy is on the horizon.[28,56] LA ART is in its inception, thus its limitations require further optimization. Generally, increasing dosing intervals beyond a month towards a bi-annual goal would make the therapy more

attractive to patients for maintenance and PrEP alike. Therefore, our previous work has demonstrated that generating hydrophobic prodrugs of existing ARVs and manufacturing LASER-ART formulations could substantially improve PK and BD.[66,67,70,71] Our current work reports the nanoformulation and testing of a myristoylated RPV prodrug (NM3RPV). NM3RPV generated RPV plasma concentrations above the PA-IC$_{90}$ for 25 weeks, while concurrently producing a substantial tissue depot, after in single IM injection in *BALB/cJ* mice. Furthermore, NM3RPV provided 13- and 26-fold increases in RPV $t_{1/2}$ and MRT, respectively, compared with NRPV. Therefore, our current work demonstrates proof-of-concept for the development and further optimization of nanoformulated RPV prodrugs

3.2 Materials and Methods

3.3.1 Reagents

RPV was purchased from LeapChem (Hangzhou, China). Ciprofloxacin, paraformaldehyde (PFA), 3-(4,5-dimethylthiazol-2-yl)-2,5-diphenyltetrazolium bromide (MTT), 3,3'-diaminobenzidine (DAB) and pluronic F127 (P407) was purchased from Sigma-Aldrich (St. Louis, MO). Pluronic F108 (P338) was purchased from BASF (Florham Park, NJ). Acetonitrile (ACN), methanol (MeOH), cell-culture grade water (endotoxin-free), KH$_2$PO$_4$, bovine serum albumin (BSA), Triton X-100, and gentamicin were purchased from Fisher Scientific (Hampton, NH). Dulbecco's Modified Eagle Medium (DMEM) was purchased from Corning Life Sciences (Tewksbury, MA). Polymer-based HRP-conjugated anti-mouse Envision+ secondary antibody was purchased from Dako (Carpinteria, CA).

3.3.2 Quantification of RPV and M3RPV by UPLC-UV/Vis

Drug concentration was assayed on a Waters ACQUITY ultra performance liquid chromatography (UPLC) H-Class system with TUV detector and Empower 3 software (Milford, MA). RPV and M3RPV samples were separated on a Phenomenex Kinetex 5 μm C18 column (150 x 4.6 mm) (Torrance, CA). RPV was detected at 285 nm, using a mobile phase consisting of 65% (50 mM KH_2PO_4 pH 3.2) and 35% (ACN) and a flow rate of 1.0 mL/min. M3RPV was detected at 230 nm, using a mobile phase consisting of 90% ACN and 10% H_2O and a flow rate of 1.0 mL/min. Drug content was determined relative to peak areas from drug standards (0.05-50 μg/mL).

3.3.3 Solubility

Aqueous and 1-octanol solubility were evaluated by mixing excess RPV in each solvent for 24 hours. Centrifugation at 20,000 *g* for 10 min pelleted any undissolved drug. Aqueous supernatants were frozen, lyophilized, and subsequently re-suspended in MeOH for analysis. 1-Octanol supernatants were prepared for analysis by dilution into MeOH. Collected samples were analyzed for drug content by UPLC-UV/Vis as described above.

3.3.4 Nanoparticle manufacture and characterization

Nanoformulations of RPV and M3RPV (NRPV and NM3RPV) were manufactured using an Avestin EmulsiFlex-C3 high-pressure homogenizer (Ottawa, ON, Canada). NRPV was prepared to best replicate Janssen's RPV-LA currently in clinical trials.[37] Specifically, P338 1% (w/v) was dispersed in H_2O, followed by the addition of 10% (w/v) RPV-free base and mixing overnight. Similarly, NM3RPV contained 2.1% P407 and 21% M3RPV in H_2O. Formulations were homogenized at (20,000 psi) to generate homogeneous nanocrystals of uniform size and polydispersity (pdi). Nanoparticle physicochemical characterization for size (nm),

polydispersity (PDI) and zeta potential (mV) were evaluated by dynamic light scattering (DLS, Malvern Nano-ZS Worcestershire, UK). NM3RPV and NRPV drug quantitation was analyzed by UPLC-UV/Vis as described above.

3.3.5 Macrophage cellular uptake and retention studies

Human monocytes were obtained by leukapheresis from HIV-1/2 seronegative donors and subsequently purified by counter-current centrifugal elutriation.[92] Monocytes were grown in culture media containing DMEM (4.5 g/L glucose, L-glutamine, and sodium pyruvate) supplemented with 10% pooled human serum (heat-inactivated), 10 µg/mL ciprofloxacin, and 50 µg/mL gentamicin. Additionally, cells were maintained at 37°C in a 5% CO_2 incubator. Human monocytes were plated in 12, 24, or 96-well plates at 1.0×10^6, 0.5×10^6, or 0.15×10^6 cells/mL respectively. Recombinant human macrophage colony stimulating factor (MCSF, 1000 U/mL) was added to culture media for 7 days to facilitate monocyte-derived macrophages (MDMs) differentiation and vitality in culture. MDM uptake and retention studies were performed in 12-well plates, with each treatment group completed in triplicate. Briefly, MDMs were treated with NM3RPV or NRPV at concentrations of 10 or 30 µM and cells were collected 1, 2, 4, 8 hours later. For cellular retention studies, drug was removed after 8 hours. Cells were washed with PBS and replenished with fresh media. Cellular samples were collected at 1, 5, 10, 20 and 30 days to assay intracellular drug concentration. For both studies, MDMs were collected by removing media, PBS washing, and scraping the cells into suspension. Cells were subsequently counted using an Invitrogen Countess Automated Cell Counter (Carlsbad, CA). Collected MDMs were centrifuged at 3,000 rpm for 8 min. Cell pellets were sonicated in MeOH to extract intracellular drug and subsequently centrifuged at 14,000 rpm for 10 min. Samples were analyzed by UPLC-UV/Vis for intracellular drug content as

described above. Furthermore, to test cytotoxicity, an MTT was performed. Briefly, MDM were plated in 96-well plates at a density of 0.15×10^6 cells per well and treated with NRPV or NM3RPV (1-1000 µM) for a period of 8 hours. After treatment, cells were washed and incubated with MTT solution (5 mg/mL; 100 µL/well) at 37°C for 45 min. Next, MTT was aspirated and 200 µL of DMSO was subsequently added. Plates were gentled shaken to mix and absorbance was measured on a Molecular Devices SpectraMax M3 plate reader with SoftMax Pro 6.2 software (Sunnyvale, CA) at 490 nm.

3.3.6 Assay of antiretroviral activities in MDM

To assess long-term antiretroviral activity, MDMs were plated in 24-well plates at a density of 0.5×10^6 cells/well. Cells were treated with 10 or 30 µM NM3RPV or NRPV for 8 hours, followed by a PBS wash and addition of fresh media. Cells were then challenged with HIV-1$_{ADA}$ at a multiplicity of infection (MOI) 0.1 at 1, 5, 10, 20 or 30 days after treatment for 16 hours. After viral challenge, cells were washed with PBS and replenished with fresh media. Supernatants were collected 10 days after challenge and assayed for reverse transcriptase (RT) activity.[85,86] Replicate cells were fixed with 4% PFA and stained for HIV-1 p24 antigen by immunohistochemistry.[86]

3.3.7   Plasma cleavage kinetics

Plasma cleavage kinetics of M3RPV was evaluated from mouse, rat, rabbit, dog, monkey, and human plasma. M3RPV (1 µM) was incubated in 100 µL plasma at 37°C. At 0, 2, 6, and 24 hours samples were quenched with 1 mL of MeOH and vortexed for 3 min. Samples were the centrifuged at 15,000 *g* for 10 min; upon which supernatants were analyzed for RPV and/or M3RPV by UPLC-MS/MS. Heat-

inactivated plasma was used as a negative control for enzymatic cleavage and hydrolysis testing.

3.3.8 Transmission Electron Microscopy (TEM)

Morphology of NRPV and NM3RPV was assessed by FEI Tecnai G2 Spirit TEM (Hillsboro, OR) using negative staining. Briefly, 10 μL of diluted nanoformulation was applied to a formavar/silicone monoxide coated 200 mesh copper grid and allowed to absorb for 5 min. Excess samples were removed with filter paper and subsequently dried for an additional 2-5 minutes. Next, Nanovan negative stain was pipetted onto the grid for staining before imaging under TEM.

3.3.9 Pharmacokinetics (PK) and biodistribution (BD)

Male *BALB c/J* mice (6-8 weeks, Jackson Labs, Bar Harbor, ME) were administered 45, 75, or 100 mg/kg RPV-eq. NM3RPV or NRPV by a single intramuscular (IM; caudal thigh muscle) injection at 40 μL/ 25 g. Following injection, blood samples were collected into heparinized tubes 24 hours later, as well as weekly for the 46 week study duration. Collected blood (25 μL) was immediately diluted into 1 mL ACN and stored at -80°C until drug analysis. Remaining blood samples were centrifuged at 2,000 *g* for 5 min. Plasma supernatants were collected and stored at -80°C until further analysis. Animals were humanly euthanized with isoflurane, followed by cervical dislocation at 56 and 323 days after drug treatment to obtain spleen, lymph node, liver, lung, gut, kidney, brain and rectal tissue for drug content determinations. Drug concentrations in plasma, tissue and whole blood were determined by UPLC-MS/MS using a Waters ACQUITY UPLC-Xevo TQ-S micro mass spectrometry system (Milford, MA). RPV was separated using an AQUITY UPLC-BEH shield RP18 column (1.7 μm, 2.1 mm x 100 mm) using a 7 min gradient mobile

phase consisting of A (7.5 mM ammonium bicarbonate in Optima-grade water adjusted to pH 7 using acetic acid) and B (100% Optima-grade MeOH) at a flow rate of 0.25 mL/min. Initial conditions of 70% mobile phase B remained for 4.75 min, followed by an increase to 95% B in 0.25 min and held constant for 0.75 min. Mobile phase B was reset to 70% in 0.25 min and the column equilibrated for 1.0 min before the next injection. A cone voltage of 92 volts and collision energy of 56 volts was used to detect RPV. Multiple reaction monitoring (MRM) transitions used for RPV, indinavir and lopinavir were 367.032 > 127.859, 614.14 > 97.023, and 629.177 > 155.031 m/z respectively. M3RPV was separated using an ACQUITY UPLC BEH C18 1.7 µm analytical column (2.1 mm x 30 mm) with an ACQUITY BEH C18 Vanguard column using a flow rate of 0.28 mL/min. MRM transitions of 607.34 < 379.09 m/z were used for quantification, while 60.734 < 367.12 and 607.34 < 363.12 m/z were used for identity confirmation. Mobile phase A (7.5 mM ammonium formate in water, adjusted to pH 3.0 with formic acid) and mobile phase B (100% MeOH) ran isocratic at 15 % A for 5 minutes. In order to wash the column, mobile phase A decreased to 5% for 1 min, then returning to 15% over the next 2 min. For drug analysis 50 µL of plasma was mixed with 1 mL of ice cold ACN and subsequently spiked with 10 µL of internal standards. (IS; MDTG and $^{15}N_2$-^{13}C-Lamivudine) Samples were subsequently vortexed (3 min) and centrifuged (17,000 g for 10 min). Supernatants were dried, reconstituted, and injected for UPLC-MS/MS analysis. Plasma standards were extracted at a final concentration of 0.1-1000 ng/ml. Tissue analysis required between 20-200 mg of tissue (spleen, lymph node, liver, gut, lung, kidney, brain, rectal) to be diluted with 90% MeOH and homogenized. Tissue homogenates were mixed with MeOH containing IS and vortexed (3 min), followed by centrifugation (17,000 g for 10 min). Supernatants were collected and mixed with H_2O for UPLC-MS/MS analysis. Tissue standards were extracted at a final concentration of 0.05-500 ng/g.

3.3.10 NM3RPV PK in rhesus macaques

Male rhesus macaques (4.4-6.7 kg; PrimeGen) were anesthetized with ketamine (10 mg/kg) and subsequently administered 45 mg/kg RPV eq. of NM3RPV by IM injection (0.5 mL/kg) in the gluteus maximus. Blood samples were collected in potassium-EDTA coated tubes for blood cell counts, serum metabolites and plasma drug quantitation. At 204 days after treatment lymph node, adipose tissue and rectal tissue biopsies were performed in anesthetized animals for for drug quantitation.

3.3.11 PK parameter analyses

Non-compartmental PK analyses for plasma RPV were performed using WinNonlin-5.1 (Certara USA, Inc., Princeton, NJ, USA) for *BALB/cJ* mice studies.

3.3.12 NM3RPV Pharmacodynamics in a humanized mouse model of HIV-1 infection

NOD/scid-IL-2Rγc[null] (NSG) mice were reconstituted with CD34+ human hematopoietic stem cells (HSC) isolated from umbilical cord blood.[93] Mice were administered NM3RPV (100 mg/kg RPV eq.; IM) and subsequently challenged with HIV-1$_{ADA}$ (1×10^4 TCID50; Intraperitoneal; IP) two weeks following drug treatment. Two and 4 weeks after viral challenge blood was collected by cheek puncture into EDTA-coated tubes. Blood samples were centrifuged (2,000 g for 5 min) and collected plasma was stored at -80°C until further analyses. Viral load (HIV-1 RNA) was quantified in collected plasma samples using a Roche Amplicor and TaqMan-48 system. Additionally, plasma drug concentrations were determined by UPLC-MS/MS.

3.3.13 Statistics

In-vitro studies were expressed as mean ± SEM with a minimum of 3 biological replicates, while in-vivo study results were expressed as mean ± SEM with a minimum of 4 biological replicates. GraphPad Prism 7.0 software (La Jolla, CA) was used for all statistical analysis. Specifically, comparisons between two groups utilized student's *t* test (two-tailed). Significant differences were denoted as follows: (* *P* < 0.05, ** *P* < 0.01, *** *P* < 0.001, **** *P* < 0.0001).

3.4 Results

3.4.1 M3RPV Solubility, Cleavage Kinetics, and Antiviral Activity

Prodrug synthesis enabled precise alteration of a RPV's physicochemical properties. M3RPV exhibited a 2.4-fold decrease in water (***P* < 0.01) and an 8.7-fold increase in 1-octanol solubility (****P < 0.0001) (Figure 3.6.1). This data underscores the changes in hydrophobicity and lipophilicity generated by prodrug modification. As most prodrugs are pharmacologically inactive and require enzymatic or hydrolytic activation, we tested cleavage kinetics of M3RPV in mouse, rat, rabbit, dog, monkey, and human plasma (Figure 3.6.2). Interestingly, species-specific kinetic differences were observed, whereby mouse plasma produced the most robust cleavage (94.8%) and human plasma exhibited slower prodrug breakdown (15.7%) over a 24-hour period. As successful bioconversion requires removal of the inactive moiety and release of the active compound we analyzed RPV formation during plasma cleavage. M3RPV incubated in mouse plasma efficiently released 70% of RPV within 24 hours. In comparison dog, human and monkey yielded 5, 14, and 21% RPV, respectively. Furthermore, to demonstrate there was not an abrogation of activity due to prodrug modification, M3RPV was tested against HIV-1 in both MDM and CD4+ T-cells (CEM) (Figure 3.6.3). Compared to RPV, M3RPV exhibited a 4.3-fold increase in EC_{50} for viral inhbition in

MDM (EC_{50} of 1.9 vs 8.2 nM), and a 6.8-fold increase (EC_{50} of 0.8 vs 5.5 nM) in CEM T-cells.

3.4.2 Nanoformulation characterization and particle stability

NRPV and NM3RPV were manufactured by top down synthesis utilizing high-pressure homogenization to generate stable nanosuspensions. Poloxomer (P338 and P407) surfactants provided particle surface stabilization for NRPV and NM3RPV. As clinically relevant injectable formulations must maintain their physical integrity within a range of storage conditions DLS was used to assess physicochemical stability of NRPV and NM3RPV at room temperature, 4, and 37°. Both formulations maintained particle size, polydispersity (pdi), and zeta potential for a period of 100 days. Specifically, the initial size (277 ± 9 nm), pdi (0.24 ± .02), and zeta potential (-9.2 ± 0.3 mV) of NRPV exhibited a subtle size reduction over the course of testing (239 ± 3 nm, 0.25 ± .01, -13.6 ±. 0.7 mV at day 100. (Figure 3.6.4) NM3RPV had an average particle size of 345 ± 5 nm, pdi of 0.18 ± .06 and zeta potential of -17.6 ± 0.6 mV at the time of manufacture. One hundred days later, physicochemical parameters of NM3RPV were stable (326 ± 1 nm, 0.25 ± 0.1 and -9.2 ± 0.9 mV. (Figure 3.6.4) Furthermore, temperature variation (4 or 37°) did not change the physical integrity of either NRPV or NM3RPV (Figure 3.6.4) Transmission electron microscopy (TEM) of both NRPV and NM3RPV displayed nanocrystals of an elongated cuboidal morphology (Figure 3.6.5). Importantly, we next investigated prodrug stability within NM3RPV over time. NM3RPV contained 99.72% M3RPV when analyzed for both prodrug and parent (RPV) compounds by UPLC UV/Vis after initial manufacture. By day 100 the percentage remained consistent for NM3RPV at RT and 4° (99.69 and 99.71%), while a decreasing trend was observed in formulation stored at 37°C (99.42%) (Figure 3.6.6). Furthermore, pharmacokinetic (PK) tests of NM3RPV were performed in *BALB/cJ* mice comparing freshly made formulations to

those stored at RT for 90 days. RPV plasma levels were comparable between the two formulations during the 147-day study period (Figure 3.6.6).

3.4.3 NM3RPV-macrophage interactions

The phagocytic nature of macrophages affords testing of their use as cellular drug depots. We reasoned that packaging of drug nanocrystals at sites of viral growth would facilitate the drug's antiretroviral activities. We therefore evaluated uptake of NM3RPV and NRPV in MDM at 10 and 30 μM doses. Drug formulations administered at 10 μM resulted in comparable intracellular drug levels after 8 hours for NM3RPV (2.0 μg/10^6 cells) and NRPV (2.2 μg/10^6 cells). (Figure 3.6.7) A 30 μM treatment led to drug concentrations of 6.0 μg/10^6 and 4.9 μg/10^6 cells for NRPV and NM3RPV, respectively. (Figure 3.6.9) Furthermore, NM3RPV treated cells generated detectable intracellular RPV concentrations of 95 and 140 ng/10^6 cells at 8 hours after 10 and 30 μM of drug exposure. As macrophages also have the capacity to migrate throughout the body, thereby serving as drug delivery systems to viral reservoirs, we tested their capacity to retain intracellular drug over a 30-day period following a single drug loading. Single exposure of MDM to 10 or 30 μM of NM3RPV showed enhanced intracellular drug over NRPV. Specifically, the amount of prodrug retained by MDM was 1.7 and 2.9 μg/10^6 cells 30 days after treatment with 10 and 30 μM of NM3RPV, respectively. (Figure 3.6.7; 3.6.9) Conversely, NRPV treatment yielded RPV levels that fell below the limit of quantitation within 20 days, with significantly lower drug concentrations at all time points when compared against NM3RPV treatment. Importantly, at both doses (10 and 30 μM) sustained RPV concentrations were detected for 30 days in NM3RPV-treated cells. To examine whether sustained release of drug would protect MDM against HIV-1 infection, we challenged cells with HIV-1$_{ADA}$ up to 30 days after drug loading and assayed quantitatively for RT activity, as well as qualitatively for HIV-1p24 antigen. Both 10 and

30 µM, NM3RPV suppressed HIV-1 RT activity by > 96% at all challenge time points. (Figure 3.6.8; 3.6.10) In contrast, treatment of MDM with 10 µM NRPV provided 67% reduction of RT activity when challenged 10 days post treatment, with complete viral breakthrough occurring at day 20. Similarly, 30 µM NRPV provided only 42% viral inhibition at day 30. Therefore, enhanced MDM drug uptake and retention (and continued RPV release) exhibited by NM3RPV provides superior protection against HIV-1 challenge compared with NRPV.

3.4.4 PK and BD

Prodrug modification not only alters the physicochemical properties of a compound, but also can change its pharmacokinetic profile and tissue distribution. Therefore, we administered a single IM injection of 45, 75, and 100 mg/kg RPV-eq. doses of NM3RPV or NRPV to male *BALB/cJ* mice. NM3RPV generated lower initial plasma RPV concentrations coupled with slower plasma decay kinetics compared with NRPV. Specifically, animals dosed with 45, 75, 100 mg/kg NRPV maintained RPV plasma concentrations above the PA-IC$_{90}$ (12 ng/mL) for 4, 6, and 7 weeks before falling below the limit of quantitation of 0.5 ng/mL by 10, 13, and 16 weeks. (Figures 3.6.11; 3.6.14; 3.6.17) In comparison, NM3RPV provided sustained plasma RPV concentrations above the PA-IC$_{90}$ for 4, 12, and 25 weeks at doses of 45, 75, and 100 mg/kg RPV-eq. respectively. Furthermore, NM3RPV treated animals exhibited 13- and 26-fold increases in $t_{1/2}$ and MRT compared with NRPV respectively. (Table 3.6.1) Moreover, NM3RPV significantly improved tissue biodistribution compared with NRPV. Particularly, NM3RPV provided significantly higher RPV concentrations in the spleen, liver, gut, and kidney 8 weeks following drug administration at all doses (45, 75, and 100 mg/kg). (Figures 3.6.12; 3.6.15; 3.6.18) Importantly, at the conclusion of the study (46 weeks), RPV concentrations were still detectable in most tissue tested (spleen, lymph node, liver, gut,

kidney), with a significant tissue distribution observed in the lymph nodes (145 ng/g). By comparison, RPV was not found above the limit of quantitation in any tissue collected 46 weeks after treatment with NRPV. Furthermore, we assayed all tissues for the presence of NM3RPV.   Lymph node, spleen, and liver were substantial depots for M3RPV, containing 26,941, 674, and 220 ng/g of M3RPV 46 weeks after injection, respectively. (Figure 3.6.19)

Next, to investigate whether species differences in M3RPV cleavage kinetics might generate differences in plasma and tissue distribution, NM3RPV was evaluated after a single IM injection of 45 mg/kg RPV-eq. in rhesus macaques. (Figure 3.6.20) We observed a significant presence of prodrug in plasma, whereby concentrations of M3RPV were between 2-16 fold higher than RPV across the course of 44 weeks of investigation. Furthermore, rectal, lymph node, adipose biopsies collected 204 days after NM3RPV treatment contained measurable levels of both M3RPV and RPV. Specifically, RPV concentrations of 8.7, 23.7, and 19.7 ng/g were detected in the rectal, lymph node and adipose tissue at day 204. Moreover, M3RPV was distributed and retained in the lymph node and adipose tissue (456.3 and 532.3 ng/g), with lower levels detected in rectal tissue (7.4 ng/g).

3.4. NM3RPV PrEP in humanized mice

To determine the efficacy of NM3RPV against HIV-1 challenge, we employed a CD34+ humanized mouse model for PrEP studies. Specifically, animals were given a single injection of NM3RPV (100 mg/kg) and subsequently challenged with HIV-1$_{ADA}$ (IP) 2 weeks after treatment. Plasma viral loads 2 and 4 weeks after challenge revealed plasma viral RNA levels similar to untreated controls. (Figure 3.6.21) Furthermore, plasma was collected to assay RPV concentrations at the time of viral challenge.

Specifically, RPV concentrations were ~2.5 times the PA-IC$_{90}$ at time of challenge with HIV-1$_{ADA.}$ (Figure 3.6.21)

3.5 Discussion

Treatment of HIV-1 infection requires life-long ART to maintain viral suppression, CD4+ T cell numbers and lifespan.[2,3] Since inception, ART required strict adherence for both treatment of existing infection and for pre-exposure prophylaxis.[90] While ART has evolved to formulations requiring a single daily pill,[94] LA formulations such as injectable or implants have received considerable support from large numbers of infected or at risk patients.[95,96] In sub-Saharan Africa, which bears the largest global burden of HIV-1 infections, increased use of injections or implants for contraception have laid the groundwork for LA ART.[58,59]

Monthly administration of CAB and RPV LA has seen levels of viral suppression consistent with established oral treatments.[28,56,57] Therefore, as LA ART comes closer towards approval, optimization of delivery and incorporation of a broader range of ARVs are in increasing demand. In parallel, reducing injection volume, dose frequency, injection site reactions while increasing tissue drug penetrance remain in want.[66] While implantable devices can alleviate some of these concerns, cost and access remain limitations.[60,61,64,84] In effort to improve drug biodistribution and global use, LASER ART was created. It employs a prodrug approach to incorporate ARVs into nanocrystals generating sustained plasma drug concentrations with efficient tissue and cell reservoir delivery.[67,70,71,76]

Our present studies focused on the synthesis, nanoformulation, and characterization of a myristoylated RPV (M3RPV). Prodrug modification transiently changes the structure of a compound to achieve a specific goal, such as alteration of physicochemical or pharmacokinetic properties.[69] RPV is a poorly soluble

diarylpyrimidine (DAPY) derivative extensively studied as a LA formulation (RPV-LA).[37-39] Previous research has demonstrated that synthesizing hydrophobic prodrugs of inherently low solubility compounds can be beneficial, particularly by increasing the apparent half-life and/or enhancing tissue distribution. [70,71,97,98] M3RPV was manufactured as a LA nanoparticle coined as NM3RPV using high-pressure homogenization. For comparison, we best replicated RPV-LA, with the manufacture of NRPV. In particular, we used the same surfactant (P338), generating particles of 277 nm, similar to the 200 nm RPV-LA formulations.[37,39] Both preparations use top-down approaches for manufacture.[37,39]

Stability is important for clinical translation. NM3RPV demonstrated exceptional physicochemical stability at 4° and 37°C over a period of 100 days. Furthermore, injectable formulations must provide repeatable PK results months after initial manufacture. In our studies, NM3RPV provided congruent RPV concentrations in mice plasma after injection with both new and aged formulations. Drug delivery to viral reservoirs remains a challenge.[99,100] LA injectable formulations are designed to generate slow dissolution depots at the injection site. Furthermore, infiltrating macrophages have been observed sequestering nanocrystals at the injection site facilitating their biodistribution.[71,101] These cells are phagocytic and highly mobile.[102] In particular, macrophages have large cytoplasmic volumes, such that phagocytized drug nanocrystals can be stored extended time periods.[67,70,103] Therefore, nanocrystals can develop a cell based tissue depot, but also more efficiently deliver drug to sites of viral infection. Prodrug modifications, particularly those that increase lipophilicity, have been observed to increase macrophage drug uptake and retention.[70,71,75,76] In our work, NM3RPV and NRPV both readily enter macrophages, but only NM3RPV is retained for a significant period of time, indicating that NM3RPV may establish a secondary tissue depot for RPV.

Prodrug modification not only significantly alters a compound's physicochemical properties, but also its pharmacokinetics and biodistribution.[104] In our studies, NM3RPV generated substantial differences in the duration of plasma exposure, as well as tissue distribution when compared to NRPV. We treated mice with 100 mg/kg RPV-eq. To mirror the human equivalent dose administered in clinical trials.[28,56] Prodrug modification provided a shallow plasma RPV decay curve and sustained RPV concentrations 48 weeks after injection. Specifically, RPV concentrations were above the proposed PA-IC$_{90}$ (12.5 ng/mL) for 25 weeks after administration. These results are significant when compared with 7 weeks above the PA-IC$_{90}$ observed with NRPV. Clinical trials demonstrating viral suppression with RPV-LA and CAB-LA injections every 8 weeks observed C$_{trough}$ RPV concentrations of 64 ng/mL or ~ 5 times the PA-IC$_{90}$.[28] In addition, viral breakthrough was observed in a patient after accidental HIV-1 exposure 41 days after RPV LA injection (300 mg) exhibiting approximately 10.5 ng/mL RPV in plasma on the day of exposure.[105] Therefore, future work must focus on increasing RPV plasma concentrations to at least the RPV-LA C$_{trough}$ by optimizing dosing schedules or affecting prodrug structure.

Furthermore, administration of 45 mg/kg RPV-eq. of NM3RPV to rhesus macaques resulted in sustained levels of M3RPV in the plasma over the course of 44 weeks, but provided low levels of active RPV, which quickly fell below the PA-IC$_{90}$. We observed a similar ratio of M3RPV:RPV in the plasma 24 hours after injection compared to our mice studies. Specifically, 24 hours after injection mice and rhesus macaques exhibited a M3RPV:RPV ratio of 12.4 and 10.2, respectively. Interestingly 2 weeks later, the M3RPV:RPV ratio fell to 0.19 in mice, but remained higher (6.8) in rhesus macaques. We hypothesize the stability of M3RPV in monkeys paralleled our plasma in-vitro cleavage studies where stark differences in prodrug bioconversion were observed between species (mouse and rhesus macaque). Observed differences in cleavage

kinetics may be due to the lack of abundant carboxylesterases observed in monkey, dog, and/or human plasma that are abundant in rodents.[106,107] Therefore studies focused on the specific mechanism and enzymes responsible for prodrug bioconversion are warranted.

Impending research directives will investigate formulations of shorter chain RPV prodrugs (M1RPV, M2RPV) in rhesus macaques in order to achieve more efficient prodrug bioconversion to RPV. LASER-ART employs hydrophobic and lipophilic prodrugs to enrich tissue distribution, particularly to sites of viral infection. In our mice studies, NM3RPV generated tissue depots in the lymph nodes, spleen, and liver, whereby substantial prodrug concentrations were observed 46 weeks after injection (26,941, 674, 220 ng/g, respectively). We posit that the prodrug tissue depots, coupled with the slow cleavage kinetics of M3RPV, provided sustained RPV concentrations not only in the plasma, but in tissues (spleen, lymph node, liver, gut, kidney) where RPV was still detectable 46 weeks after treatment. These findings provide significant improvements in the long-term distributions of RPV to tissues important in viral replication. Importantly, rhesus macaques also retained relevant concentrations of both M3RPV and RPV in the lymph nodes 204 days after injection.

In our studies investigating PrEP in CD34+ humanized mice we did not observe any protection from NM3RPV treatment, even with RPV plasma concentrations of more than 2x the PA-IC$_{90}$ a the time of viral challenge. Previous studies investigating RPV LA in mice models of HIV-1 infection have produced varying results. Specifically, RPV LA-dosed bone marrow lymphoid thymus (BLT) mice (300; 600 mg/kg) were challenged vaginally with HIV-1$_{CH040}$ one week after treatment and had successfully suppressed virus during the course of study.[108] While protection was observed, the treatment dose was not clinically relevant was 3-6 times higher than the dose given in our study. Additionally, they used a mucosal infection model compared with our IP viral inoculation.

Furthermore, studies in humanized CD45+ mice combined 3TC, TDF, and RPV LA to successfully suppress virus.[109] Moreover, upon viral suppression, animals were maintained on RPV LA (160 mg/kg) monotherapy, and viral rebound occurred. These studies help to frame our reported PrEP studies in context and understand the challenges and limitations of each model system when studying HIV-1 infection in mice.

In conclusion, LA ART is a significant step forward in the field of HIV-1 therapeutics. In particular, RPV LA has garnered excitement with its success coupled with CAB-LA in phase 3 clinical trials. In our studies, we aimed to generate a LASER-ART formulation of RPV by generating a series of hydrophobic prodrugs in an attempt to increase its tissue distribution and apparent half-life. Our studies provide an excellent proof-of-concept that nanoformulated prodrugs of RPV can provide sustained release of RPV and the generation of a significant secondary tissue depot. Further work studying prodrug bioconversion, PK, pharmacodynamics (PD), and injection schedules are required.

3.6 Figures

A

B
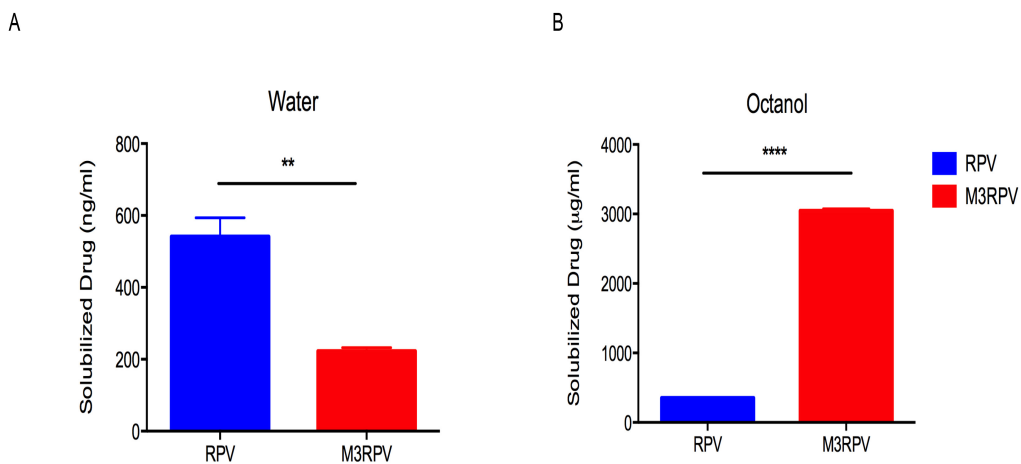
Figure 3.6.1 M3RPV Solubility.

(A) Water and (B) 1-octanol solubility of M3RPV and RPV was measured following 24 hours incubation. Data expressed as mean ± SEM for n=3 replicates (** = P < 0.01, **** = P < 0.0001)
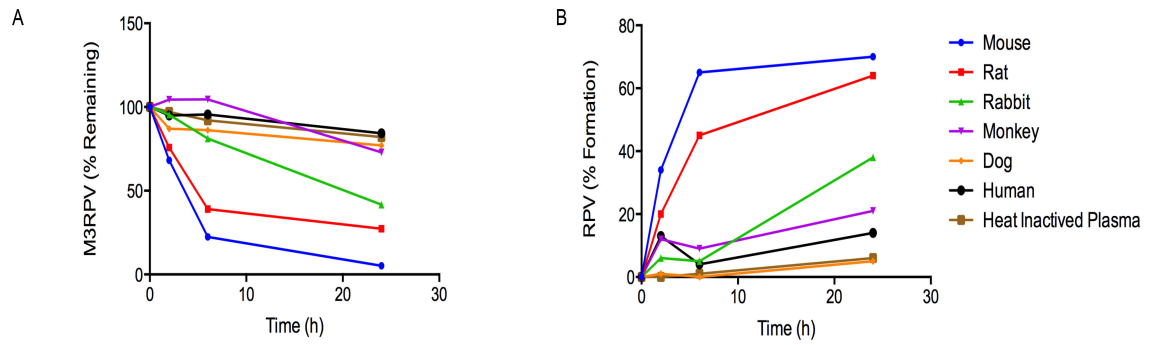
Figure 3.6.2 M3RPV Cleavage Kinetics.

Plasma cleavage kinetics of M3RPV was tested in various species (mouse, rat, rabbit, monkey, dog, and human) and **(A)** measured as loss of M3RPV, as well as **(B)** formation of RPV.
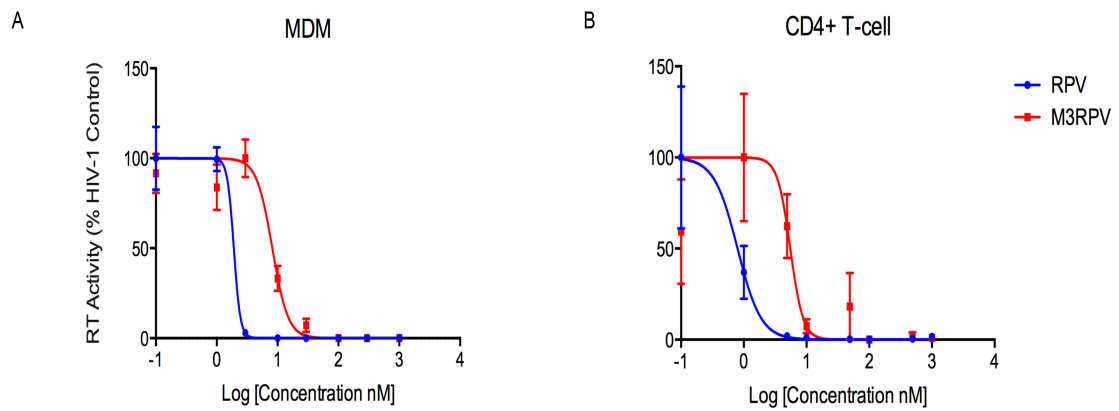
Figure 3.6.3 M3RPV Antiviral Activity.

Antiviral activity of M3RPV and RPV in **(A)** MDM and **(B)** CEM-CD4+ T-cells was assessed at a range of concentrations (0.1-1000 nm) and determined by RT activity after viral challenge with HIV-1$_{ADA}$ (MOI 0.1). Data was normalized and expressed as percentage of HIV-1 control (mean ± SEM) with a minimum of 3 biological replicates.
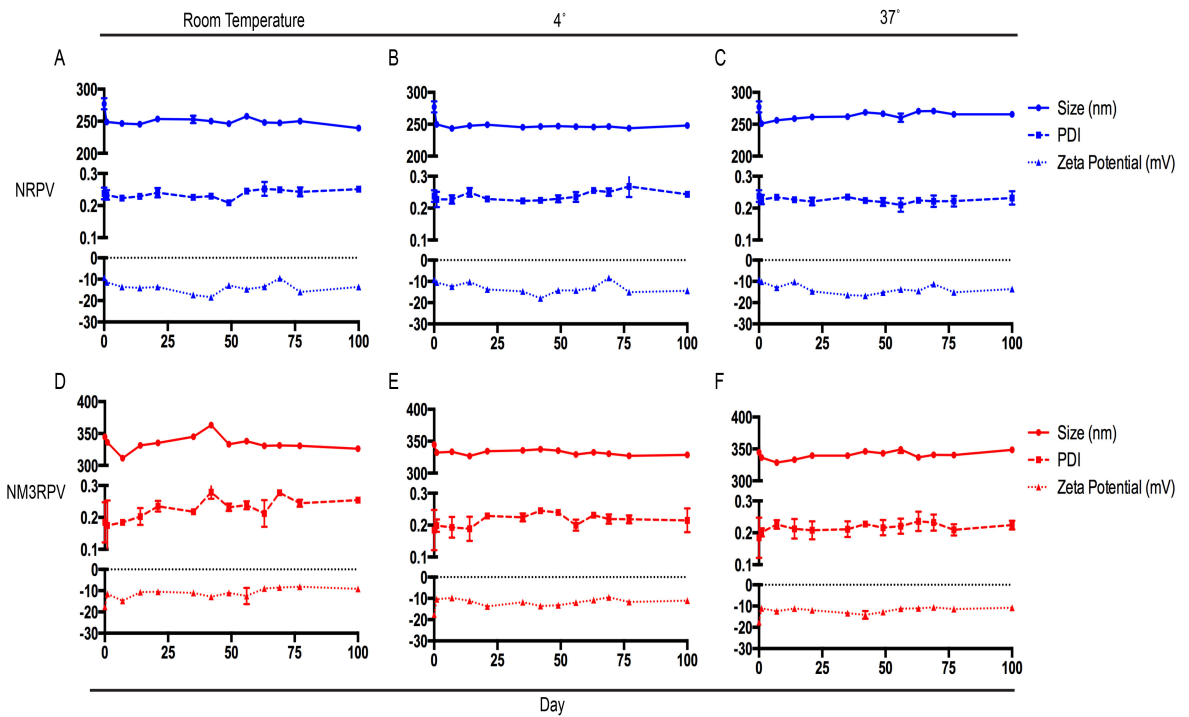
Figure 3.6.4 Physicochemical stability NM3RPV and NRPV.

(A-C) Physicochemical stability of NRPV and **(D-F)** NM3RPV were evaluated for size (nm), polydispersity (PDI), and zeta potential (mV) at multiple temperatures (RT, 4, 37°) across 100 days. Data is expressed at mean ± SD for n=3 measurements.
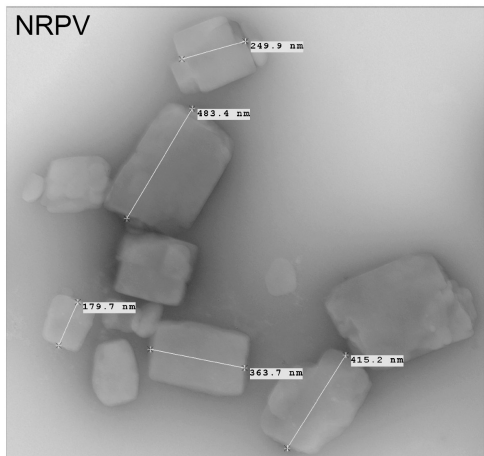
G   H
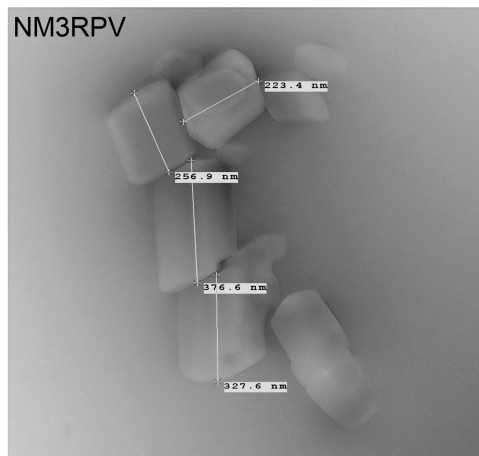
Figure 3.6.5 Morphology of NM3RPV and NRPV.

Transmission electron microscopy (TEM) provided a morphological assessment of NRPV **(G)** and NM3RPV **(H)**.

A

B
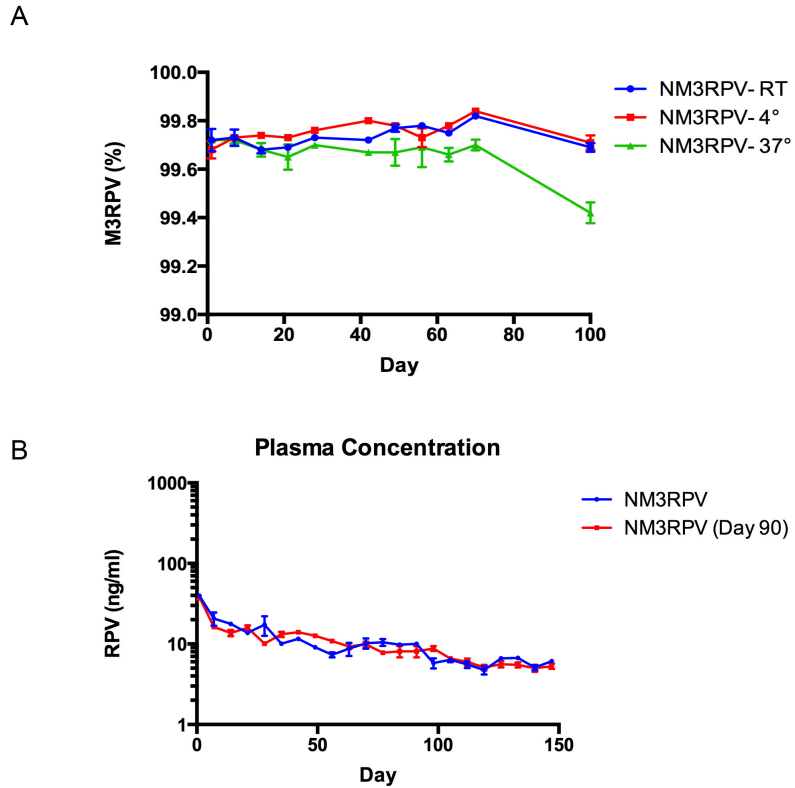
Figure 3.6.6. NM3RPV prodrug stability and PK reproducibility.

(A) Prodrug stability within nanoformulated M3RPV (NM3RPV) was determined by analyzing the ratio of M3PRV to RPV in NM3RPV over a period of 100 days. Data expressed at mean ± SEM for n=3 measurements. (**B**) *BALB c/J* mice were administered NM3RPV (45 mg/kg RPV eq.) upon initial manufacture and after 90 days of storage to determine the pharmacokinetic reproducibility of NM3RPV. Data are expresses as mean ± SEM of n=4 animals.
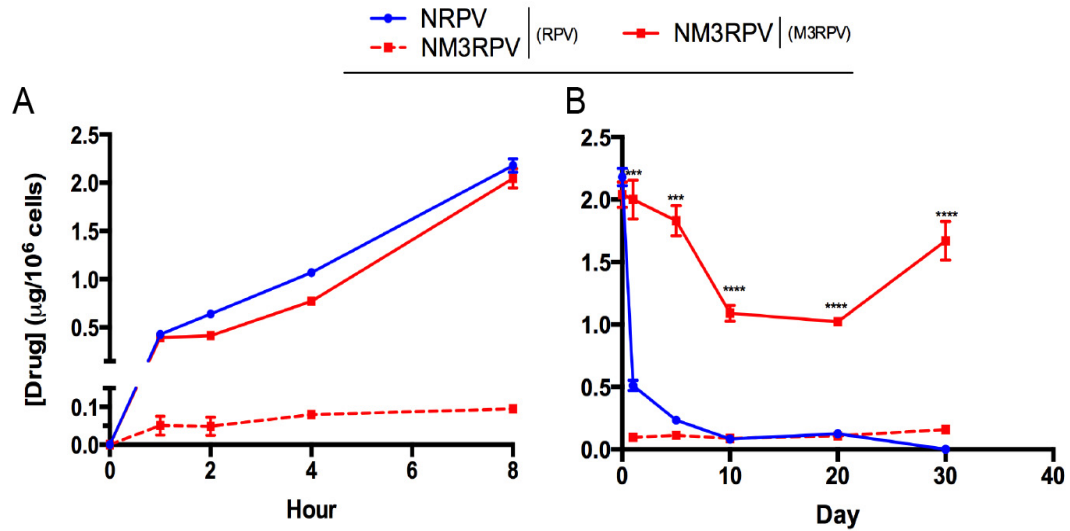
Figure 3.6.7 In-vitro characterization of NM3RPV in human macrophages (10 µM).

Nanoformulation uptake and retention was assessed in human MDMs. Specifically, NM3RPV and NRPV were evaluated for uptake **(A)** and retention **(B)** of intracellular RPV and M3RPV at a concentration of 10 µM. Data is expressed as mean ± SEM with n=3 biological replicates (* $P < 0.05$, ** $P < 0.01$, *** $P < 0.001$, **** $P < 0.0001$ as determined by Student's *t* test.)

A

B

Day
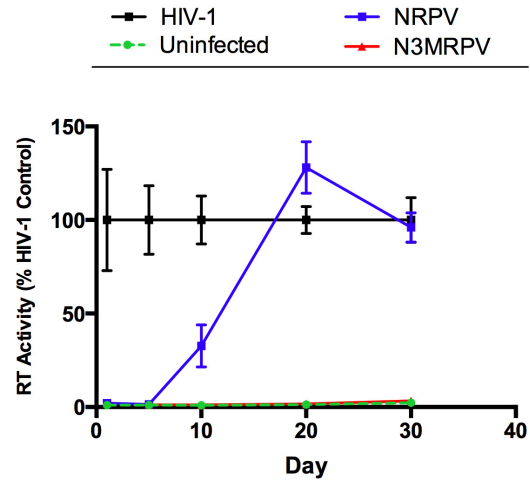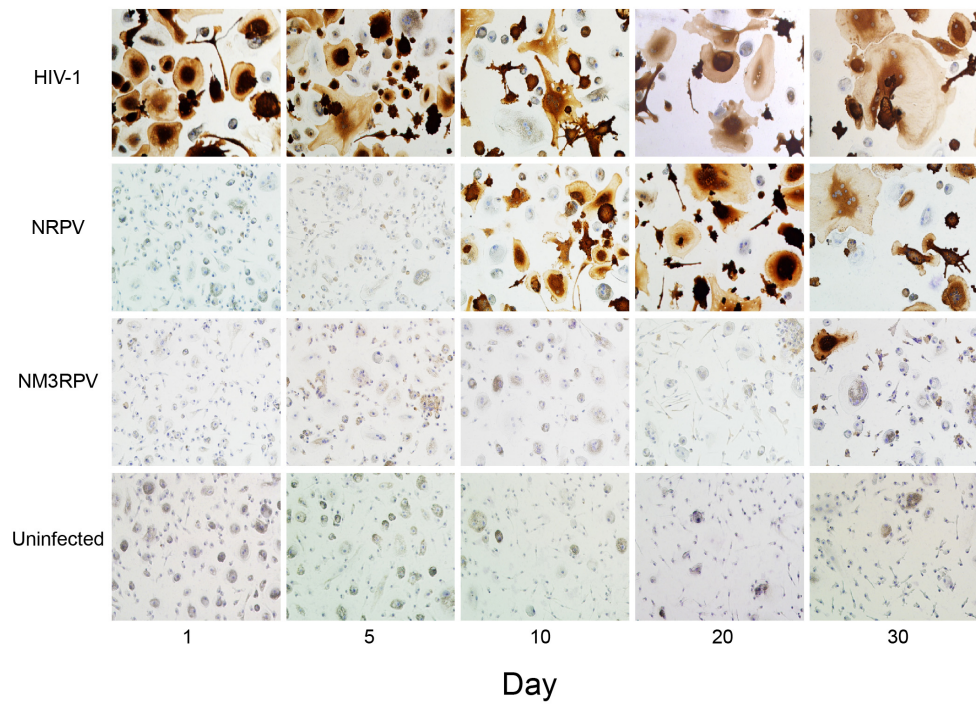
Figure 3.6.8 Long-term antiretroviral efficacy in MDMs (10 µM).

Long-term antiretroviral efficacy of NM3RPV and NRPV was examined after a single treatment of 10 µM for 8 hours, followed by HIV-1$_{ADA}$ challenge up to 30 days post treatment. Infection was characterized by RT activity **(A)** and HIV P24 antigen expression **(B)**. RT activity data was normalized as a percentage of HIV-1 positive control and expressed as mean ± SEM with n=4 biological replicates. Representative images of MDMs stained for HIV-1 p-24 antigen expression are shown.
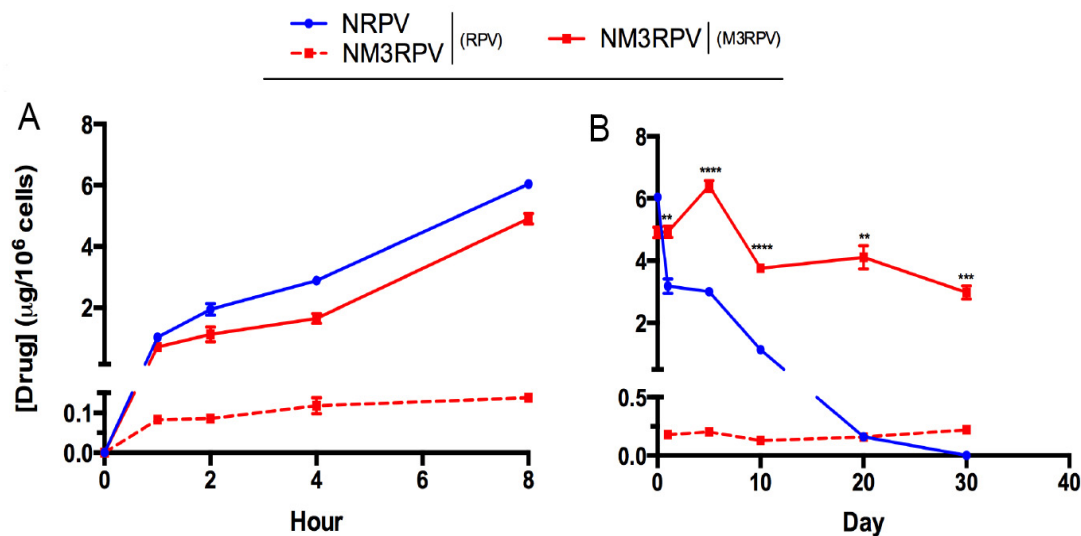
Figure 3.6.9 In-vitro characterization of NM3RPV in MDM (30 µM).

Nanoformulation uptake and retention was assessed in MDMs. Specifically, NM3RPV and NRPV was evaluated for uptake **(A)** and retention **(B)** of intracellular RPV and M3RPV at a concentration of 30 µM. Data is expressed as mean ± SEM with n=3 biological replicates (* $P < 0.05$, ** $P < 0.01$, *** $P < 0.001$, **** $P < 0.0001$ as determined by Student's *t* test.)

A

B
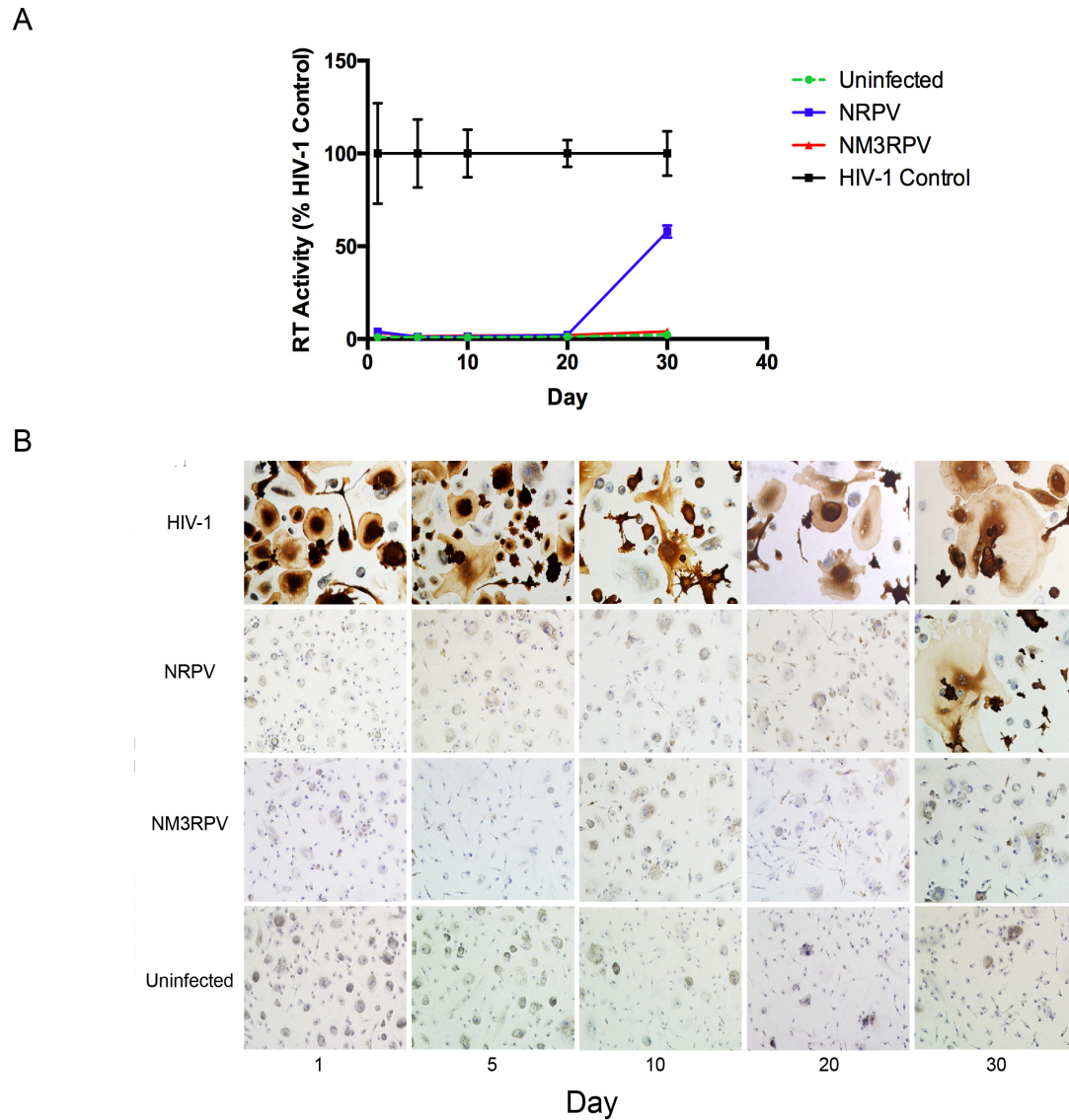
Figure 3.6.10 Long-term antiretroviral efficacy in MDMs (30 µM).

Long-term antiretroviral efficacy of NM3RPV and NRPV was examined after single treatment of 30 µM for 8 hours, followed by HIV-1$_{ADA}$ challenge up to 30 days post treatment. Infection was characterized by RT activity **(A)** and HIV-1 p-24 antigen expression **(B).** RT activity data was normalized as a percentage of HIV-1 positive control and expressed as mean ± SEM with n=4 biological replicates. Representative images of MDMs stained for HIV-1 p-24 antigen expression are shown.

Figure 3.6.11 Murine plasma RPV concentration (45 mg/kg)

Male *BALB/cJ* mice were administered a single IM injection of NM3RPV or NRPV at 45 mg/kg RPV-eq. Plasma RPV concentrations were determined by UPLC-MS/MS. Data is expressed as mean ± SEM for n = 4/5 .

Figure 3.6.12 Murine RPV tissue distribution (45 mg/kg)

Male *BALB/cJ* mice were administered a single IM injection of NM3RPV or NRPV at 45 mg/kg RPV-eq. Tissue biodistribution of RPV was assessed 56 and 323 days after injection in the spleen, lymph node, liver, gut and kidney. Data is expressed as mean ± SEM for n = 4/5 (**** *P* < 0.0001, *** *P* < 0.001, ** *P* < 0.01, * *P* < 0.05. # *P* < 0.1 by Student's *t* test).

Figure 3.6.13 Murine M3RPV tissue distribution (45 mg/kg)

Male *BALB/cJ* mice were administered a single IM injection of NM3RPV or NRPV at 45 RPV-eq. Tissue biodistribution of M3RPV was assessed 56 and 323 days after injection in the spleen, lymph node, liver, gut and kidney. Data is expressed as mean ± SEM where n = 4/5 biological replicates
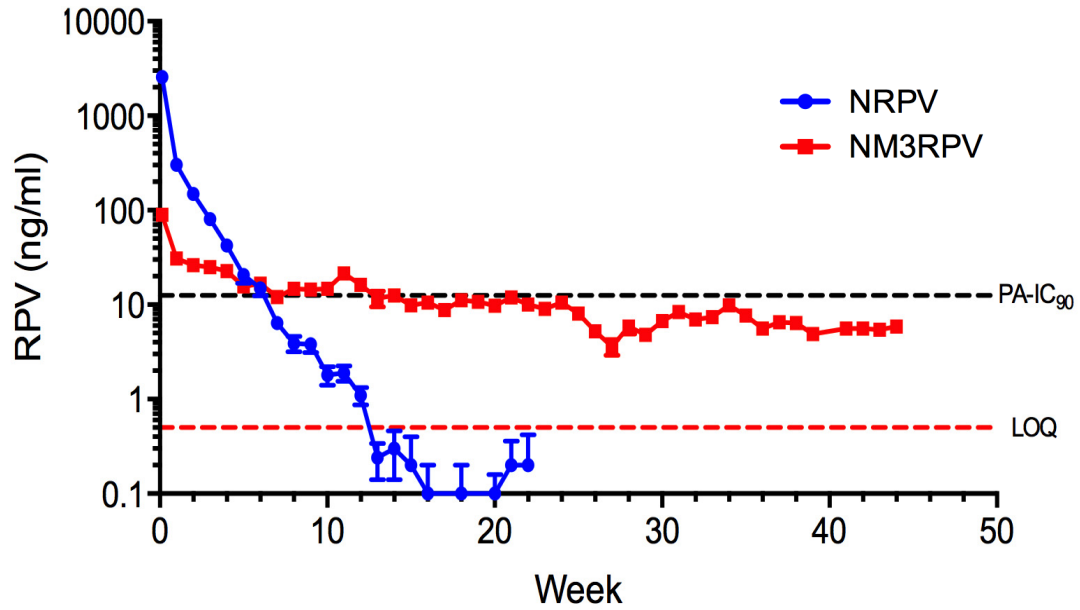
Figure 3.6.14 Murine plasma RPV concentrations (75 mg/kg)

Male *BALB/cJ* mice were administered a single IM injection of NM3RPV or NRPV at 75 mg/kg RPV-eq. Plasma RPV concentrations were determined by UPLC-MS/MS. Data is expressed as mean ± SEM where n ≥ 4 biological replicates.
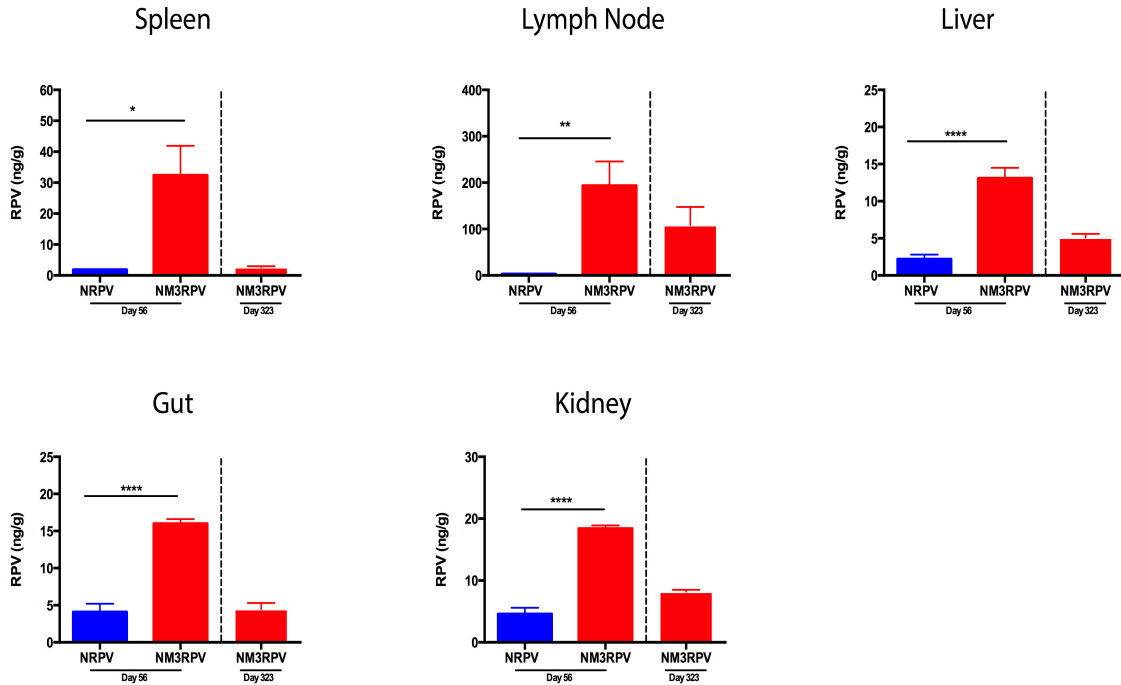
Figure 3.6.15 Murine RPV tissue distribution (75 mg/kg)

Male *BALB/cJ* mice were administered a single IM injection of NM3RPV or NRPV at 75 RPV-eq. Tissue biodistribution of RPV was assessed 56 and 323 days after injection in the spleen, lymph node, liver, gut and kidney. Data is expressed as mean ± SEM where n ≥ 4 biological replicates (**** $P < 0.0001$, *** $P < 0.001$, ** $P < 0.01$, * $P < 0.05$. # $P < 0.1$ by Student's *t* test).
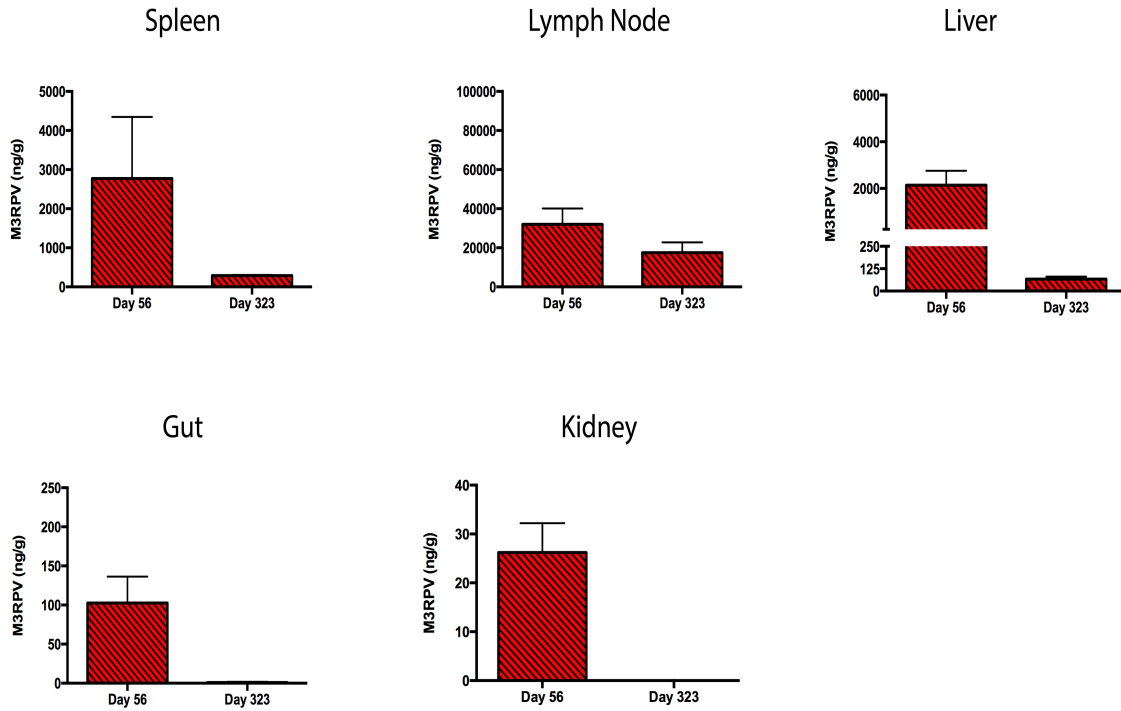
Figure 3.6.16 Murine M3RPV tissue distribution (75 mg/kg)

Male *BALB/cJ* mice were administered a single IM injection of NM3RPV or NRPV at 75 RPV-eq. Tissue biodistribution of M3RPV was assessed 56 and 323 days after injection in the spleen, lymph node, liver, gut and kidney. Data is expressed as mean ± SEM where n ≥ 4 biological replicates
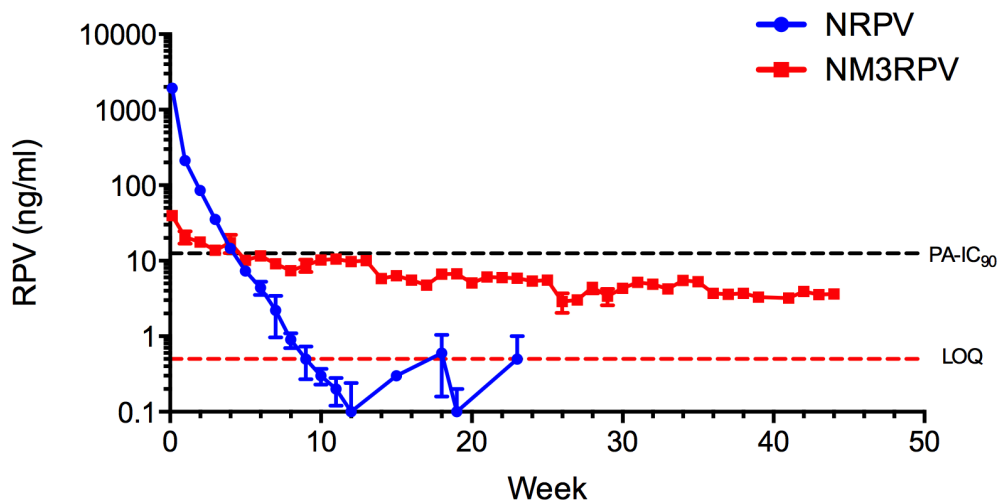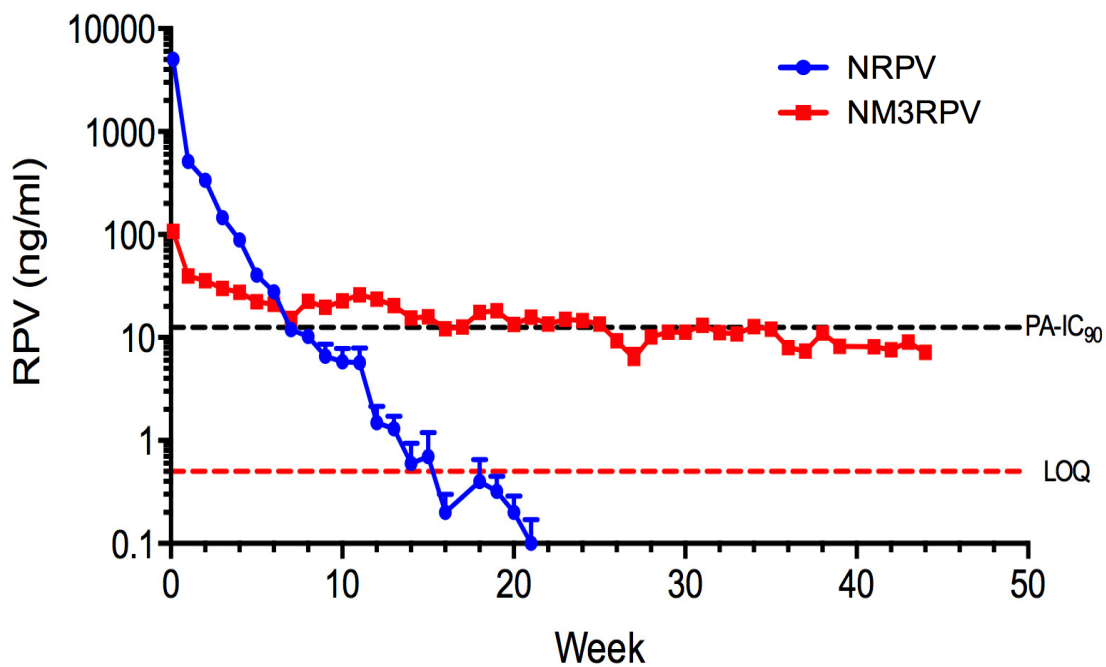
Figure 3.6.17 Murine plasma RPV concentration (100 mg/kg)

Male *BALB/cJ* mice were administered a single IM injection of NM3RPV or NRPV at 100 mg/kg RPV-eq. Plasma RPV concentrations were determined by UPLC-MS/MS. Data is expressed as mean ± SEM where n ≥ 4 biological replicates.
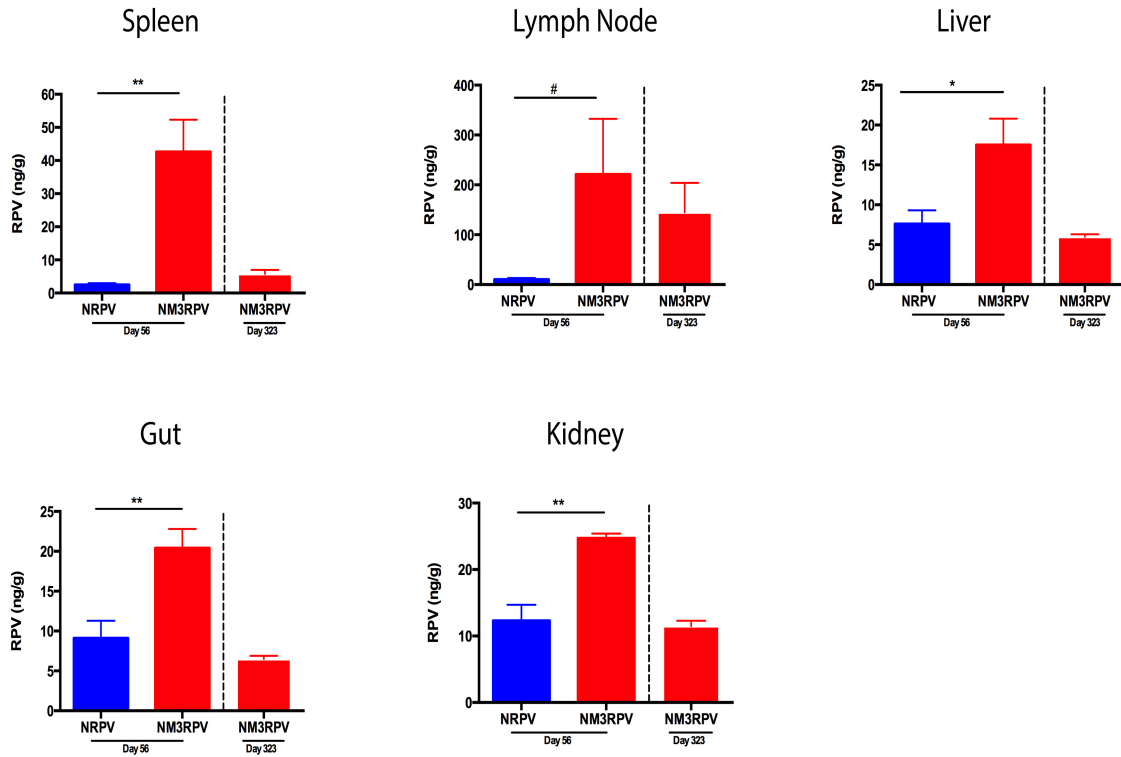
Figure 3.6.18 Murine RPV tissue distribution (100 mg/kg)

Male *BALB/cJ* mice were administered a single IM injection of NM3RPV or NRPV at 100 RPV-eq. Tissue biodistribution of RPV was assessed 56 and 323 days after injection in the spleen, lymph node, liver, gut and kidney. Data is expressed as mean ± SEM where n ≥ 4 biological replicates (**** $P < 0.0001$, *** $P < 0.001$, ** $P < 0.01$, * $P < 0.05$. # $P < 0.1$ by Student's *t* test).
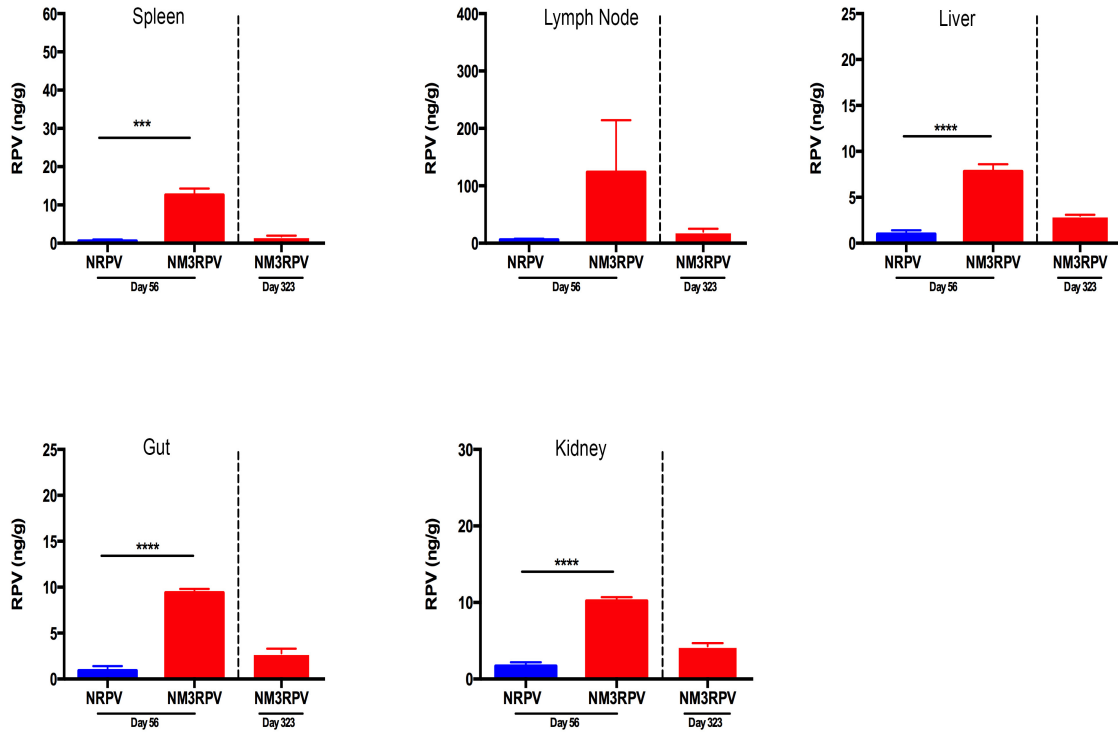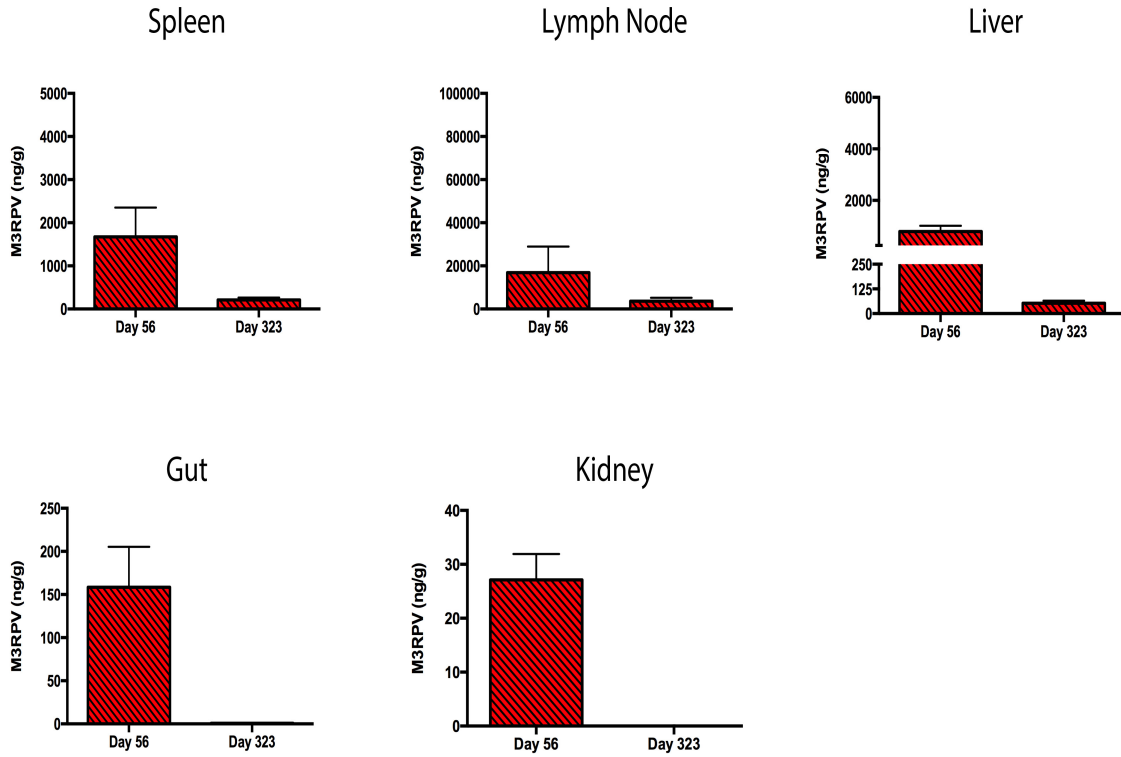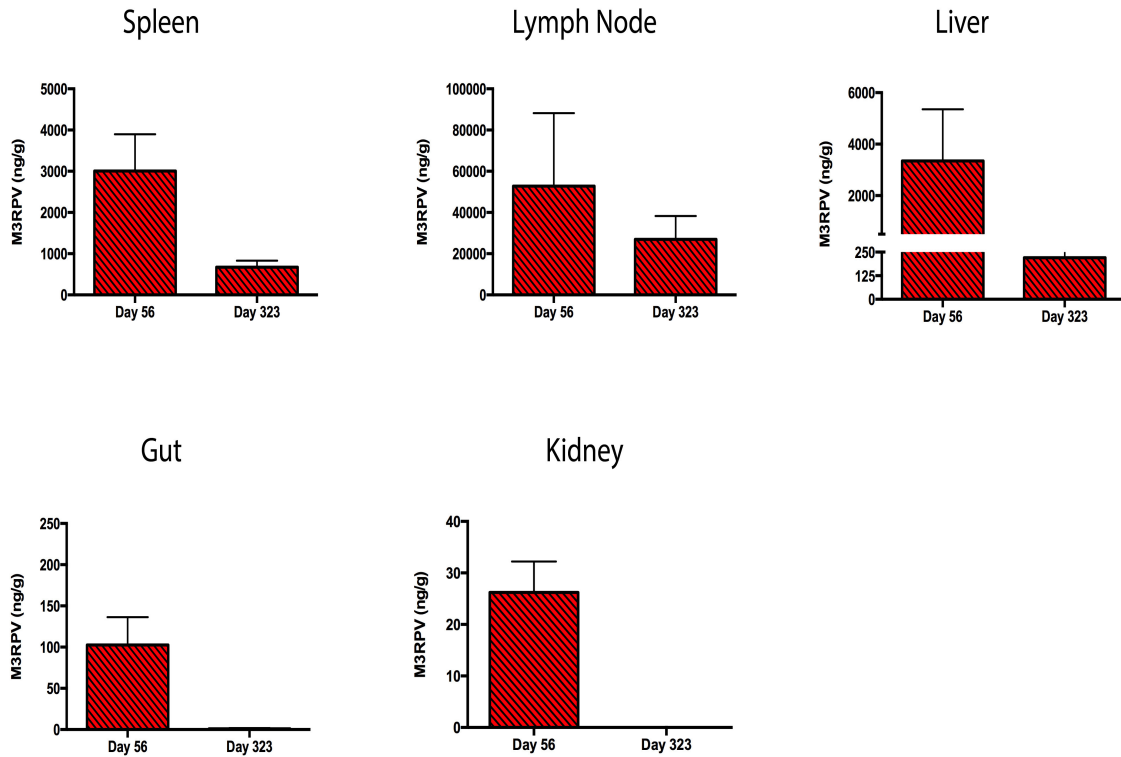
Figure 3.6.19 Murine M3RPV tissue distribution (100 mg/kg)

Male *BALB/cJ* mice were administered a single IM injection of NM3RPV or NRPV at 100 RPV-eq. Tissue biodistribution of M3RPV was assessed 56 and 323 days after injection in the spleen, lymph node, liver, gut and kidney. Data is expressed as mean ± SEM where n ≥ 4 biological replicates

85
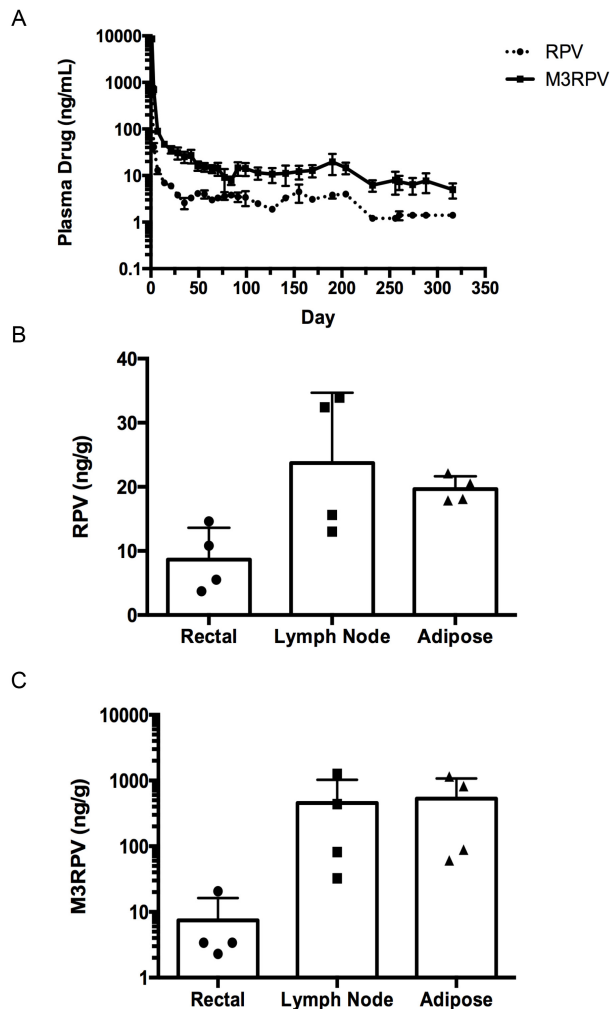
Figure 3.6.20 Rhesus macaque RPV and M3RPV plasma and tissue distribution.

Four rhesus macaques were administered 45 mg/kg RPV eq. of NM3RPV by a single intramuscular injection. **(A)** Plasma samples were collected and assayed for RPV and NM3RPV throughout the course of study (316 days). Additionally, rectal, lymph node, and adipose tissue biopsies were collected 204 days after drug administration. Tissue samples were assayed for RPV **(B)** and NM3RPV **(C)** content. Both plasma and tissue drug concentrations were determined by UPLC-MS/MS. Data is expressed as mean ± SEM where n = 4 biological replicates.

A
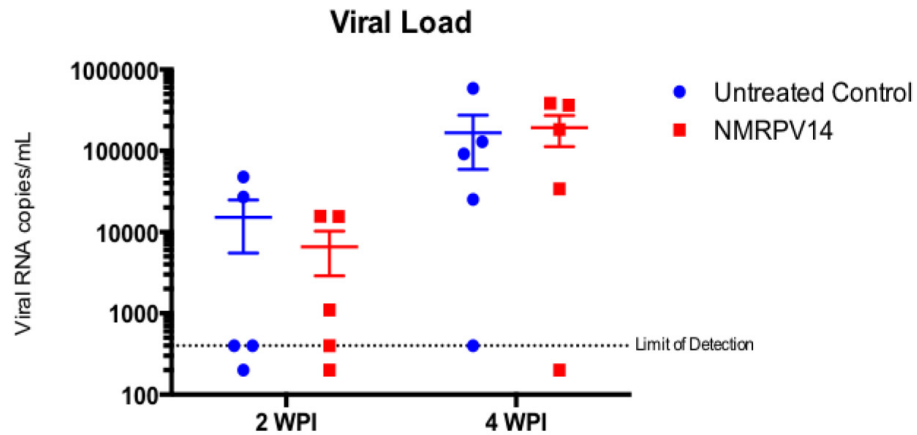
B
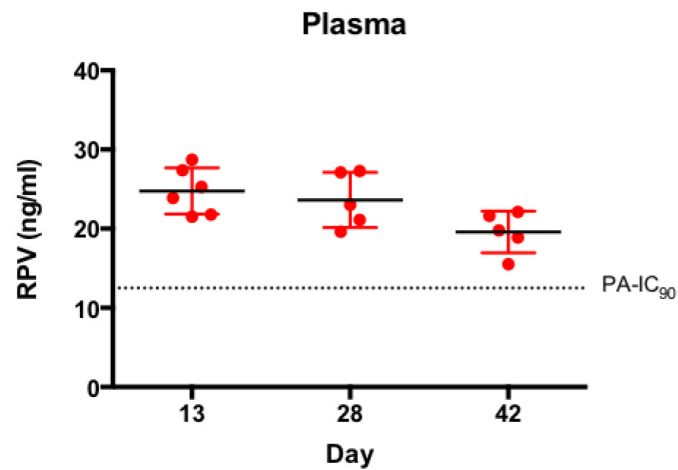
Figure 3.6.21 NM3RPV humanized mice PrEP study.

CD34+ humanized mice were administered 100 mg/kg RPV eq. NM3RPV and subsequently challenged with HIV-1$_{ADA}$ 2 weeks after drug treatment. Animals without treatment served as HIV-1+ controls. (A) Plasma viral loads analyzed 2 and 4were detected for each condition. (B) Plasma collected from NM3RPV treated animals were analyzed by UPLC-MS/MS to quantify RPV concentrations 13, 28, and 42 days after injection.

3.7 Tables

PK Parameters	NRPV 45 mg/kg	NM3RPV 45 mg/kg	NRPV 75 mg/kg	NM3RPV 75 mg/kg	NRPV 100 mg/kg	NM3RPV 100 mg/kg
λz (h^{-1})	0.1040	0.0058	0.0729	0.0050	0.0686	0.0050
$t_{1/2}$ (day)	6.7	119.2	9.5	137.7	10.1	139.8
$MRT_{0-\infty}$ (day)	5.6	174.9	8.4	215.9	8.3	221.5

Table 3.7.1 PK parameters

Non-compartmental PK analysis of NM3RPV and NRPV doses at 45, 75, and 100 mg/kg RPV eq. in BALB/cJ mice.

CHAPTER 4

THE POTENTIAL APPLICATION OF MVC AS A LA THERAPUETIC

4.1 Abstract

MVC (MVC; Selzentry) is a well-known CCR5 co-receptor antagonist used as part of combination antiretroviral therapy (cART) for HIV-1 infected people with CCR5-tropic (R5) virus. A twice-daily dosing regimen, low bioavailability, and rapid metabolism limit its maximal efficacy. We sought to overcome known limitations of MVC by developing a LA parenteral formulation. A variety of formulation techniques ranging from polymeric nanoparticles to solid drug nanosuspensions were employed to facilitate extended release of MVC. Additionally, prodrugs and hydrophobic salts were generated to aid nanoparticle development. Multiple nanoformulations and prodrugs were produced for MVC, although a functional LA MVC formulation is still elusive and will require further study.

4.2 Introduction

ART provides sustained suppression of HIV replication, restoration of immune function, and reduction in disease morbidity and mortality. Strict life-long adherence is required to achieve the effects of ART. Particularly, in the context of PrEP, adherence is essential as drug concentrations strongly correlate to protection.[110] Unfortunately, even in clinical setting, adherence is remarkably low.[111] Thus, the potential use of LA therapy

for PrEP is currently being researched.[83] Among prospective drug candidates for LA PrEP is maraviroc (MVC). Acting as a CCR5 inhibitor, MVC prevents viral entry of R5 tropic strains of HIV-1 that are most commonly encountered during infection. Furthermore, MVC is readily distributed to vaginal and rectal tissue, and can also be found in semen after oral administration.[42,43] MVC oral regimens require twice-daily 150-600 mg doses depending on whether patients are receiving a CYP3A inducer or inhibitor.[112] Therefore to simplify treatment and generate a better dosage form for PrEP, our studies focused on prodrug and hydrophobic salt synthesis for successful development of a LA MVC therapy. We successfully synthesized two distinct MVC prodrugs (MVC14; MVC-PRO), a hydrophobic salt (MVC-PA), and a multitude of diverse nanoformulations. Ultimately, a LA MVC amenable for PrEP remained elusive and will require further research.

4.3 Materials and Methods

4.3.1 Reagents

Maraviroc (MVC) was a generous gift from ViiV Healthcare (Research Triangle Park, NC). Dichloromethane (DCM), tetrahydrofuran (THF), *N,N*-dimethylformamide (DMF), Chloroform, sodium bis(trimethylsilyl) amide (NaHMDS,1 M in THF), hexanes, ethyl acetate, dimethyl sulfoxide (DMSO), myristoyl chloride, pamoic acid, zinc chloride ($ZnCl_2$), sodium iodide (NaI), deuterated chloroform, celite, *tert*-Butylmagnesium chloride (1.0 M in THF), ciprofloxacin, paraformaldehyde (PFA), 3,3'-diaminobenzidine (DAB) and Pluronic F127 (P407) was purchased from Sigma-Aldrich (St. Louis, MO). Heptyl chloroformate was purchased from Boc Sciences (Shirley, NY). 1,2-distearoyl-syn-glycero-3-phosphocholine (DSPC), 1,2-distearoyl-sn-glycero-3-phospho-(1'rac-glycerol) (DSPG), and 1,2-distaroyl-syn-glycero-3-phosphoethanolamine-N-

[methoxy(polyethylene glycol)-2000] (DSPE-PEG$_{2000}$) were purchased from Avanti Polar Lipids, Inc. (Alabaster, AL). Acetonitrile (ACN), methanol (MeOH), cell-culture grade water (endotoxin-free), KH$_2$PO$_4$, bovine serum albumin (BSA), Triton X-100, and gentamicin were purchased from Fisher Scientific (Hampton, NH). Flash column chromatography was performed on 32-63 μm flash silica gels, while thin layer chromatography utilized pre-coated silica plates (250 μm, F-254) both from SiliCycle Inc. (Quebec, Canada) and Dulbecco's Modified Eagle Medium (DMEM) were purchased from Corning Life Sciences (Tewksbury, MA). Polymer-based HRP-conjugated anti-mouse Envision+ secondary antibody was purchased from Dako (Carpinteria, CA).

4.3.2 MVC Hydrophobic salt formation

MVC and pamoic acid (PA) were added to separate glass beakers and stirred in water at 40°C to form a suspension. Next, hydrochloric acid (HCL; 3M) was added dropwise to the MVC suspension until all MVC was dissolved resulting in a clear solution. Furthermore, sodium hydroxide (NaOH; 3M) was added dropwise to the PA mixture until complete solubilization yielded a clear yellow liquid. Subsequently, the solubilized MVC solution was added to the PA solution in a dropwise manner. Upon addition an immediate precipitate formed and the mixture was stirred for an additional 30 min at RT. Next, the mixture containing MVC:PA salt was centrifuged (10,000 *g* for 30 min) and subsequently washed with water. Collected pellets were dried and lyophilized to yield a fine yellow powder.

4.3.3 Manufacture of nanoformulated MVC (nMVC)

Single emulsion solvent evaporation was used to nanoformulate MVC. Specifically, DSPC, DSPE-PEG$_{2000}$, and DSPG (7:1:0.7 molar ratio) were dissolved in chloroform and subsequently evaporated to generate a thin film at the bottom of the

glass vial. Samples were dried in a desiccator for a minimum of 2 hours before being resuspended with water. Poly(lactic-co-glycolic) acid (PLGA; 75:25) and MVC were dissolved in DCM and added to the aqueous solution of hydrated lipids. Next, samples were sonicated in an ice bath for 7 minutes followed by rotary evaporation to remove organic solvent (DCM). Following evaporation, formulations were centrifuged at 5,000 g for 5 min, followed by 10,000 g for 15 min. The resultant pellets were resuspended with water and centrifuged at 200 g for 3 min to yield the final nanoformulation. nMVC was characterized by dynamic light scattering (DLS, Malvern Nano-ZS, Worcestershire, UK) for size (nm), polydispersity (PDI), and zeta potential (mV) and analyzed for drug content as described below.

4.3.4 Synthesis of chloromethyl tetradecanoate

Myristoyl chloride was reacted with 1.0 equivalent (eq.) PFA and 0.025 eq. $ZnCl_2$ under reflux conditions for up to 16 hours. The reaction mixture was then cooled to RT and partitioned between DCM and saturated aqueous sodium bicarbonate in a separatory funnel. The aqueous layer was back-extracted twice with DCM. Organic extracts were combined, washed with brine and dried from sodium sulfate. The solvents were evaporated on a rotary evaporator followed by isolation of the desired compound using silica column chromatography eluting with a mobile phase of 9:1 hexanes-ethyl acetate.

4.3.5 Synthesis of iodomethyl tetradecanoate

Chloromethyl tetradecanoate (1 eq.) and NaI (2.5 eq.) were dissolved in a 2:1 mixture of ACN/DCM under an argon atmosphere. The reaction proceeded for 90 hours at RT under light protection. Upon completion, the mixture was concentrated and partitioned between DCM and water. The aqueous layer was further extracted with DCM

followed by sequential washing of the combined organic extracts with saturated sodium bicarbonate and brine. The sample solution was then dried from sodium sulfate, concentrated and purified by silica column chromatography eluting with 9:1 hexanes-ethyl acetate.

4.3.6 Synthesis of MVC-14

Briefly, NaHMDS (2.0 eq.) was dissolved in anhydrous THF and cooled to 0°C on ice. Next, a solution of MVC (1.0 eq.) in THF was slowly added to the reaction mixture and allowed to warm to RT over the course of 30 min under argon atmosphere. Next, iodomethyl tetradecanoate (3.0 eq.) was added slowly to the reaction over the course of 5 min. The reaction continued at 60°C under reflux conditions for at least 48 hours. Upon completion, the reaction was cooled to 0°C and quenched with saturated NH_4Cl. Next, the reaction mixture was extracted between DCM and brine. The aqueous layer was washed twice with DCM. Afterwards, combined organic layers were washed with water and subsequently dried from sodium sulfate and concentrated by rotary evaporation. MVC-14 was purified by silica column chromatography using a mobile phase of 9:1 DCM:MeOH. Purified product was collected, dried, and analyzed by ^1H NMR yielding brown colored oil. Furthermore, MVC-14 oil was dissolved in MeOH (60°C) and stirred in the presence of carbon/10% palladium for 10 min. Next, the sample was filtered through celite and dried to yield a sticky solid. Precipitation in hexanes yielded a white solid.

4.3.7 Synthesis of MVC-PRO

MVC was suspended in anhydrous toluene, evaporated, and dried on a lyophilizer for at least 16 hours. Next, MVC was dissolved in anhydrous THF and cooled to -78°C in a dry ice/acetone bath under argon atmosphere. Thereafter, tert-butyl magnesium chloride (2.0 eq.) was added to the reaction mixture dropwise and mixed for

10 min. Heptyl chloroformate (1.1 eq.) was subsequently added dropwise and the reaction was allowed to warm to RT over time and ultimately proceeded for a minimum of 16 hours. MVC-PRO was purified by silica column chromatography and the isolated product analyzed by ^{1}H NMR to confirm chemical modification.

4.3.8 Nanoformulation of MVC-PA and MVC-PRO

Nanoformulations of MVC-PA (L-MVC-PA; P-MVC-PA) and MVC-PRO (nMVC-PRO) were manufactured using an Avestin EmulsiFlex-C3 high-pressure homogenizer (Ottawa, ON, Canada). Briefly, pre-suspension of L-MVC-PA contained MVC-PA (2% w/v), 1,2-distearoyl-sn-glycero-3-phosphocholine (DSPC) (0.1% w/v), and 1,2-disteroyl-sny-glycero-3-phosphoethanolamine-N-[amino(polyethylene glycol)-2000 (DSPE-PEG_{2000}) (0.03% w/v) in water. P-MVC-PA required dispersion of P407 (0.6% w/v), DSPE-PEG_{2000} (0.3% w/v), and MVC-PA (2% w/v) in water. Furthermore, nMVC-PRO was manufactured by dispersing P407 (1% w/v) and MVC-PRO (2% w/v) in water. All formulations were homogenized at 20,000 psi and characterized by dynamic light scattering (DLS, Malvern Nano-ZS, Worcestershire, UK) for size (nm), polydispersity (PDI), and zeta potential (mV). L-MVC-PA and P-MVC-PA were purified by tangential flow filtration (TFF; Spectrum Laboratories, Inc., CA, USA) using a mPES MidiKros Filter Module (cut-off size: 0.2 um; surface area 20 cm^2). Suspensions starting at 15 mL were concentrated to 3 mL followed by diafiltration with 5 or 10 diavolumes (DV) of water. nMVC-PRO was concentrated by centrifugation, whereby homogenized samples were centrifuged (10,000 g for 10 min) and the subsequent pellet was resuspened in a solution of 0.2% P407. Prodrug or MVC content in the nanoformulations were analyzed by UPLC-UV/Vis after dilution in MeOH and centrifugation (14,000 rpm for 10 min) as described below.

4.3.9 Quantification of MVC and MVC-PRO by UPLC-UV/Vis

Drug concentration was assayed on a Waters ACQUITY ultra performance liquid chromatography (UPLC) H-Class system with TUV detector and Empower 3 software (Milford, MA). MVC and MVC-PRO samples were separated on a Phenomenex Kinetex 5 µm C18 column (150 x 4.6 mm) (Torrance, CA). MVC was detected at 192 nm, using a mobile phase consisting of 74% 50 mM KH_2PO_4, pH 3.2, and 26% ACN and a flow rate of 1.0 mL/min. MVC-PRO was detected at 250 nm, using a mobile phase consisting of 50% 50 mM KH_2PO4, pH 3.2, and 50% ACN and a flow rate of 1.0 mL/min with an elution time of 7.2 min. Drug content was determined by comparing peak areas to peak areas from drug standards (0.05-50 µg/mL).

4.3.10 Plasma Cleavage Studies

Sprague Dawley rat plasma was used to determine the in vitro bioconversion of MVC-PRO to MVC. Specifically, MVC-PRO (dissolved in DMSO) was spiked into rat plasma at a concentration of 5 µg/mL. Samples were collected (0, 15, 30, 60 min; 2, 4, 7, 24 hour; D3, D5, D7) by immediately diluting 100 µL plasma into 1 mL ACN and stored at -20°C. For analysis, samples were vortexed for 5 min, followed by centrifugation (17,000 g for 10 min). Resultant supernatants were transferred to a new tube and dried on a speedvac. Samples were resuspended with 200 µL of MeOH and analyzed for MVC and MVC-PRO content by UPLC-UV/Vis.

4.3.11 Half-maximum effective concentration (EC_{50}) assays

Studies to determine the EC_{50} of MVC and MVC-PRO in MDMs were performed in 96-well plates at a density of 0.15 x 10^6 cells/well. Specifically, cells were treated with 0.1-10,000 nM MVC or MVC-PRO for 2 hours, followed by HIV-1$_{ADA}$ challenge at a MOI of 0.1 for 16 hours. Following viral challenge, cells were washed

with PBS, and given fresh 0.1-10,000 nM drug containing media. Supernatants were collected 10 days after challenge and assayed for HIV reverse transcriptase (RT) activity.[85,86] Replicate cells were fixed with 4% PFA and stained for HIV-1 p24 antigen by immunohistochemistry.[86]

4.3.12 Macrophage cellular uptake and retention studies

Human monocytes were obtained by leukapheresis from HIV-1/2 seronegative donors and subsequently purified by counter-current centrifugal elutriation.[92] Monocytes were grown in culture media containing DMEM (4.5 g/L glucose, L-glutamine, and sodium pyruvate) supplemented with 10% pooled human serum (heat-inactivated), 10 μg/mL ciprofloxacin, and 50 μg/mL gentamicin. Additionally, cells were maintained at 37°C in a 5% CO_2 incubator. Human monocytes were plated in 12, 24, or 96-well plates at $1.0x10^6$, $0.5x10^6$, or $0.15x10^6$ cells/mL respectively. Recombinant human macrophage colony stimulating factor (MCSF, 1000 U/mL) was added to culture media for 7 days to facilitate monocyte-derived macrophages (MDMs) differentiation and vitality in culture.MDM uptake and retention studies were performed in 12-well plates, with each treatment group completed in triplicate. Briefly, MDMs were treated with 100 μM MVC, nMVC, nMVC-PRO, L-MVC-PA, or P-MVC-PA and cells were collected 1, 2, 4,or 8 hours later. For cellular retention studies, drug was removed after 8 hours. Cells were washed with PBS and replenished with fresh media. Cellular samples were collected at 1, 5, 10, and 15 days to assay intracellular drug concentration. Specifically, MDMs were collected by removing media, washing 2 times with PBS, and scraping the cells into PBS. Cells were subsequently counted using an Invitrogen Countess Automated Cell Counter (Carlsbad, CA). Collected MDMs were centrifuged at 956 g for 8 min. Cell pellets were sonicated in 200 μL MeOH to extract intracellular drug and subsequently centrifuged at 20,000 g for 10

min. Samples were analyzed by UPLC-UV/Vis for intracellular drug content as described above.

4.3.13 Murine Pharmacokinetic Studies

Male *BALB/cJ* mice (6-8 weeks, Jackson Labs, Bar Harbor, ME) were used for all PK studies. Specifically, for studies involving nMVC animals were administered 100 mg/kg subcutaneous (SC) injection of MVC-HCL or nMVC. Studies with MVC-PA proceeded with intramuscular (IM; caudal thigh muscle) injections of 50 mg/kg L-MVC-PA, P-MVC-PA, or MVC-PA (sesame oil). For studies of MVC-PRO, animals were administered 50 mg/kg NMVC-PRO, MVC-HCL, or MVC-PRO (sesame oil) by IM injection. For all studies, blood samples were collected by cheek puncture into heparinized tubes and centrifuged at 2,000 g for 5 min. Plasma supernatants were collected and stored at -80°C until further analysis. Plasma drug concentrations were determined by UPLC-MS/MS using a Waters ACQUITY UPLC-Xevo TQ-S micro mass spectrometry system (Milford, MA) and an ACQUITY UPLC BEH shield, RP18 (1.7 µm, 2.1 x 100 mm) column. For analyte separation, a mobile phase consisting of A (7.5 mM ammonium acetate in Optima-grade water; pH adjusted to 5 with acetic acid) and B (100% ACN) and a flow rate of 0.25 mL/min was used. The mobile phase gradient used was as follows: 3 min (70% A/ 30% B), 4.5 min (40% A/ 60% B), 5.5 min (5% A /95% B), 6.25 min (70% A /30% B) for a run time totaling 8 min. MRM transitions used for MVC were 514.40>389.2, 514.0>280.0 and 514.0>117.0 and for IDV (the internal standard; IS) were 614.4>421.0 and 614.4>97.10. For drug analysis 25 µL of plasma was mixed with 1 mL of ice cold ACN and subsequently spiked with 10 µL of IS. Samples were vortexed (3 min) and centrifuged (17,000 g for 10 min). Supernatants were dried, reconstituted with 50% ACN, and injected for UPLC-MS/MS analysis. Plasma standards were extracted at a final concentration of 0.1-1000 ng/ml.

4.5 Results

4.5.1 Characterization of the physicochemical properties of nMVC

Polymeric lipid-coated nanoparticles successfully encapsulating MVC (nMVC) were manufactured using single emulsion-solvent evaporation. nMVC had an average size of 281 nm. Furthermore, particles exhibited a zeta potential of -37 mV and a PDI of 0.29. Drug loading, which can be defined as the amount of drug present in a defined weight of lyophilized nanoparticle powder ((MVC)/(Total weight of lyophilized powder) x 100) was assessed by UPLC-UV/Vis. Analysis determined drug loading of nMVC nanoparticles to be 6.4 %.

4.5.2 nMVC MDM uptake and retention

Cell cultures of monocyte-derived macrophages (MDM) were used to assess the cellular uptake and retention of nMVC compared to MVC. MDM were treated with 100 µM nMVC or MVC and intracellular drug levels examined after 1, 2, 4, and 8 hours. nMVC demonstrated significantly higher uptake compared with MVC, with intracellular MVC concentrations of 2.2 and 0.78 µg/10^6 respectively (*** $P < 0.001$). To assess the potential for macrophage drug depot development, intracellular MVC was analyzed 1, 2, 4, 6, 8, and 10 days after initial 8-hour treatment. nMVC treated cells retained detectable amounts of MVC for the duration of study (10 days), while MVC treated cells fell below the limit of detection (0.05 µg/mL) by day 1.

4.5.3 nMVC MDM antiretroviral efficacy

To determine if improved MDM intracellular uptake and retention specified enhanced antiviral activity, cells were challenged with HIV-1$_{ADA}$ 1, 5, 10, and 15 days after drug treatment (nMVC or MVC). Specifically, viral breakthrough was witnessed in

cells treated with MVC 1 day after treatment. Conversely, nMVC treated cells exhibited 95% viral inhibition as measured by RT activity 15 days after treatment. Furthermore, HIV p24 antigen expression revealed significant infection in MVC treated cells at all time points. nMVC treatment provided substantial protection, whereby a small percentage of p24 positive cells can be detected at 10 and 15 days after treatment.

4.5.4 nMVC PK and BD

Male *BALB/cJ mice* were administered a 100 mg/kg (SC) injection of nMVC or MVC to determine its plasma PK profile. nMVC treatment generated significantly higher MVC plasma concentrations at 8 hours, as well as 1 and 2 days after injection compared to MVC treatment (* $P < 0.05$, *** $P < 0.001$, ** $P < 0.01$ respectively). Specifically, nMVC treatment resulted in MVC plasma concentrations of 1634, 548.9, and 41.0 ng/mL at 8, 24 and 48 hours respectively. Conversely, MVC treated animals had 914.7, 190.5, and 7.4 ng/mL in the plasma at the same time points.

4.5.5 Synthesis and characterization of MVC-14

MVC was successfully modified with a 14-carbon fatty acid moiety to generate a hydrophobic prodrug (MVC-14). ^{1}H NMR confirmed the presence of the attached aliphatic chain with signals at 0.84 and 1.24 ppm, representing the protons of the terminal methyl group and (R-C$\mathbf{H_2}$-R) respectively. Furthermore, mass spectrometry analysis confirmed MVC-14 by detecting a compound of the correct molecular weight (754 m/z). MVC-14 did not readily form a nanosuspension after testing with an assortment of surfactants (P407, P188, P338, Tween 20, Tween 80, TPGS) and was not further studied.

4.5.6 Manufacture, characterization, and nanoformulation of MVC-PA

MVC and pamoic acid (PA) were co-precipitated to form a hydrophobic salt with a proposed interaction between the carboxylic acids of PA and the protonated tropane and triazole nitrogen groups of MVC. UPLC-UV/Vis analysis determined MVC-PA powder to be 49.6% MVC by weight. Nanoformulations of MVC-PA, were generated using a top-down manufacturing process and subsequently concentrated by TFF. Specifically, P-MVC-PA had an average particle size of 484 nm, while L-MVC-PA particles averaged 548 nm. Nanoformulated MVC-PA (L-MVC-PA; P-MVC-PA) was administered to MDM (100 µM) to test intracellular uptake. After 8 hours of treatment, cells treated with nanoformulations of MVC-PA generated intracellular drug concentrations similar to native MVC. Furthermore, *BALB/cJ* animals were administered 50 mg/kg MVC, L-MVC-PA, or P-MVC-PA by a single IM injection. Minimal plasma MVC concentrations were observed 24 hours after injection with L-MVC-PA and P-MVC-PA (50 mg/kg) respectively (35.5 and 13.2 ng/mL).

4.5.7 MVC-PRO synthesis, characterization, and nanoformulation

In further studies, MVC was modified by heptyl chloroformate to generate a short-chain carbamate prodrug (MVC-PRO). ^{1}H NMR spectra analysis revealed signals at 0.88 and 1.20-1.37 ppm corresponding to the terminal methyl and (R-CH_2-R) protons respectively. Prodrug modification generated substantial changes in aqueous solubility, exhibiting an ~1000-fold reduction (2,600 and 2.4 µg/mL) for MVC and MVC-PRO respectively. Additionally, we hypothesized our prodrug modification occurred at the secondary amine of MVC. To indirectly test this hypothesis, we performed a pH dependent solubility study. MVC has two ionizable nitrogen groups, with a pKa of 3.3 and 7.7, respectively. Therefore, we should observe a similar solubility curve for both MVC and MVC-PRO if those groups remained unmodified. MVC exhibited a clear pH

dependent solubility with increased solubility below pH 7 and lower solubility at pH 9 and 11. MVC-PRO exhibited a similar pattern with solubilities of 131.8, 76.9 and 2.4 µg/mL at pH 3, 5, and 7, respectively. Soluble MVC-PRO in samples at pH 9 and 11 was below the limit of our detection method (0.05 µg/mL). To further characterize MVC-PRO we examined its antiviral activity in MDMs. Specifically, MVC exhibited a low-nanomolar EC_{50} value (4.7 nM) consistent with its high antiviral potency. MVC-PRO displayed decreased antiviral activity (EC_{50} = 96 nM), possibly due to relatively slow cleavage of MVC from the carbamate prodrug. Therefore we examined the cleavage kinetics of MVC-PRO in rat plasma. MVC-PRO effectively released active MVC, but it proceeded slowly over the course of multiple days. Specifically, after 24 hours, 29.5% of MVC-PRO remained. Importantly, after 24 hours 74% of possible MVC had been released ensuring that active compound could be released from MVC-PRO. Importantly, MVC-PRO was nanoformulated (nMVC-PRO) successfully using high-pressure homogenization. In particular, nMVC-PRO exhibited an average size of 410 nm and PDI of 0.24.

4.5.8 In vitro and In vivo characterization of nMVC-PRO

To determine cellular uptake and retention, MDMs were treated with nMVC-PRO, MVC-PRO, or MVC (100 µM). After 8 hours of incubation, MDMs treated with nMVC-PRO showed a 44-fold increase in intracellular drug levels compared to MVC treatment. Additionally, non-formulated MVC-PRO was equally as efficient in terms of intracellular drug delivery. MVC was detected at all times points in cells treated with nMVC-PRO and MVC-PRO, thus indicating prodrug bioconversion. Next, to test MDM retention cells were collected 1,3, 5, 7, and 10 days after an initial 8 hour treatment. Intracellular drug concentrations of MVC treated cells quickly fell below the limit of detection after a single day. Moreover, both nMVC-PRO and MVC-pro exhibited similar retention patterns with precipitous decreases in cellular retention occurring within the first day, eventually falling

below the limit of detection by day 5. To understand how nanoformulation uptake and retention may affect antiretroviral efficacy, we challenged cells with HIV-1$_{ADA}$ at 1, 3, 5, 7, and 10 days after drug loading. Viral breakthrough was observed at all timepoints in MDMs treated with MVC. Interestingly, both nMVC-PRO and MVC-PRO provided 78 and 88% reduction in RT activity 10 days after drug treatment. RT activity data was qualitatively supported by p24 antigen staining where robust infection is observed at all times points after MVC treatment. Minimal p24 positive cells were observed after nMVC-PRO and MVC-PRO loading when challenged at 7 and 10 days after treatment, corresponding to the results of our RT assays. Furthermore, male *BALB/cJ mice* were administered 50 mg/kg MVC-eq. of nMVC-PRO, MVC-PRO (Seasme oil), MVC, or MVC-PA (Seasme oil) by IM injection. Plasma MVC concentrations 24 hours after injection demonstrated 4.2, 15.9, 90.2, and <1 ng/mL for nMVC-PRO, MVC-PRO, MVC-PA, and MVC respectively. Unfortunately, MVC plasma concentrations fell below the limit of quantitation (0.5 ng/mL) 3 days after treatment for all groups.

4.6 Discussion

MVC, the first and only entry inhibitor approved for HIV-1 treatment, has generated significant research interest based upon observations of slow disease progression in individuals harboring the Δ32 CCR5 mutant.[40] A long-acting formulation of MVC would be particularly beneficial in PrEP considering its action early in the viral life cycle and the observation that most early infection strains are R5 tropic. Furthermore, MVC is present in vaginal and rectal tissue, as well as semen after oral dosing.[42,43] Therefore, our studies aimed to evaluate the potential of MVC as a LA HIV-1 therapeutic.

MVC is moderately soluble in an aqueous environment in part due to its ionization at physiological pH. Certainly, its solubility is not as high as most NNRTI

compounds, although it is substantially more soluble than CAB and RPV, compounds currently under long-acting development. Early attempts at top-down nanoformulation were unsuccessful, even after screening numerous commonly used surfactants. Based on these observations we transitioned to PLGA-based nanoparticles (nMVC) and successfully manufactured particles with an average size of 281 nm. Subsequent studies in MDM determined nMVC improved intracellular uptake and provided detectable intracellular MVC concentrations 10 days after treatment. Furthermore, nMVC exhibited protection against HIV-1 infection, whereby 95% inhibition was observed 15 days after treatment. Moreover, in vivo testing in *BALB/cJ* mice exhibited increased plasma MVC concentrations up to 3 days following a single SC injection of nMVC compared with MVC. These results offered proof-of concept MVC could not only be nanoformulated successfully, but could enhance in vitro antiretroviral efficacy and in vivo PK. Ultimately, the in-vivo changes were short-acting and therefore did not represent a truly long-acting option for further development. Therefore, we investigated alternative approaches to alter the physicochemical properties of MVC and facilitate LA nanoformulation development.

Prodrug synthesis is an approach often employed to transiently modify the physicochemical properties of a compound. In particular hydrophilic molecules such as 3TC and ABC have been converted into hydrophobic prodrugs and ultimately successfully nanoformulated.[74-76] Reactive and accessible functional groups are required for prodrug synthesis. Therefore, we focused our synthetic schemes on the amide group present within MVC. Amides are less reactive than other secondary amines due to the electron withdrawing nature of its adjacent carbonyl, resulting in partial double bond character due to resonance. A significant amount of time and optimization was required to synthesize MVC-14, although subsequent nanoformulation was unsuccessful after screening a multitude of surfactants. Further prodrug synthesis generated a carbamate

prodrug of MVC-PRO. Carbamates are relatively stable due to the partial double bond character formed by its possible resonance structures.[113] Therefore to ensure MVC-PRO released its active form (MVC), we analyzed prodrug bioconversion in rat plasma. MVC-PRO readily released MVC over a 5-day period, demonstrating its potential utility in subsequent efficacy studies. Subsequent in vitro studies revealed its significant intracellular uptake and antiretroviral efficacy. Ultimately, PK studies in *BALB/cJ mice* exhibited detectable concentrations of MVC for only a single day following IM injection. These results may be due to rapid metabolism of MVC or the lack of conversion of MVC-PRO in vivo. Further UPLC-MS/MS method development is required to quantitate prodrug concentrations in the plasma and tissue.

Next, using olanzapine pamoate (ZYPREXA RELPREVV) as a model, we aimed to develop an extended release formulation for MVC by generating a hydrophobic pamoate salt (MVC-PA).[114] Ultimately, PK studies in *BALB/cJ mice* determined MVC-PA did not extend MVC release, providing minimal concentrations of MVC in the plasma for just a single day.

Transitioning MVC into a LA therapeutic has been extremely challenging. LA solid drug nanoformulations in clinical development have focused on highly potent hydrophobic compounds such as CAB and RPV. In comparison MVC possesses higher aqueous solubility and requires delivery of large amounts of drug due to its rapid metabolism.[112,115,116] Furthermore, in conjunction with laborious prodrug synthesis, creating a MVC LA formulation remains a significant challenge.

Recently the manufacture of MVC solid drug nanoparticles (SDN) resulted in detectable MVC concentrations for 10 days after IM injection.[117] In particular, the terminal half-life ($t_{1/2}$) increased from 53.2 hours for conventional MVC to 140.7 hours in MVC SDN, generating a step towards a LA injectable formation of MVC. Furthermore, proof-of-concepts studies incorporating MVC into topical gels were able to prevent HIV

infection in a humanized mouse model and SIV infection in rhesus macaques.[118,119] Thus, transitioning MVC into an extended release formulation is challenging, but its potential application in PrEP, as well as treating other disease states, such as cancer and graft-versus–host (GVHD) disease, will continue to foster extensive research into its therapeutic potential.[120]

4.7 Figures
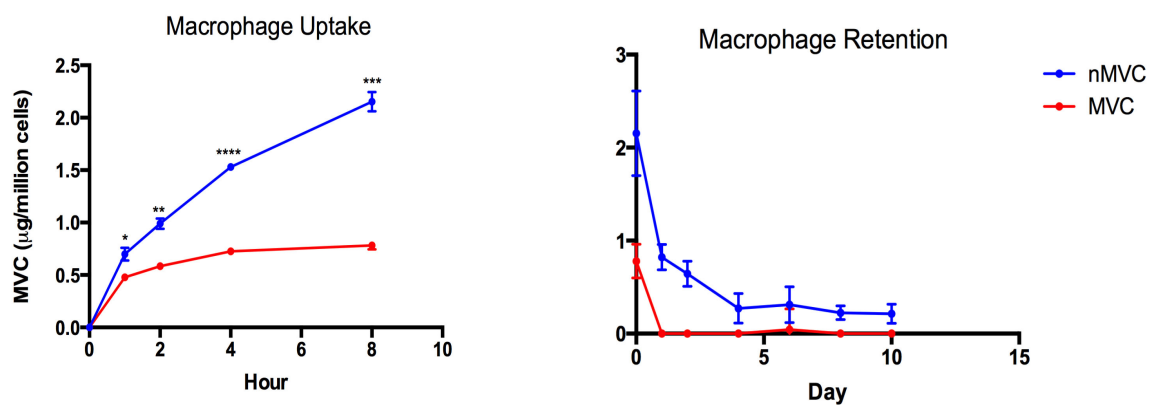
Figure 4.7.1 NMVC macrophage uptake and retention.

NMVC and MVC were evaluated for their MDM intracellular uptake and retention after 100 μM treatment. Data is expressed as mean ± SEM with n=3 biological replicates (* P < 0.05, ** P < 0.01, *** P < 0.001, **** P < 0.0001 as determined by Student's t test).
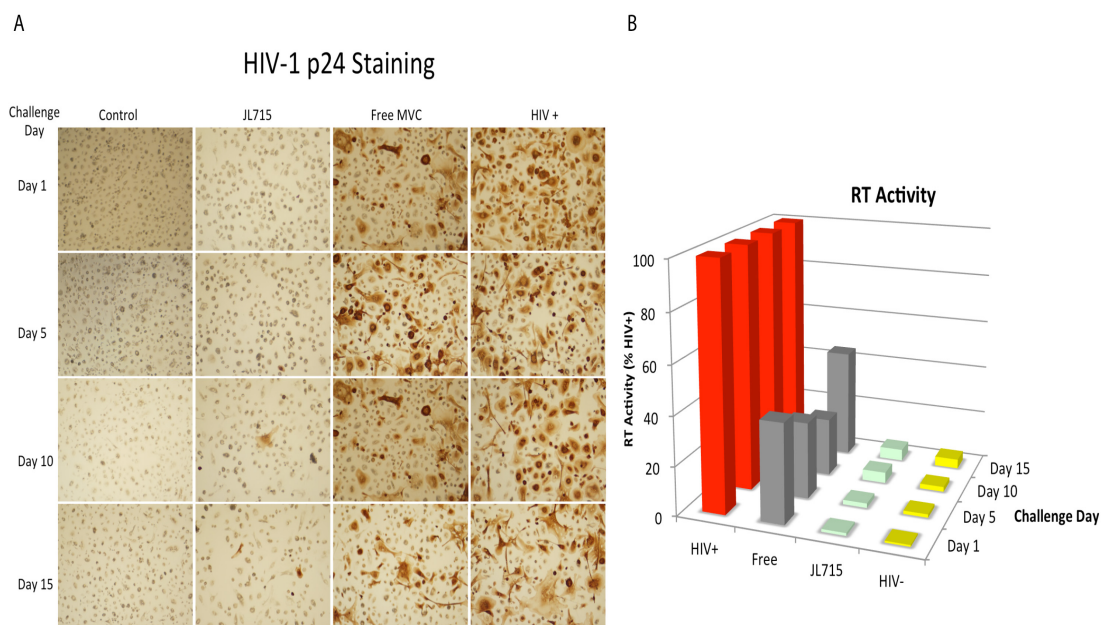
Figure 4.7.2 Comparison of antiretroviral activity of NMVC and MVC in MDM.

(A) HIV-1p24 antigen expression in MDMs challenged with HIV-1 at 1, 5, 10, and 15 days after initial 8-hour treatment with 100 µM NMVC or MVC. (B) RT activity was determined in medium of cells loaded with NMVC or MVC for 8 hours, then challenged with HIV-1$_{ADA}$ 1, 5, 10, and 15 days post treatment. Data represents mean ± SEM for n=3 biological samples.
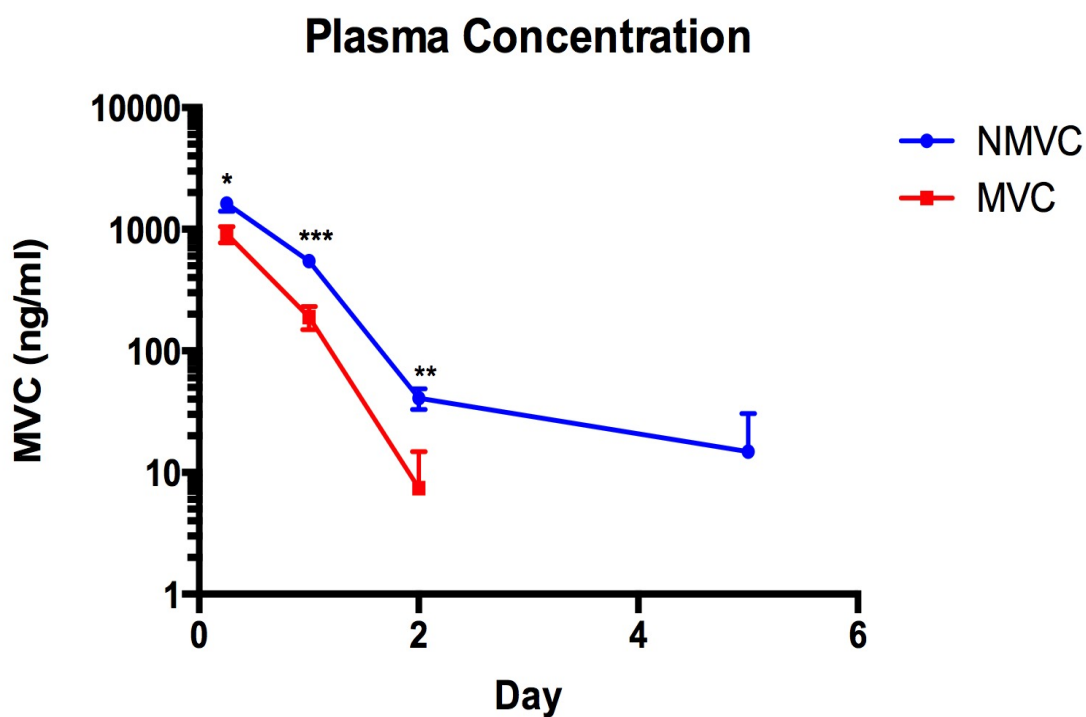
Figure 4.7.3 Murine pharmacokinetic evaluation of NMVC.

Male *BALB/cJ* mice were administered a single 100 mg/kg subcutaneous (SC) injection of NMVC or MVC. MVC plasma concentrations were evaluated for a period of 5 days post treatment. Data is expressed as mean ± SEM for n ≥ 10 biological replicates. (* $P <$ 0.05, ** $P < 0.01$, *** $P < 0.001$)
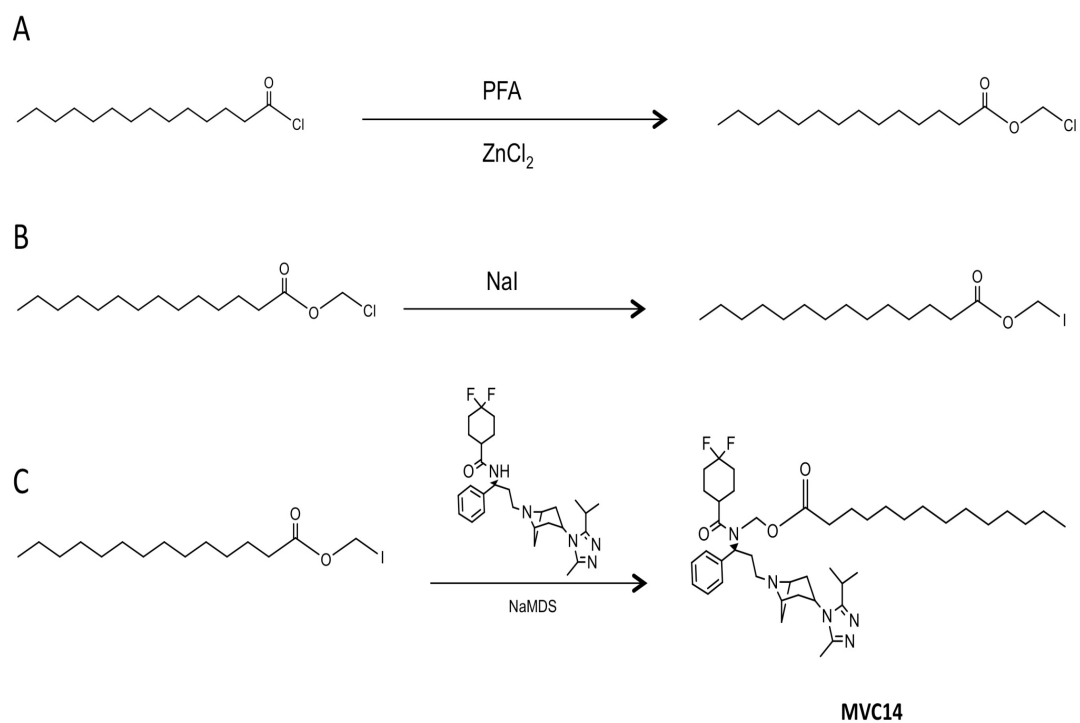
Figure 4.7.4 Synthesis of iodomethyl chloroformate and MVC14.

(A) Myristoyl chloride was reacted with PFA and ZnCl$_2$ under reflux conditions to generate chloromethyl chloroformate. **(B)** Chloromethyl chloroformate was reacted with NaI to generate Iodomethyl chloroformate. **(C)** MVC was reacted with iodomethyl chloroformate to generate a hydrophobic prodrug of MVC (MVC14).

A
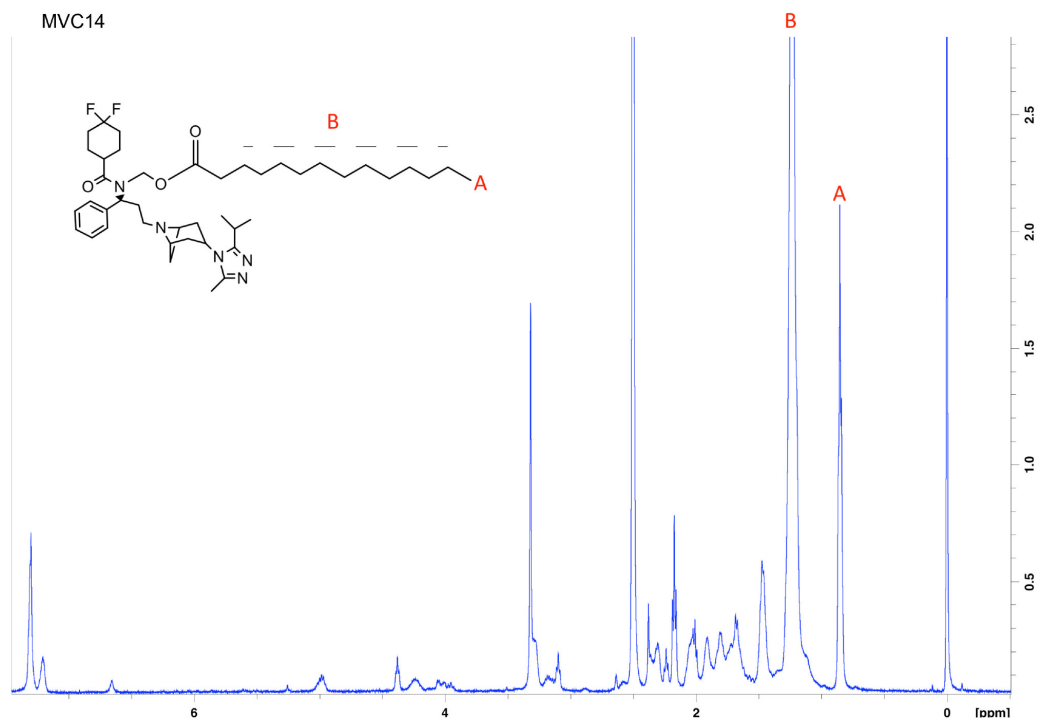
MVC14

B
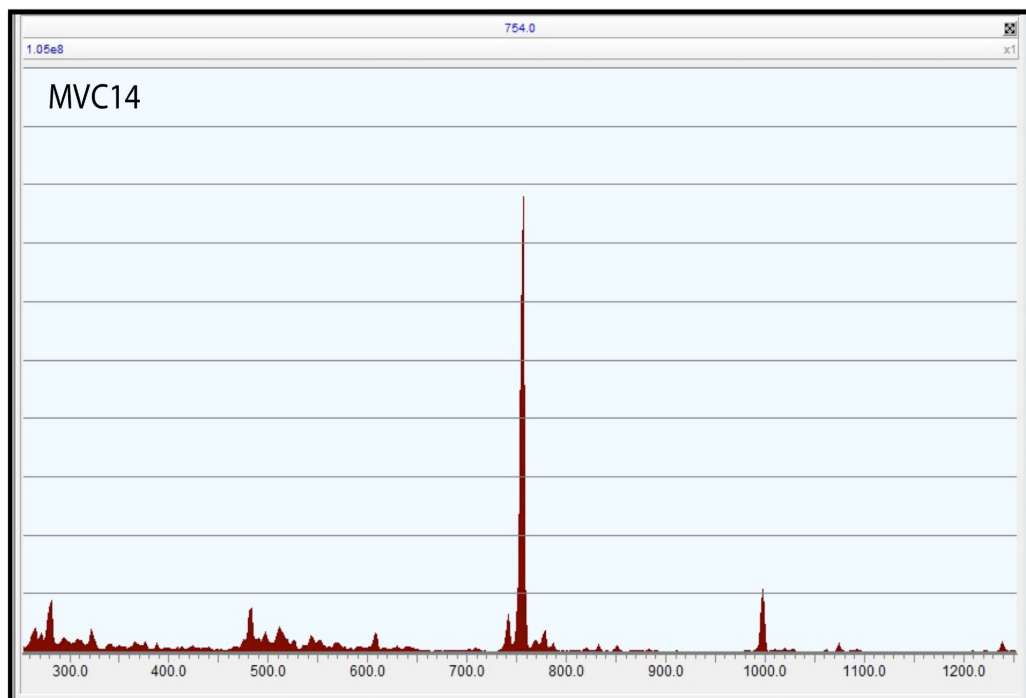
Figure 4.7.5 Chemical characterization of MVC14

(A) MVC was modified to generate methylene ester prodrug (MVC14) with an attached 14-carbon aliphatic chain. ^{1}H NMR spectra revealed signals at 0.84 and 1.24 ppm corresponding to the protons of terminal methyl group and (R-C**H$_2$**-R) respectively. (B) Positive electrospray ionization mass spectrometry (ESI-MS) analysis generated a strong signal for MVC14 at its predicted molecular weight.
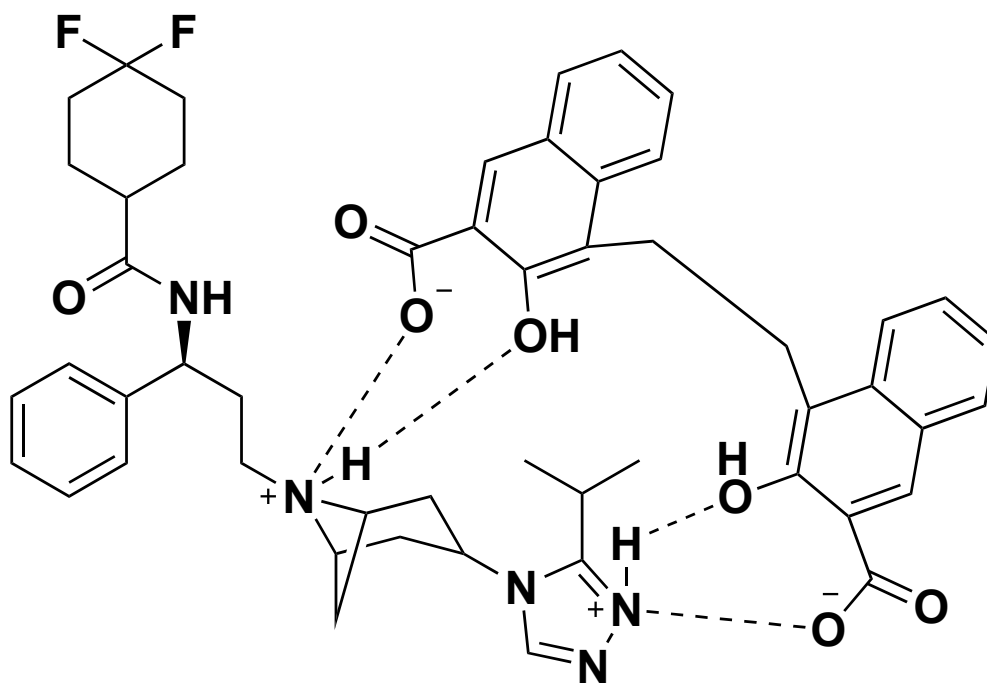
Figure 4.7.6 Proposed structure of MVC:pamoic acid (MVC-PA) salt

MVC and pamoic acid were co-precipitated to form a hydrophobic salt. The proposed electrostatic and hydrogen bond interactions between MVC and pamoic acid is depicted above.

A

Formulation	Preparation Process	Excipients	Purification Process
P-MVC-PA	Homogenization	P407, DSPE-PEG2000	TFF
L-MVC-PA	Homogenization	DSPE-PEG2000, DSPC	TFF
MVC	Drug Solution		0.22 um Filtration
Formulation	**Hydrodynamic Diameter (nm)**	**Polydispersity (PDI)**	**Zeta Potential (mV)**
P-MVC-PA	484 ± 41	0.24 ± 0.02	−26 ± 2
L-MVC-PA	548 ± 40	0.22 ± 0.02	−20 ± 2

B

Macrophage Uptake

MVC
P-MVC-PA
L-MVC-PA

C

Plasma Concentration
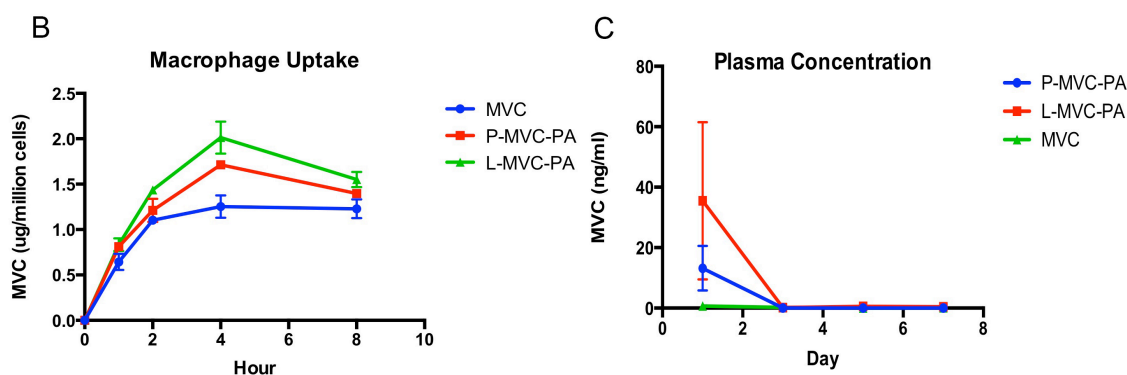
P-MVC-PA
L-MVC-PA
MVC

Figure 4.7.7 Development of nanoformulated MVC-PA

(A) Nanoformulations of MVC-PA (L-MVC-PA; P-MVC-PA) were manufactured by high-pressure homogenization, concentrated by TFF, and characterized by dynamic light scattering. (B) MDM intracellular uptake of MVC, L-MVC-PA, and P-MVC-PA over the course of 8 hours of treatment (100 µM). Data is expressed as mean ± SEM in n = 3 biological replicates. (C) MVC plasma concentrations from *BALB/cJ* mice given a 50 mg/kg intramuscular (IM) injection of MVC, L-MVC-PA, or P-MVC-PA. Data is expressed as mean ± SEM in n ≥ 3 biological replicates.

A

B
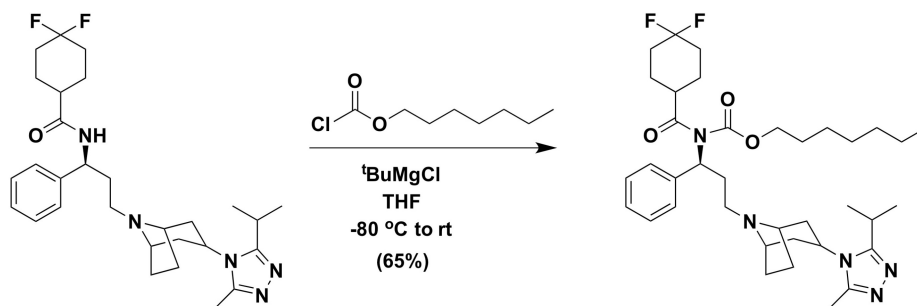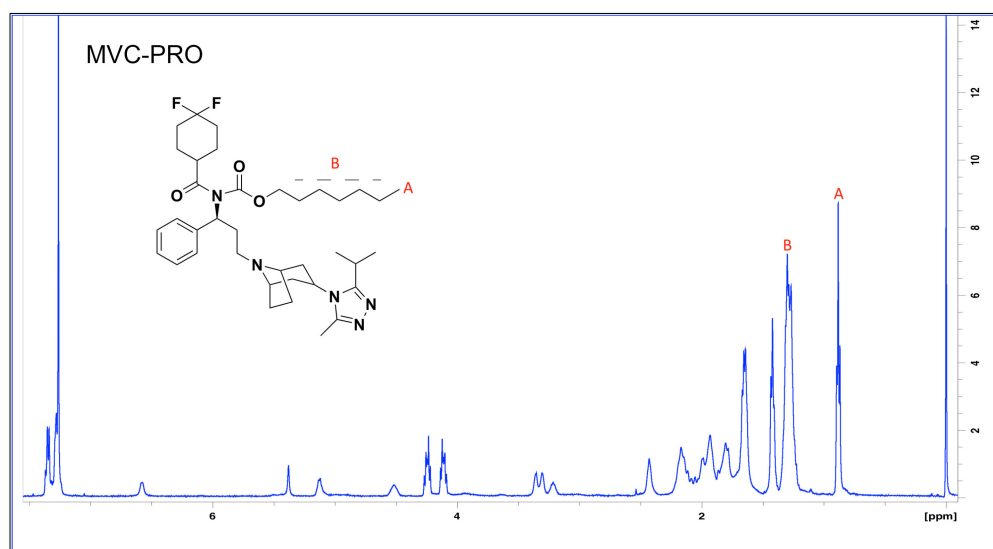
Figure 4.7.8 MVC-PRO chemical characterization

(A) MVC was reacted with heptyl chloroformate in the presence of *tert*-butylmagnesium chloride to generate a carbamate prodrug (MVC-PRO) (B) ^{1}H NMR spectra revealed signals at 0.88 and 1.20-1.37 ppm corresponding to the protons of the terminal methyl group and (R-C**H₂**-R) respectively.
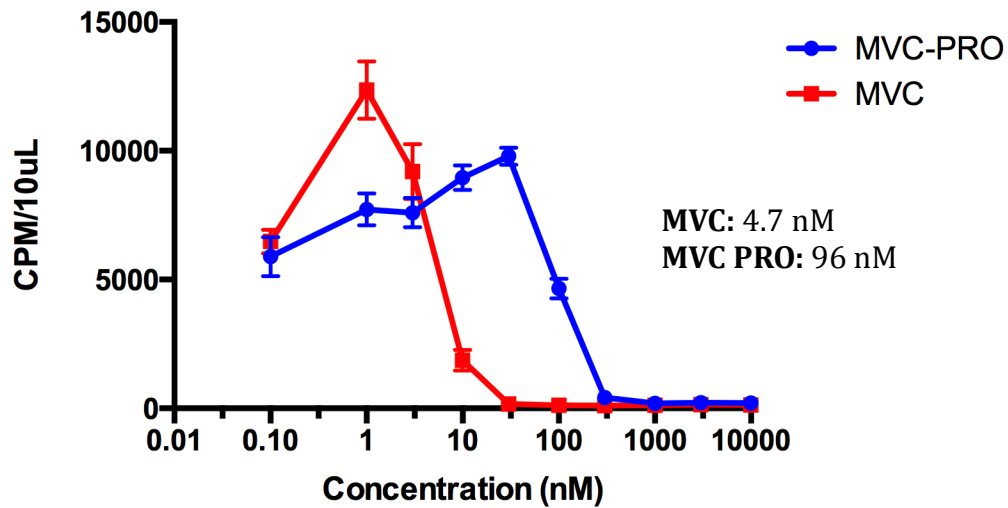
Figure 4.7.8 Antiviral activity of MVC-PRO in MDMs.

The antiviral activities of MVC and MVC-PRO were tested at a range of concentrations (0.1-10,000 nM) in MDMs. RT activity was determined after viral challenge with HIV-1_{ADA}. Data represents mean ± SEM with a minimum of 3 biological replicates.
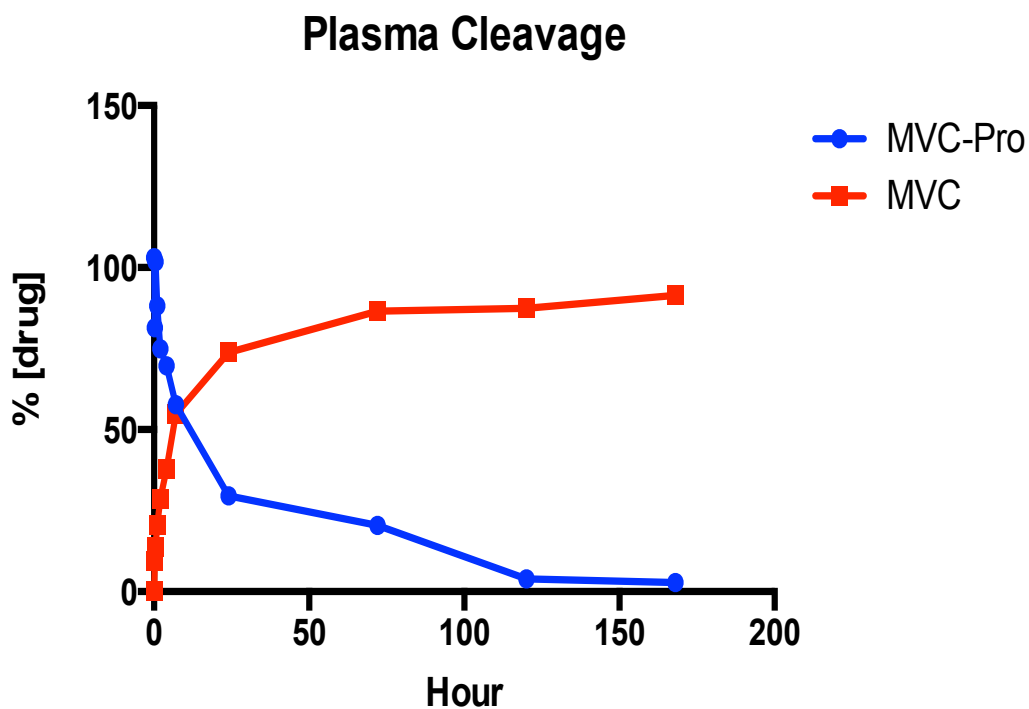
Figure 4.7.9 MVC-PRO plasma bioconversion

Plasma cleavage kinetics of MVC-Pro was tested in rat plasma. Briefly, 5 μg/mL MVC-Pro was spiked in rat plasma and collected at defined time points. Plasma samples were immediately spiked in ACN and stored at -80°C until further processing. Drug analysis was performed by UPLC-UV/Vis for MVC and MVC-PRO content.
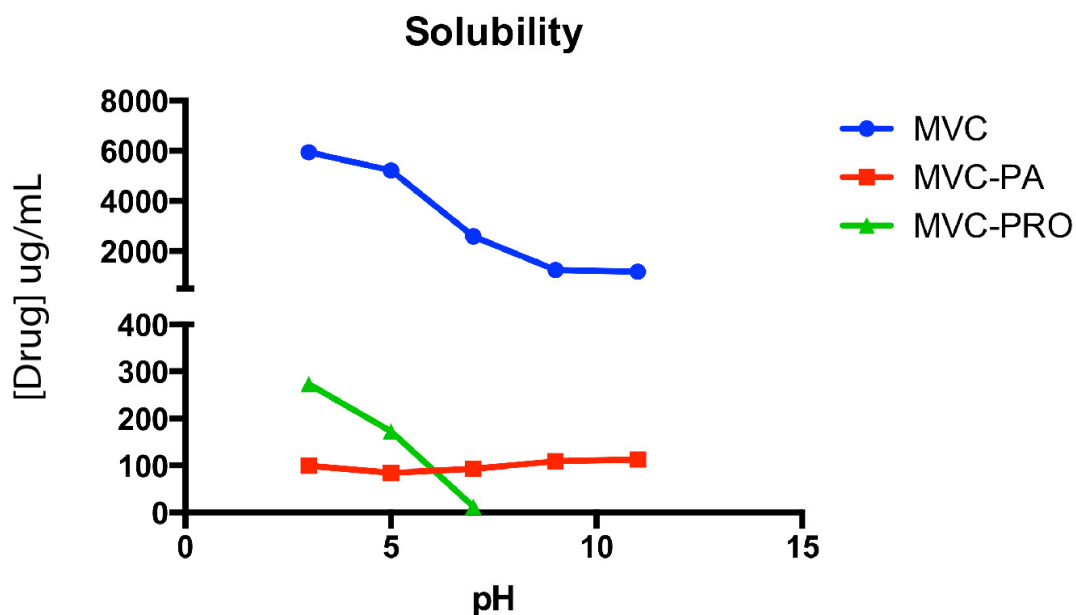
Solubility

Figure 4.7.10 MVC-PRO pH dependent solubility

MVC, MVC-PRO and MVC-PA were incubated in aqueous solutions of varying pH (3, 5, 7, 9, 11) for solubility analysis. Samples were collected after 24 hours of mixing, centrifuged to remove unsolubilized drug, and the supernatant analyzed for drug content by UPLC-UV/vis.

A
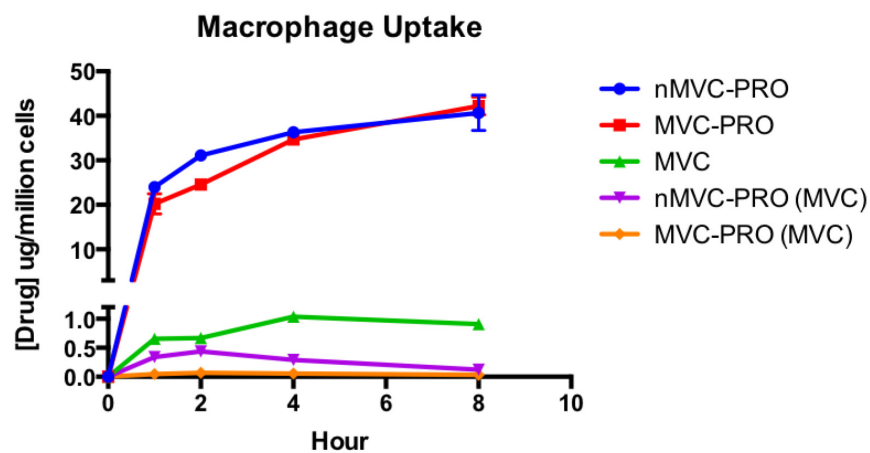
B
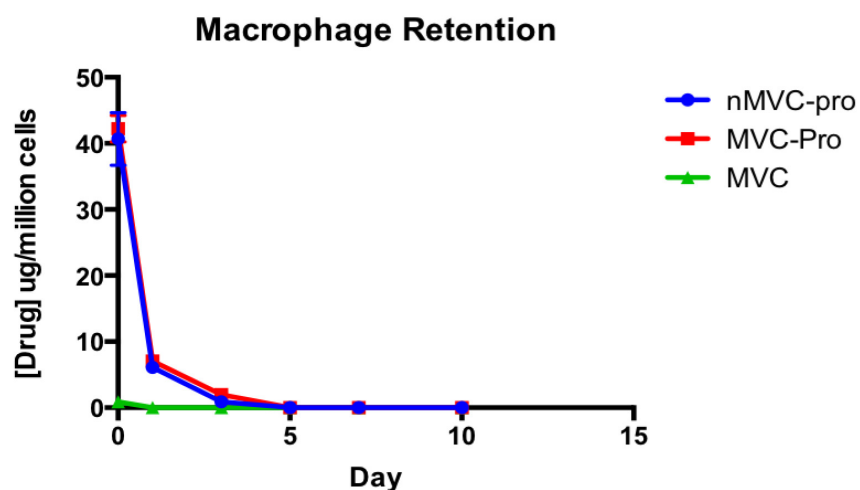
Figure 4.7.11 NMVC-PRO Macrophage uptake and retention.

Nanoformulated MVC-PRO (nMVC-PRO) and MVC were evaluated for MDM intracellular uptake (A) and retention (B) after 100 µM treatment. Intracellular MVC-PRO and MVC concentrations were quantified by UPLC-UV/Vis. Data is expressed as mean ± SEM with n=3 biological replicates.
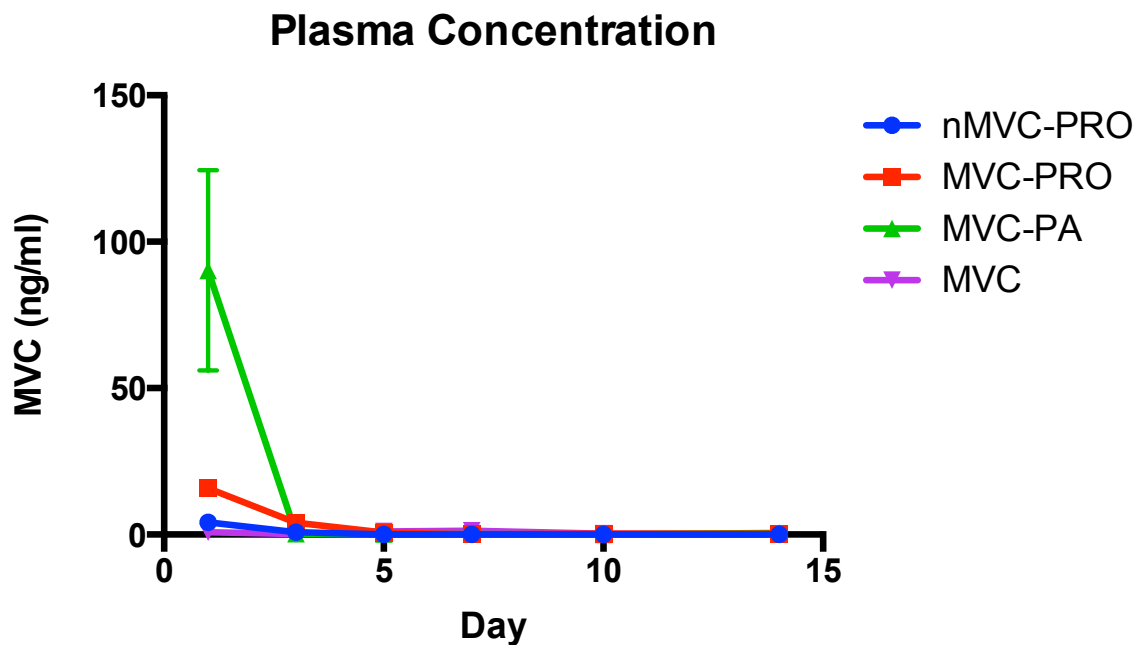
Figure 4.7.7 PK characterization of MVC-PRO

Male *BALB/cJ mice* were administered 50 mg/kg nMVC, MVC-PRO, MVC-PA, or MVC by IM injection. Blood was collected for 2 weeks after injection for MVC plasma quantitation by UPLC-MS/MS. Data is expressed as mean ± SEM in n = 5 biological replicates

CHAPTER 5

DISCUSSION

5.1 Discussion

Treatment of patients infected with HIV-1 is approaching an inflection point. Widespread application of oral ART completely changed the narrative surrounding HIV-1 infection. Once, an HIV diagnosis meant ostracization and impending death. ART enabled infected patients the opportunity to live a longer life, in which they could manage HIV-1 as more of a chronic condition, albeit requiring strict adherence to treatment protocols. Nevertheless, gaps still exist in HIV-1 therapy. Regions such eastern and southern Africa harbor most of the global disease burden with over 19 million individuals infected.[1] Furthermore, only 51% percent of infected patients are currently virally suppressed.[121] In order to make significant headway, a paradigm shift must take place. Ultimately a LA revolution in HIV-1 therapy may be on the horizon.

LA formulations have a number of benefits in the context of HIV-1 therapy. First, oral ART is effective when strict adherence is maintained. Since HIV-1 remains integrated in the host cells of infected patients even while on ART, viral rebound will occur if treatment ceases.[122] Furthermore, missed doses can lead to suboptimal drug concentrations and facilitate the development of resistance mutations. Thus, HIV-1 requires a life-long battle and any means by which treatment can be simplified is advantageous. LA formulations may provide an opportunity for simplification and increased effectiveness.

Furthermore, LA formulations have the potential to significantly impact PrEP and its associated patient populations. Oral PrEP is successful across vulnerable populations of varying sexes and sexual contact, but its effectiveness is contingent on consistent adherence.[123] Currently, the World Health Organization (WHO) suggests the implementation of PrEP for people at substantial risk of HIV-1 infection (> 3% incidence).[124] Young African women are particularly vulnerable and carry a disproportionate burden of HIV infections.[125] Unfortunately, clinical trials with oral PrEP in young African women have revealed very poor adherence (< 30%) rendering preventative measures ineffective.[126,127] LA PrEP measures could substantially impact this vulnerable subpopulation by administering LA ART during doctor visits and significantly increasing prevention effectiveness.

RPV- and CAB LA represent the first generation of HIV-1 LA formulations and have primarily been studied as monthly injections for maintenance therapy.[28,56] Although, early investigations into their application for PrEP have been undertaken.[53,128] Despite preliminary returns of clinical success, limitations have arisen and need to be addressed as HIV LA therapy is advanced. Injection site reactions (ISR) are the most commonly reported side effect with RPV and CAB LA (~97%) and may be due to the large dosage volumes that are necessary for delivery.[28,129] Furthermore, there are concerns regarding potential toxicity and/or unwanted side effects from treatment, which would be irreversible upon injection. Therefore, oral lead-in therapy to determine drug safety and tolerance may be necessary. Additionally, discontinuation of therapy is more complex in LA treatments. Whereas oral therapy discontinuation would generate precipitous drops in plasma drug concentrations, missing a LA injection or ceasing treatment would generate a long tail of suboptimal drug concentrations, leading to the potential rise in resistance mutations.

LA implants provide an alternative to injectable formulations for HIV-1 treatment and prevention. Slow drug release and sustained plasma drug concentration are the hallmark of LA implants and are well suited for PrEP. Additionally, a broad range of ARVs have been incorporated into implantable devices, unlike injectable forms which are limited to those with low solubility. Implants would improve PrEP adherence, but often require more advanced technical procedures than a simple injection for insertion and removal. Therefore, biodegradable implants delivered by subcutaneous injection are particularly attractive. Moreover, implants delivering a single ARV may not be sufficient, thus may require insertion of multiple implants or development of multi-drug sustained release devices. Lastly, implantable devices do not readily improve drug distribution to viral reservoirs, whereas observed macrophage infiltration in the muscle following LA injections may be advantageous for tissue delivery.

Working towards the next generation in HIV-1 therapy, our lab has developed a LA delivery approach deemed LASER-ART. Specifically, LASER-ART utilizes prodrug modification of existing ARVs to enhance nanoformulation entry into tissue and cellular reservoirs and provide sustained release of efficacious drug concentrations to the plasma and sites of viral infection. Furthermore, combining LASER-ART with novel CRISPR technologies targeting integrated HIV-1 proviral DNA provided viral elimination in a subset of humanized mice.[130] Together, these observations led us to develop a library of RPV prodrugs with the goal extending the apparent half-life and tissue distribution of RPV LA.

Four RPV prodrugs were successfully synthesized with varying carbon chain lengths (7,12,14,18). M3RPV, our 14-carbon modified prodrug was selected as the lead compound. In vitro studies determined delivery of nanoformulated M3RPV facilitated improved cellular drug retention and antiretroviral efficacy. These results suggested NM3RPV could provide a significant tissue depot in-vivo. Moreover, PK studies in

BALB/cJ mice demonstrated prodrug modification could significantly alter terminal half-life, MRT, and biodistribution. Specifically, NM3RPV generated 13 and 26-fold increases in $t_{1/2}$ and MRT respectively compared with NRPV. Additionally, NM3RPV exhibited plasma concentrations above the PA-IC$_{90}$ for 25 weeks compared with 7 weeks for NRPV. Moreover, both prodrug (M3RPV) and active compound (RPV) were detected in the spleen, lymph node, and liver 323 days after initial treatment.

NM3RPV provided extended RPV release into the plasma, but absolute levels did not reach the C$_{trough}$ concentrations observed for RPV-LA in clinical trials. It is necessary to continue to optimize our delivery mechanism to allow higher plasma exposure. Additionally, when we tested NM3RPV in rhesus macaques, plasma RPV concentrations rapidly declined. We witnessed extended release of the prodrug (M3RPV) in monkey plasma, a finding starkly different from our studies in mice. Interestingly, we did observe detectable levels of both RPV and M3RPV in tissue biopsies collected from lymph node, adipose tissue, and rectal tissue 204 days after injection. These results demonstrate further research is necessary to elucidate the reasons for the observed species differences and what measures can be taken to address these concerns. Furthermore, it could be reasonable to test some of the shorter-chain prodrugs in higher species to observe if they can release RPV in a more efficient manner than M3RPV.

Our presented research provides a proof-of-concept for RPV prodrug modification and its effects on PK and BD. As LA HIV injectable formulations become available for prevention and maintenance, new alternatives must be developed. LA ARVs largest impact will be for PrEP in vulnerable populations, particularly young African women. Therefore, research aimed towards making LA ARVs more efficient and user friendly will ultimately derive the greatest impact. Transitioning LA treatments from once a month to a quarterly or bi-annual schedule, if achieved would be substantial. Bi-

annual dosing provides the option of mass-drug administration to highly vulnerable populations, similar to what is done in Africa for other highly endemic diseases. Therefore, our work provides a small step towards this goal. Ultimate realization will require the development of novel compounds. Current LA formulations use existing ARVs originally developed for oral therapy. Therefore, future compounds will need to be highly potent, possess a long inherent half-life, and be specifically designed for LA formulation. Furthermore, optimizations such as prodrug modification, nanoformulation design, and/or novel implantable devices may be required to achieve extended sustained release and tissue distribution requisite for bi-annual therapy.

BIBLIOGRAPHY

1. UNAIDS. Global HIV & AIDS Statistics- 2018 Fact Sheet. (2018).
2. May, M.T.*, et al.* Impact on life expectancy of HIV-1 positive individuals of CD4+ cell count and viral load response to antiretroviral therapy. *Aids* **28**, 1193-1202 (2014).
3. Antiretroviral Therapy Cohort, C. Survival of HIV-positive patients starting antiretroviral therapy between 1996 and 2013: a collaborative analysis of cohort studies. *The lancet. HIV* **4**, e349-e356 (2017).
4. Organization, W.H. HIV/AIDS Fact Sheet. (2018).
5. Dalgleish, A.G.*, et al.* The CD4 (T4) antigen is an essential component of the receptor for the AIDS retrovirus. *Nature* **312**, 763-767 (1984).
6. Dragic, T.*, et al.* HIV-1 entry into CD4+ cells is mediated by the chemokine receptor CC-CKR-5. *Nature* **381**, 667-673 (1996).
7. Melikyan, G.B. Common principles and intermediates of viral protein-mediated fusion: the HIV-1 paradigm. *Retrovirology* **5**, 111 (2008).
8. Hu, W.S. & Hughes, S.H. HIV-1 reverse transcription. *Cold Spring Harbor perspectives in medicine* **2**(2012).
9. Craigie, R. & Bushman, F.D. HIV DNA integration. *Cold Spring Harbor perspectives in medicine* **2**, a006890 (2012).
10. Das, A.T., Harwig, A. & Berkhout, B. The HIV-1 Tat protein has a versatile role in activating viral transcription. *Journal of virology* **85**, 9506-9516 (2011).
11. Sundquist, W.I. & Krausslich, H.G. HIV-1 assembly, budding, and maturation. *Cold Spring Harbor perspectives in medicine* **2**, a006924 (2012).

12. Maartens, G., Celum, C. & Lewin, S.R. HIV infection: epidemiology, pathogenesis, treatment, and prevention. *Lancet* **384**, 258-271 (2014).

13. Brenchley, J.M.*, et al.* CD4+ T cell depletion during all stages of HIV disease occurs predominantly in the gastrointestinal tract. *The Journal of experimental medicine* **200**, 749-759 (2004).

14. Gottlieb, M.S.*, et al.* Pneumocystis carinii pneumonia and mucosal candidiasis in previously healthy homosexual men: evidence of a new acquired cellular immunodeficiency. *The New England journal of medicine* **305**, 1425-1431 (1981).

15. Fischl, M.A.*, et al.* The efficacy of azidothymidine (AZT) in the treatment of patients with AIDS and AIDS-related complex. A double-blind, placebo-controlled trial. *The New England journal of medicine* **317**, 185-191 (1987).

16. Hammer, S.M.*, et al.* A controlled trial of two nucleoside analogues plus indinavir in persons with human immunodeficiency virus infection and CD4 cell counts of 200 per cubic millimeter or less. AIDS Clinical Trials Group 320 Study Team. *The New England journal of medicine* **337**, 725-733 (1997).

17. Moore, R.D. & Chaisson, R.E. Natural history of HIV infection in the era of combination antiretroviral therapy. *Aids* **13**, 1933-1942 (1999).

18. Gulick, R.M.*, et al.* 3-year suppression of HIV viremia with indinavir, zidovudine, and lamivudine. *Annals of internal medicine* **133**, 35-39 (2000).

19. Palella, F.J., Jr.*, et al.* Declining morbidity and mortality among patients with advanced human immunodeficiency virus infection. HIV Outpatient Study Investigators. *The New England journal of medicine* **338**, 853-860 (1998).

20. Craig, J.C.*, et al.* Antiviral properties of Ro 31-8959, an inhibitor of human immunodeficiency virus (HIV) proteinase. *Antiviral research* **16**, 295-305 (1991).

21. Koup, R.A.*, et al.* Inhibition of human immunodeficiency virus type 1 (HIV-1) replication by the dipyridodiazepinone BI-RG-587. *The Journal of infectious diseases* **163**, 966-970 (1991).

22. Wild, C.T., Shugars, D.C., Greenwell, T.K., McDanal, C.B. & Matthews, T.J. Peptides corresponding to a predictive alpha-helical domain of human immunodeficiency virus type 1 gp41 are potent inhibitors of virus infection. *Proceedings of the National Academy of Sciences of the United States of America* **91**, 9770-9774 (1994).

23. Dorr, P.*, et al.* Maraviroc (UK-427,857), a potent, orally bioavailable, and selective small-molecule inhibitor of chemokine receptor CCR5 with broad-spectrum anti-human immunodeficiency virus type 1 activity. *Antimicrobial agents and chemotherapy* **49**, 4721-4732 (2005).

24. Summa, V.*, et al.* Discovery of raltegravir, a potent, selective orally bioavailable HIV-integrase inhibitor for the treatment of HIV-AIDS infection. *Journal of medicinal chemistry* **51**, 5843-5855 (2008).

25. Mathias, A.A.*, et al.* Bioequivalence of efavirenz/emtricitabine/tenofovir disoproxil fumarate single-tablet regimen. *Journal of acquired immune deficiency syndromes* **46**, 167-173 (2007).

26. Cohen, M.S.*, et al.* Prevention of HIV-1 infection with early antiretroviral therapy. *The New England journal of medicine* **365**, 493-505 (2011).

27. Guidelines for the Use of Antiretroviral Agents in Adults and Adolescents with HIV. (U.S Department of Health and Human Services, 2019).

28. Margolis, D.A.*, et al.* Long-acting intramuscular cabotegravir and rilpivirine in adults with HIV-1 infection (LATTE-2): 96-week results of a randomised, open-label, phase 2b, non-inferiority trial. *Lancet* **390**, 1499-1510 (2017).

29. UNAIDS. 90-90-90: An ambitious treatment target to help end the AIDS epidemic. (2014).

30.   Sharma, M. & Saravolatz, L.D. Rilpivirine: a new non-nucleoside reverse transcriptase inhibitor. *The Journal of antimicrobial chemotherapy* **68**, 250-256 (2013).

31.   Janssen, P.A*., et al.* In search of a novel anti-HIV drug: multidisciplinary coordination in the discovery of 4-[[4-[[4-[(1E)-2-cyanoethenyl]-2,6-dimethylphenyl]amino]-2- pyrimidinyl]amino]benzonitrile (R278474, rilpivirine). *Journal of medicinal chemistry* **48**, 1901-1909 (2005).

32.   Martinez, E*., et al.* Hepatotoxicity in HIV-1-infected patients receiving nevirapine-containing antiretroviral therapy. *Aids* **15**, 1261-1268 (2001).

33.   Decloedt, E.H. & Maartens, G. Neuronal toxicity of efavirenz: a systematic review. *Expert opinion on drug safety* **12**, 841-846 (2013).

34.   Garvey, L. & Winston, A. Rilpivirine: a novel non-nucleoside reverse transcriptase inhibitor. *Expert opinion on investigational drugs* **18**, 1035-1041 (2009).

35.   Guidelines for the Use of Antiretroviral Agents in Pediatric HIV Infection.

36.   Llibre, J.M*., et al.* Efficacy, safety, and tolerability of dolutegravir-rilpivirine for the maintenance of virological suppression in adults with HIV-1: phase 3, randomised, non-inferiority SWORD-1 and SWORD-2 studies. *Lancet* **391**, 839-849 (2018).

37.   Baert, L*., et al.* Development of a long-acting injectable formulation with nanoparticles of rilpivirine (TMC278) for HIV treatment. *European journal of pharmaceutics and biopharmaceutics : official journal of Arbeitsgemeinschaft fur Pharmazeutische Verfahrenstechnik e.V* **72**, 502-508 (2009).

38.   Verloes, R*., et al.* Safety, tolerability and pharmacokinetics of rilpivirine following administration of a long-acting formulation in healthy volunteers. *HIV medicine* **16**, 477-484 (2015).

39.   Williams, P.E., Crauwels, H.M. & Basstanie, E.D. Formulation and pharmacology of long-acting rilpivirine. *Current opinion in HIV and AIDS* **10**, 233-238 (2015).

40.   Huang, Y*., et al.* The role of a mutant CCR5 allele in HIV-1 transmission and disease progression. *Nature medicine* **2**, 1240-1243 (1996).

41.   Hutter, G*., et al.* Long-term control of HIV by CCR5 Delta32/Delta32 stem-cell transplantation. *The New England journal of medicine* **360**, 692-698 (2009).

42.   Brown, K.C*., et al.* Single and multiple dose pharmacokinetics of maraviroc in saliva, semen, and rectal tissue of healthy HIV-negative men. *The Journal of infectious diseases* **203**, 1484-1490 (2011).

43.   Dumond, J.B*., et al.* Maraviroc concentrates in the cervicovaginal fluid and vaginal tissue of HIV-negative women. *Journal of acquired immune deficiency syndromes* **51**, 546-553 (2009).

44.   Brissos, S., Veguilla, M.R., Taylor, D. & Balanza-Martinez, V. The role of long-acting injectable antipsychotics in schizophrenia: a critical appraisal. *Therapeutic advances in psychopharmacology* **4**, 198-219 (2014).

45.   Park, E.J*., et al.* Long-acting injectable formulations of antipsychotic drugs for the treatment of schizophrenia. *Archives of pharmacal research* **36**, 651-659 (2013).

46.   Wu, L., Janagam, D.R., Mandrell, T.D., Johnson, J.R. & Lowe, T.L. Long-acting injectable hormonal dosage forms for contraception. *Pharmaceutical research* **32**, 2180-2191 (2015).

47.   Curtis, K.M. & Peipert, J.F. Long-Acting Reversible Contraception. *The New England journal of medicine* **376**, 461-468 (2017).

48.   Daghistani, N. & Rey, J.A. Invega Trinza: The First Four-Times-a-Year, Long-Acting Injectable Antipsychotic Agent. *P & T : a peer-reviewed journal for formulary management* **41**, 222-227 (2016).

49.   Stewart, O.H.C.a.B.H. Physicochemical and drug-delivery considerations for oral drug bioavailability. *Drug Discovery Today* **1**, 461-473 (1996).

50.   in *Consolidated Guidelines on the Use of Antiretroviral Drugs for Treating and Preventing HIV Infection: Recommendations for a Public Health Approach* (ed. nd) (Geneva, 2016).

51.   Trezza, C., Ford, S.L., Spreen, W., Pan, R. & Piscitelli, S. Formulation and pharmacology of long-acting cabotegravir. *Current opinion in HIV and AIDS* **10**, 239-245 (2015).

52.   Spreen, W.*, et al.* GSK1265744 pharmacokinetics in plasma and tissue after single-dose long-acting injectable administration in healthy subjects. *Journal of acquired immune deficiency syndromes* **67**, 481-486 (2014).

53.   Andrews, C.D.*, et al.* Cabotegravir long acting injection protects macaques against intravenous challenge with SIVmac251. *Aids* **31**, 461-467 (2017).

54.   Andrews, C.D.*, et al.* Long-acting integrase inhibitor protects macaques from intrarectal simian/human immunodeficiency virus. *Science* **343**, 1151-1154 (2014).

55.   Radzio, J.*, et al.* The long-acting integrase inhibitor GSK744 protects macaques from repeated intravaginal SHIV challenge. *Science translational medicine* **7**, 270ra275 (2015).

56.   Taylor, B.S., Tieu, H.V., Jones, J. & Wilkin, T.J. CROI 2019: advances in antiretroviral therapy. *Topics in antiviral medicine* **27**, 50-68 (2019).

57.   Kerrigan, D.*, et al.* Experiences with long acting injectable ART: A qualitative study among PLHIV participating in a Phase II study of cabotegravir + rilpivirine (LATTE-2) in the United States and Spain. *PloS one* **13**, e0190487 (2018).

58.   Kharsany, A.B. & Karim, Q.A. HIV Infection and AIDS in Sub-Saharan Africa: Current Status, Challenges and Opportunities. *The open AIDS journal* **10**, 34-48 (2016).

59.   Rattan, J.*, et al.* Rapid Contraceptive Uptake and Changing Method Mix With High Use of Long-Acting Reversible Contraceptives in Crisis-Affected Populations in Chad and the Democratic Republic of the Congo. *Global health, science and practice* **4 Suppl 2**, S5-S20 (2016).

60.   Gunawardana, M.*, et al.* Pharmacokinetics of long-acting tenofovir alafenamide (GS-7340) subdermal implant for HIV prophylaxis. *Antimicrobial agents and chemotherapy* **59**, 3913-3919 (2015).

61.   Kovarova, M.*, et al.* Ultra-long-acting removable drug delivery system for HIV treatment and prevention. *Nature communications* **9**, 4156 (2018).

62.   Sartor, O. Eligard: leuprolide acetate in a novel sustained-release delivery system. *Urology* **61**, 25-31 (2003).

63.   Michailidis, E.*, et al.* 4'-Ethynyl-2-fluoro-2'-deoxyadenosine (EFdA) inhibits HIV-1 reverse transcriptase with multiple mechanisms. *The Journal of biological chemistry* **289**, 24533-24548 (2014).

64.   Barrett, S.E.*, et al.* Extended-Duration MK-8591-Eluting Implant as a Candidate for HIV Treatment and Prevention. *Antimicrobial agents and chemotherapy* **62**(2018).

65.   Baeten, J.M.*, et al.* Use of a Vaginal Ring Containing Dapivirine for HIV-1 Prevention in Women. *The New England journal of medicine* **375**, 2121-2132 (2016).

66.   Gendelman, H.E., McMillan, J., Bade, A.N., Edagwa, B. & Kevadiya, B.D. The Promise of Long-Acting Antiretroviral Therapies: From Need to Manufacture. *Trends in microbiology* **27**, 593-606 (2019).

67. Edagwa, B., McMillan, J., Sillman, B. & Gendelman, H.E. Long-acting slow effective release antiretroviral therapy. *Expert opinion on drug delivery* **14**, 1281-1291 (2017).

68. Albert, A. Chemical aspects of selective toxicity. *Nature* **182**, 421-422 (1958).

69. Rautio, J*., et al.* Prodrugs: design and clinical applications. *Nature reviews. Drug discovery* **7**, 255-270 (2008).

70. Sillman, B*., et al.* Creation of a long-acting nanoformulated dolutegravir. *Nature communications* **9**, 443 (2018).

71. Zhou, T*., et al.* Creation of a nanoformulated cabotegravir prodrug with improved antiretroviral profiles. *Biomaterials* **151**, 53-65 (2018).

72. McMillan, J*., et al.* Pharmacokinetics of a Long-Acting Nanoformulated Dolutegravir Prodrug in Rhesus Macaques. *Antimicrobial agents and chemotherapy* **62**(2018).

73. McMillan, J*., et al.* Pharmacokinetic testing of a first-generation cabotegravir prodrug in rhesus macaques. *Aids* **33**, 585-588 (2019).

74. Guo, D*., et al.* Creation of a Long-Acting Nanoformulated 2',3'-Dideoxy-3'-Thiacytidine. *Journal of acquired immune deficiency syndromes* **74**, e75-e83 (2017).

75. Singh, D*., et al.* Development and characterization of a long-acting nanoformulated abacavir prodrug. *Nanomedicine* **11**, 1913-1927 (2016).

76. Lin, Z*., et al.* ProTide generated long-acting abacavir nanoformulations. *Chemical communications* **54**, 8371-8374 (2018).

77. Shubber, Z*., et al.* Patient-Reported Barriers to Adherence to Antiretroviral Therapy: A Systematic Review and Meta-Analysis. *PLoS medicine* **13**, e1002183 (2016).

78. Osterberg, L. & Blaschke, T. Adherence to medication. *The New England journal of medicine* **353**, 487-497 (2005).

79. Winner, B*., et al.* Effectiveness of long-acting reversible contraception. *The New England journal of medicine* **366**, 1998-2007 (2012).

80. Adams, C.E., Fenton, M.K., Quraishi, S. & David, A.S. Systematic meta-review of depot antipsychotic drugs for people with schizophrenia. *The British journal of psychiatry : the journal of mental science* **179**, 290-299 (2001).

81. Gulick, R.M. & Flexner, C. Long-Acting HIV Drugs for Treatment and Prevention. *Annual review of medicine* **70**, 137-150 (2019).

82. van 't Klooster, G*., et al.* Pharmacokinetics and disposition of rilpivirine (TMC278) nanosuspension as a long-acting injectable antiretroviral formulation. *Antimicrobial agents and chemotherapy* **54**, 2042-2050 (2010).

83. Spreen, W.R., Margolis, D.A. & Pottage, J.C., Jr. Long-acting injectable antiretrovirals for HIV treatment and prevention. *Current opinion in HIV and AIDS* **8**, 565-571 (2013).

84. Flexner, C. Antiretroviral implants for treatment and prevention of HIV infection. *Current opinion in HIV and AIDS* **13**, 374-380 (2018).

85. Kalter, D.C*., et al.* Epidermal Langerhans cells are not principal reservoirs of virus in HIV disease. *Journal of immunology* **146**, 3396-3404 (1991).

86. Nowacek, A.S*., et al.* Nanoformulated antiretroviral drug combinations extend drug release and antiretroviral responses in HIV-1-infected macrophages: implications for neuroAIDS therapeutics. *Journal of neuroimmune pharmacology : the official journal of the Society on NeuroImmune Pharmacology* **5**, 592-601 (2010).

87. Reading, E.*, et al.* Elucidation of Drug Metabolite Structural Isomers Using Molecular Modeling Coupled with Ion Mobility Mass Spectrometry. *Analytical chemistry* **88**, 2273-2280 (2016).

88. Sanrame, C.N.*, et al.* Prodrugs of pioglitazone for extended-release (XR) injectable formulations. *Molecular pharmaceutics* **11**, 3617-3623 (2014).

89. Rohde, M.*, et al.* Biological conversion of aripiprazole lauroxil - An N-acyloxymethyl aripiprazole prodrug. *Results in pharma sciences* **4**, 19-25 (2014).

90. Haberer, J.E. Current concepts for PrEP adherence in the PrEP revolution: from clinical trials to routine practice. *Current opinion in HIV and AIDS* **11**, 10-17 (2016).

91. Ekstrand, M.L.*, et al.* Suboptimal adherence associated with virological failure and resistance mutations to first-line highly active antiretroviral therapy (HAART) in Bangalore, India. *International health* **3**, 27-34 (2011).

92. Gendelman, H.E.*, et al.* Efficient isolation and propagation of human immunodeficiency virus on recombinant colony-stimulating factor 1-treated monocytes. *The Journal of experimental medicine* **167**, 1428-1441 (1988).

93. Gorantla, S.*, et al.* Human immunodeficiency virus type 1 pathobiology studied in humanized BALB/c-Rag2-/-gammac-/- mice. *Journal of virology* **81**, 2700-2712 (2007).

94. Gandhi, M. & Gandhi, R.T. Single-pill combination regimens for treatment of HIV-1 infection. *The New England journal of medicine* **371**, 248-259 (2014).

95. Williams, J.*, et al.* Long-acting parenteral nanoformulated antiretroviral therapy: interest and attitudes of HIV-infected patients. *Nanomedicine* **8**, 1807-1813 (2013).

96. Murray, M.I.*, et al.* Satisfaction and acceptability of cabotegravir long-acting injectable suspension for prevention of HIV: Patient perspectives from the ECLAIR trial. *HIV clinical trials* **19**, 129-138 (2018).

97. Turncliff, R., Hard, M., Du, Y., Risinger, R. & Ehrich, E.W. Relative bioavailability and safety of aripiprazole lauroxil, a novel once-monthly, long-acting injectable atypical antipsychotic, following deltoid and gluteal administration in adult subjects with schizophrenia. *Schizophrenia research* **159**, 404-410 (2014).

98. Bishara, D. Once-monthly paliperidone injection for the treatment of schizophrenia. *Neuropsychiatric disease and treatment* **6**, 561-572 (2010).

99. Wong, J.K. & Yukl, S.A. Tissue reservoirs of HIV. *Current opinion in HIV and AIDS* **11**, 362-370 (2016).

100. Lorenzo-Redondo, R.*, et al.* Persistent HIV-1 replication maintains the tissue reservoir during therapy. *Nature* **530**, 51-56 (2016).

101. Darville, N.*, et al.* Intramuscular administration of paliperidone palmitate extended-release injectable microsuspension induces a subclinical inflammatory reaction modulating the pharmacokinetics in rats. *Journal of pharmaceutical sciences* **103**, 2072-2087 (2014).

102. Aderem, A. & Underhill, D.M. Mechanisms of phagocytosis in macrophages. *Annual review of immunology* **17**, 593-623 (1999).

103. Nowacek, A.S.*, et al.* NanoART synthesis, characterization, uptake, release and toxicology for human monocyte-macrophage drug delivery. *Nanomedicine* **4**, 903-917 (2009).

104. Huttunen, K.M., Raunio, H. & Rautio, J. Prodrugs--from serendipity to rational design. *Pharmacological reviews* **63**, 750-771 (2011).

105. Penrose, K.J.*, et al.* Selection of Rilpivirine-Resistant HIV-1 in a Seroconverter From the SSAT 040 Trial Who Received the 300-mg Dose of Long-Acting

Rilpivirine (TMC278LA). *The Journal of infectious diseases* **213**, 1013-1017 (2016).

106. Bahar, F.G., Ohura, K., Ogihara, T. & Imai, T. Species difference of esterase expression and hydrolase activity in plasma. *Journal of pharmaceutical sciences* **101**, 3979-3988 (2012).

107. Wang, D.*, et al.* Human carboxylesterases: a comprehensive review. *Acta pharmaceutica Sinica. B* **8**, 699-712 (2018).

108. Kovarova, M.*, et al.* Nanoformulations of Rilpivirine for Topical Pericoital and Systemic Coitus-Independent Administration Efficiently Prevent HIV Transmission. *PLoS pathogens* **11**, e1005075 (2015).

109. Nischang, M.*, et al.* Humanized mice recapitulate key features of HIV-1 infection: a novel concept using long-acting anti-retroviral drugs for treating HIV-1. *PloS one* **7**, e38853 (2012).

110. Donnell, D.*, et al.* HIV protective efficacy and correlates of tenofovir blood concentrations in a clinical trial of PrEP for HIV prevention. *Journal of acquired immune deficiency syndromes* **66**, 340-348 (2014).

111. Nieuwkerk, P.T.*, et al.* Limited patient adherence to highly active antiretroviral therapy for HIV-1 infection in an observational cohort study. *Archives of internal medicine* **161**, 1962-1968 (2001).

112. Services, U.S.D.o.H.a.H. Gudelines for the Use of Antiretroviral Agents in Adults and Adolescents with HIV. (2019).

113. Ghosh, A.K. & Brindisi, M. Organic carbamates in drug design and medicinal chemistry. *Journal of medicinal chemistry* **58**, 2895-2940 (2015).

114. Lindenmayer, J.P. Long-acting injectable antipsychotics: focus on olanzapine pamoate. *Neuropsychiatric disease and treatment* **6**, 261-267 (2010).

115. Walker, D.K.*, et al.* Preclinical assessment of the distribution of maraviroc to potential human immunodeficiency virus (HIV) sanctuary sites in the central nervous system (CNS) and gut-associated lymphoid tissue (GALT). *Xenobiotica; the fate of foreign compounds in biological systems* **38**, 1330-1339 (2008).

116. Siccardi, M.*, et al.* Maraviroc is a substrate for OATP1B1 in vitro and maraviroc plasma concentrations are influenced by SLCO1B1 521 T>C polymorphism. *Pharmacogenetics and genomics* **20**, 759-765 (2010).

117. Tatham, L.M.*, et al.* Towards a Maraviroc long-acting injectable nanoformulation. *European journal of pharmaceutics and biopharmaceutics : official journal of Arbeitsgemeinschaft fur Pharmazeutische Verfahrenstechnik e.V* **138**, 92-98 (2019).

118. Neff, C.P., Kurisu, T., Ndolo, T., Fox, K. & Akkina, R. A topical microbicide gel formulation of CCR5 antagonist maraviroc prevents HIV-1 vaginal transmission in humanized RAG-hu mice. *PloS one* **6**, e20209 (2011).

119. Malcolm, R.K.*, et al.* Pharmacokinetics and efficacy of a vaginally administered maraviroc gel in rhesus macaques. *The Journal of antimicrobial chemotherapy* **68**, 678-683 (2013).

120. Woollard, S.M. & Kanmogne, G.D. Maraviroc: a review of its use in HIV infection and beyond. *Drug design, development and therapy* **9**, 5447-5468 (2015).

121. (CDC), C.f.D.C. HIV Prevention and Care Outcomes. (2015).

122. Davey, R.T., Jr.*, et al.* HIV-1 and T cell dynamics after interruption of highly active antiretroviral therapy (HAART) in patients with a history of sustained viral suppression. *Proceedings of the National Academy of Sciences of the United States of America* **96**, 15109-15114 (1999).

123. Fonner, V.A.*, et al.* Effectiveness and safety of oral HIV preexposure prophylaxis for all populations. *Aids* **30**, 1973-1983 (2016).

124. Organization, W.H. Guideline on When to Start Antiretroviral Therapy and on Pre-Exposure Prophylaxis for HIV. (2015).
125. Celum, C.L.*, et al.* Rethinking HIV prevention to prepare for oral PrEP implementation for young African women. *Journal of the International AIDS Society* **18**, 20227 (2015).
126. Van Damme, L.*, et al.* Preexposure prophylaxis for HIV infection among African women. *The New England journal of medicine* **367**, 411-422 (2012).
127. Marrazzo, J.M.*, et al.* Tenofovir-based preexposure prophylaxis for HIV infection among African women. *The New England journal of medicine* **372**, 509-518 (2015).
128. Jackson, A.G.*, et al.* A compartmental pharmacokinetic evaluation of long-acting rilpivirine in HIV-negative volunteers for pre-exposure prophylaxis. *Clinical pharmacology and therapeutics* **96**, 314-323 (2014).
129. Owen, A. & Rannard, S. Strengths, weaknesses, opportunities and challenges for long acting injectable therapies: Insights for applications in HIV therapy. *Advanced drug delivery reviews* **103**, 144-156 (2016).
130. Dash, P.K.*, et al.* Sequential LASER ART and CRISPR Treatments Eliminate HIV-1 in a Subset of Infected Humanized Mice. *Nature communications* **10**, 2753 (2019).